ČESKÉ VYSOKÉ UČENÍ TECHNICKÉ V PRAZE

Fakulta stavební

Katedra hydrauliky a hydrologie

Proudění nenewtonských komplexních směsí v potrubí

Pipe flow of non-Newtonian complex slurries

DISERTAČNÍ PRÁCE

Ing. Mikoláš Kesely

Doktorský studijní program: Stavební inženýrství

Studijní obor: Vodní hospodářství a vodní stavby

Školitel: prof. Dr. Ing. Václav Matoušek

Praha, 2020

ČESKÉ VYSOKÉ UČENÍ TECHNICKÉ V PRAZE
Fakulta stavební
Thákurova 7, 166 29 Praha 6

PROHLÁŠENÍ

Jméno doktoranda: Mikoláš Kesely

Název disertační práce: Proudění nenewtonských komplexních směsí v potrubí

Prohlašuji, že jsem uvedenou disertační práci vypracoval/a samostatně pod vedením školitele prof. Dr. Ing. Václava Matouška.
Použitou literaturu a další materiály uvádím v seznamu použité literatury.

Disertační práce vznikla v souvislosti s řešením projektů:
SGS17/063/OHK1/1T/11; SGS18/052/OHK1/1T/11; SGS19/044/OHK1/1T/11

V Praze dne 25. 9. 2020

podpis

ABSTRAKT

Tato práce řeší následující stěžení cíle: 1. vytvoření predikčního modelu tlakových ztrát třením při turbulentním proudění komplexních směsí v potrubí, do jehož výpočtu nevstupují parametry, které v projektové fázi návrhu nejsou k dispozici, 2. prozkoumání vlivu pevných částic na přechod mezi laminárním a turbulentním prouděním v nenewtonské nosné kapalině, 3. nalezení vhodného přístupu k určení kritické rychlosti, při níž dojde k tvorbě statického lože z hrubých částic na dně potrubí s nenewtonskou nosnou kapalinou.

V rámci plnění cílů byla vytvořena unikátní a rozsáhlá experimentální databáze obsahující informace o chování směsí se značným rozpětím tokových vlastností. Experimentální směs byla tvořena skleněnými kuličkami v nosné kapalině typu Herschel-Bulkley čerpaných v laboratorním trubním okruhu s vnitřním průměrem 50 mm. Za účelem určení přechodu mezi laminárním a turbulentním prouděním byly analyzovány přístupy autorů Metzner a Reed (1955), Slatter (1999), Chilton a Stainsby (1998), Swamee a Aggarwal (2011) a Hanks (1963). Pro výpočet tlakových ztrát třením při turbulentním proudění nenewtonských kapalin byly testovány modely autorů Torrance (1963), Wilson a Thomas (1985) a Slatter (1999). Za účelem predikce tlakových ztrát třením při proudění komplexních směsí byl analyzován tříkomponentní model od autorů Pullum et al. (2015).

Pro výpočet tlakových ztrát třením při proudění komplexních směsí v potrubí je v této práci prezentována modifikace tříkomponentního modelu Pullum et al. (2015). Modifikovaný model byl kalibrován sadou vlastních experimentálních dat a následně validován na základě nezávislých experimentálních dat vlastních i poskytnutých od CSIRO a GIW Industries Inc. Experimentální databáze určená pro validaci obsahuje tokové křivky pro různé materiály (skleněné kuličky, písek, štěrk) a různé průměry potrubí. Predikce modifikovaného modelu ukazují menší, než 10% odchylku od experimentálně získaných dat vlastních i poskytnutých.

Experimentální analýza vlivu pevných částic na přechod mezi laminárním a turbulentním prouděním ukazuje jasný vliv hrubých částic. Malé objemové koncentrace hrubých částic v kapalině mají za následek dřívější přechod do turbulentního proudění. V případě, že objemová koncentrace hrubých částic překročí 8%, proudění je naopak stabilnější, což má za následek pozdější přechod do turbulentního proudění. Na základě experimentálních dat byla vytvořena empirická rovnice počítající vliv hrubých částic na kritickou hodnotu Reynoldsova čísla, při které dojde k přechodu z laminárního proudění do turbulentního.

Pro výpočet kritické rychlosti, při které dojde k vytvoření nepohyblivého lože na dně potrubí, se v nenewtonské nosné kapalině jako vhodná metoda ukazuje výpočet pomocí vrstevnatého modelu (model od autorů Matoušek et al. 2015). Předpovědi tohoto modelu se pohybují v přijatelné odchylce od experimentálně získaných dat.

KLÍČOVÁ SLOVA

Nenewtonské kapaliny, reologické parametry, kritická rychlost, přechod mezi laminárním a turbulentním prouděním, proudění směsí, tlakové ztráty třením, predikční model pro určení tlakových ztrát třením

ABSTRACT

This thesis was developed with the following principle objectives: 1. to develop a frictional head loss predictive model for turbulent flows of complex slurries, which does not rely on parameters that are not available to a process engineer in the basic engineering phase of a project, 2. to analyse effect of particles on the laminar/turbulent transition in non-Newtonian carrier fluid, 3. to present a suitable approach to determination of the deposition limit velocity for coarse particles in non-Newtonian carrier fluid.

Unique and extensive experimental data base covering wide ranges of slurry properties and flow conditions using a laboratory analogue in the form of three different fractions of glass beads in Herschel-Bulkley type carrier fluid in 50 mm

pipe was created. Techniques of predicting the laminar/turbulent transition by Metzner and Reed (1955), Slatter (1999), Chilton and Stainsby (1998), Swamee and Aggarwal (2011) and Hanks (1963) were investigated. For turbulent flow head loss predictions, models by Torrance (1963), Wilson and Thomas (1985) and Slatter (1999) were tested. For flow of complex slurries, model by Pullum et al. (2015) was found to be relevant to this thesis. For frictional head loss in turbulent flows of complex slurries a reliable and robust modification of Pullum et al. (2015) model is presented. Modified model was calibrated using own experimental data and validated by comparison with both own and provided experimental data by CSIRO and GIW Industries Inc. Experimental database used for validation contains flow curves for different materials (glass beads, sand, gravel) and different pipe diameters. Model predictions show less than 10% deviation, when compared to own experimental data and to data base graciously provided by CSIRO and GIW Industries Inc.

Experimental analysis of effect of coarse particles on the laminar/turbulent transition shows an evident influence of coarse particles. Low concentration of coarse particles in the mixture results in earlier occurrence of laminar/turbulent transition, while volumetric concentrations of solids larger than 8% tend to stabilize the flow and therefore delaying the laminar/turbulent transition. Based on the experimental evidence, approximation of the critical Reynolds number is presented.

To calculate the deposition limit velocity of coarse particles in non-Newtonian fluid, use of layered model (method by Matoušek et al., 2015) proves to be viable approach. Reasonably accurate results were achieved when predictions were compared to own experimental data.

KEY WORDS

Non-Newtonian liquids, rheological properties, deposition limit velocity, laminar/turbulent transition, complex slurries, frictional head loss, predictive modelling of friction losses

PODĚKOVÁNÍ

Rád bych poděkoval níže jmenovaným za vynaloženou podporu:

Veliké díky patří mému školiteli prof. Dr. Ing. Václavu Matouškovi za to, že mi byl svými radami a zkušenostmi vždy nápomocný a mnohými konzultacemi mi pomohl zformovat mé vědomosti a experimentální výzkum do podoby prezentované v této práci.

Dále bych zde chtěl poděkovat Ing. Tomáši Pickovi, Ph.D, za jeho aktivní přístup k řešení problémů experimentálního výzkumu a mnohé konzultace.

Veliké poděkování zároveň patří všem kolegům, přátelům a rodině, kteří mi v období doktorského studia byli oporou a přispěli pomocnou rukou, kdykoliv bylo potřeba.

My thanks go to CSIRO (Australia) and GIW Industries, Inc. (USA) for graciously providing their experimental data base.

LIST OF CONTENTS

1. INTRODUCTION 1

2. REVIEW OF SOLID-LIQUID FLOW THEORY 2

2.1 Introduction to flow of fluids 2

2.1.1 Laminar flow 2

2.1.2 Turbulent flow 2

2.1.3 Laminar/turbulent transition 3

2.2 Rheology 3

2.2.1 Rheological models 5

2.2.1.1 Mathematical model for Newtonian fluids 5

2.2.1.2 Mathematical model for shear-thinning (thickening) behaviour 6

2.2.1.3 Mathematical models for viscoplastic behaviour 7

2.3 Viscometry 9

2.3.1. Rotational viscometers 10

2.3.1.1 Cone and plate configuration 10

2.3.1.2 Concentric cylinder configuration 10

2.3.1.3 Parallel plate configuration 11

2.3.2. Tube viscometers 11

2.4 Frictional head loss in pipe flows and effect of non-Newtonian viscosity 11

2.4.1. Introduction 11

2.4.2. Flow regimes of non-settling slurries 14

2.4.1.1 Laminar flow of non-settling slurries 14

2.4.1.2 Laminar/Turbulent transition 15

2.4.1.3 Turbulent flow of non-settling slurries 20

2.4.3. Interaction between carrier fluid and solid particles 24
2.4.3.1 Flow with a stationary bed 25
2.4.3.2 Flow with a sliding bed 25
2.4.3.3 Heterogeneous suspension or asymmetric flow 25
2.4.4. Flows of complex slurries 26
2.4.4.1 Laminar flow of settling slurries with non-Newtonian carrier and its predictive modelling 26
2.4.4.2 Turbulent flow of complex slurries and its predictive modelling 30
2.4.4.3 Deposition limit velocity 33
2.5 Conclusion 35
2.5.1. Laminar flow of homogeneous non-Newtonian slurries and rheology 36
2.5.2. Laminar/turbulent transition 36
2.5.3. Turbulent flow of homogeneous non-Newtonian slurries 36
2.5.4. Flows of complex slurries 36
2.5.5. Deposition limit velocity in non-Newtonian fluids 37
3. LABORATORY EXPERIMENTS 38
3.1 Experimental apparatus 38
3.2 Characterization of materials 39
3.3 Methodology and procedure 40
3.4 Test series overview 41
3.4.1. New experimental data 41
3.4.2. CSIRO experimental database 43
3.4.3. GIW experimental database 44
3.5 Results and discussion 46

4. ANALYSIS OF PULLUM ET AL. 2015 3-COMPONENT MODEL 48
4.1 Analysis of components contribution to total pressure drop 48
4.2 Sensitivity analysis of turbulent-flow models to rheological parameters 49
4.2.1 Sensitivity of the Torrance model 50
4.2.2 Sensitivity of the Wilson - Thomas model 51
4.2.3 Sensitivity of the Slatter model 52
4.2.4 Discussion of the sensitivity of the turbulent-flow models 54
4.3 Analysis of the scaling constant k_1 55
4.4 Analysis of reference velocity V_{50} 55
4.5 Conclusion 57
5. NEW ANALYSIS 59
5.1 Modified approach to determine the pressure drop from the heterogeneous component 59
5.2 Laminar/Turbulent transition 60
5.3 Prediction of deposition limit velocity 65
5.4 Experimental identification of scaling coefficients 67
5.5 Comparison of modified 3-component model predictions with experimental data 70
5.5.1. Results of model calibration 70
5.5.2. Results of model validation 72
5.6 Concluding comments 75
6. SUMMARY, CONCLUSIONS AND RECOMMENDATIONS 76
6.1 Summary 76
6.2 Conclusions 79
6.2.1. Laminar/turbulent transition 80

6.2.2. Deposition limit velocity 80
6.2.3. Turbulent flow predictive modelling 80
6.2.4. Experimental work 80
6.3 Future research recommendations 81
REFERENCES 82
NOMENCLATURE 87
Greek letters 88
Index 89
Appendix A – Detailed pipeline test results i
Appendix B – Photographs of the experimental test loop and instrumentation i
Appendix C– Recommended procedure for frictional head loss predictions in turbulent flows of complex slurries – straight circular pipes i
C.1 INTRODUCTION i
C.2 DETERMINATION OF SLURRY PROPERTIES i
C.3 MODEL INPUT VALUES i
C.4 REGIME DETERMINATION ii
C.5 DETERMINATION OF DEPOSITION LIMIT VELOCITY iii
C.6 TURBULENT FLOW HEAD LOSS iii
C.6. 1. Equivalent component iii
C.6. 2. Heterogeneous fraction component iv
C.6. 3. Stratified fraction component iv
C.6. 4. Total pressure drop iv

1. INTRODUCTION

As water is becoming a scarce and expensive commodity, many slurries of industrial interest (for example, mixtures of thickened tailings and process water in recycle operations) exhibit a non-Newtonian behaviour due to the high concentration of fine particles in a carrier fluid. Often, fractions of larger particles are present in the mixture as well, creating a complex slurry that overlaps more than one of the flow patterns. Pipeline design for complex slurries is problematic and not much research has been conducted in this field, even though pipeline hydraulic transport has been considered a progressive technology for conveying large quantities of bulk materials (this includes long distance hauling of coal, minerals, ore and solid commodities, dredging and filling, collection and disposal of solid waste and material processing). Compared to a mechanical transport, the use of a slurry pipeline ensures a dust free environment, demands substantially less space, makes full automation possible, while minimum number of operating staff is required. On the other hand, high quality of pumping equipment and control systems is a demand.

Reliable prediction of pressure drop versus flow rate is essential for pipeline design. In practice, a majority of non-Newtonian fluids are viscoplastic, which means that they express some yield stress. If fluid of this sort is subjected to a shear stress, no strain rate is produced until the applied shear stress exceeds the yield stress. For homogeneous fluids, laminar flow predictions analytical formulae exist, but transitional velocity and turbulent flow predictions remain a practical problem. Various semi-empirical or empirical models exist for pressure drop predictions in turbulent flow regime, but literature review does not conclusively show which of these is the most consistent and reliable. For solid-fluid flows of complex slurries, reliable and robust model still needs to be presented. To approach the predictive modelling for complex slurry flows, knowledge of the effect of transported particles on the structure of turbulent flow and of the interactions between particles and flow boundaries (typically a pipeline wall) is required. The present knowledge still does not meet the needs of engineering practice.

2. REVIEW OF SOLID-LIQUID FLOW THEORY

This chapter serves as an introduction to the mechanics of non-Newtonian fluids and slurries. Its primary intention is to review knowledge related to the research aspects of this thesis. Due to the strong historical influence of Newtonian fluid behaviour, differences between Newtonian and non-Newtonian fluids are briefly approached in this review as well as types of non-Newtonian behaviour. In further sections, several modelling approaches to flows of homogeneous non-Newtonian slurries as well as rather complex multiphase flows of slurries with non-Newtonian carrier are discussed. Note, that this chapter provides only a very brief survey required for proper understanding of particular subjects introduced in this thesis and there is much more that could be discussed.

2.1 Introduction to flow of fluids

Flow of fluids can be divided into three sections: laminar, turbulent and laminar/turbulent transition.

2.1.1 Laminar flow

This flow can be described as smooth and steady flow in parallel adjacent layers without lateral mixing. The laminar pipe flow behaviour can be understood and analytical solutions can be readily derived. Due to the steady behaviour of the laminar flow, velocity distribution in the pipe cross-section is much smoother than in its turbulent counterpart (Fig. 2.1)

2.1.2 Turbulent flow

When the flow cease being steady and becomes agitated and fluctuating, it is called turbulent. As random fine-scale fluctuations of turbulent flow cannot be simulated analytically, most turbulent flow theory is semi-empirical based on physical reasoning.

2.1.3 Laminar/turbulent transition

The changeover between laminar and turbulent flow regime is called transition and although there are several methods for the identification of the transition in the literature, there is no unified concept or a guideline as to which approach should be used, when it comes to non-Newtonian behaviour.

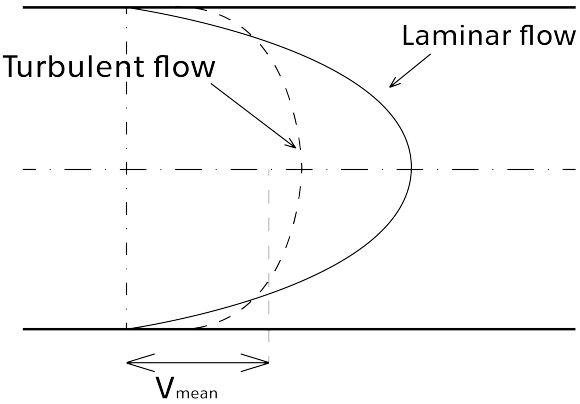

Figure 2. 1 – Comparison of laminar and turbulent velocity profiles in pipe flows

2.2 Rheology

Rheology, from Greek "rheos" – flow and "logos" – knowledge, is a science of deformation and flow of matter. In this thesis, rheology is taken as the viscous characteristics of a fluid.

In a very crude characterisation a fluid can be described as Newtonian or non-Newtonian. The difference can be demonstrated on rather simple example. Consider a fluid element, as in Fig. 2.2 (where y is thickness of the gap between two parallel plates), sheared in one plane by a single shear stress τ. While the plate at $y = 0$ is stationary, the plate at $y = Y$ is moving with steady velocity U.

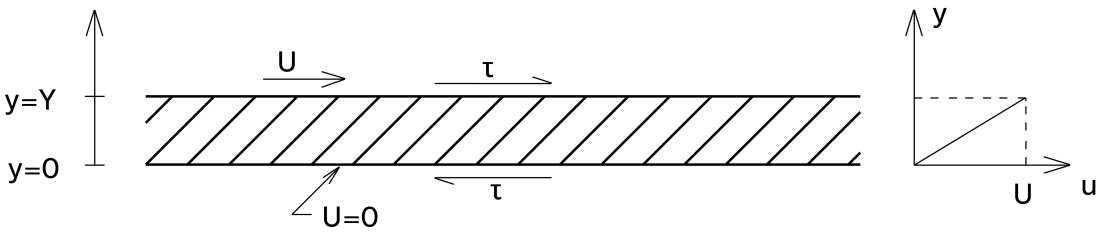

Figure 2. 2 - Shear deformation of fluid (Wilson et al., 2006)

At each plate, the fluid maintains the same velocity as the plate itself (phenomenon called non-slip boundary condition). The fluid velocity U at any

position between the plates is *y*U/Y* and the ratio *U/Y* is the velocity gradient of the fluid. As the force must be applied to the moving plate, to maintain the steady motion, shear stress is then defined as the force on plate per unit area.

Common fluids such as water or air show linear relationship between applied shear stress and resulting strain rate in laminar flow conditions. These fluids are said to be Newtonian. Any fluid which exhibit non-liner relationship or yield-stress are said to be non-Newtonian. Even though there is an infinite number of possible relationships between shear stress and shear rate, non-Newtonian fluids may be conveniently grouped into general classes (Fig 2.3):

(i) Dilatant – These fluids are *shear-thickening*, the resistance increases with increasing shear rate. Example suspensions would be corn starch, sand in water or quick sand

(ii) Pseudo plastic – A *shear-thinning* fluids are less resistant at higher strain rates. Classical examples are polymer solutions, blood plasma, paper pulp in water or latex paints.

(iii) Yield-plastic – the yield stress has to be exceeded before the fluid begins to flow. Some examples are clay suspensions, drilling mud or toothpaste.

(iv) Rheopectic – To maintain a constant strain rate, gradually increasing shear stress is required.

(v) Thixotropic – opposite case to rheopectic fluids, fluid that thins out with time.

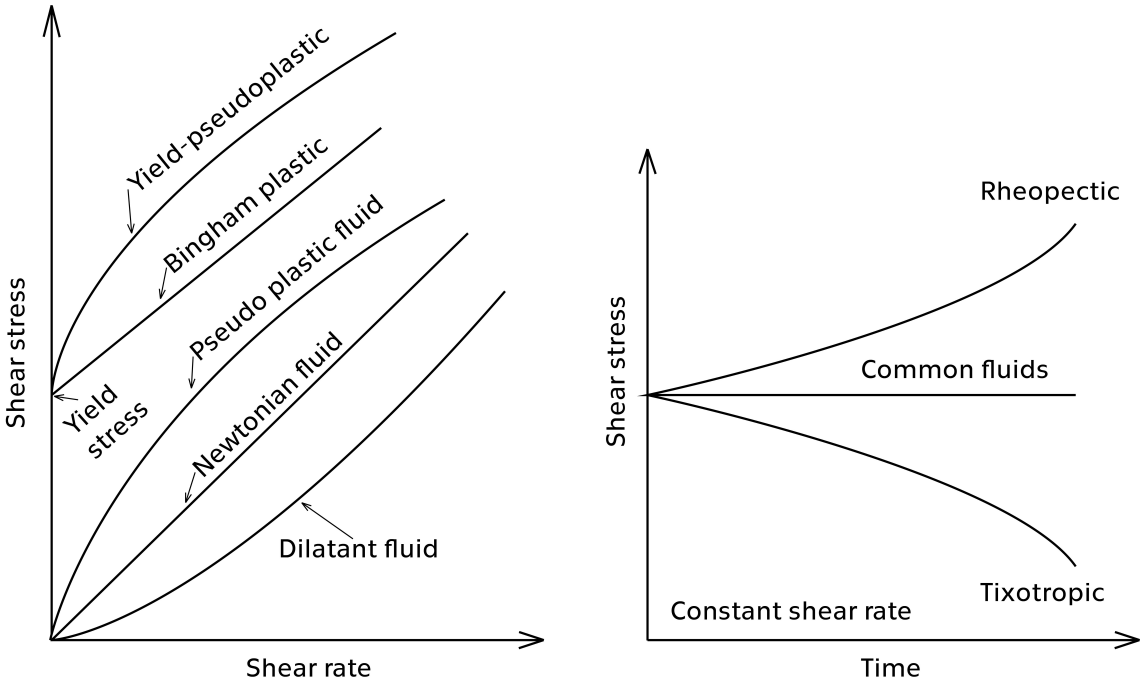

Figure 2. 3 – Rheological behaviour of various viscous materials

2.2.1 Rheological models

To form a basis for subsequent calculations, several rheological models describing the dominant non-Newtonian characteristics of the fluid can be identified. Many mathematical expressions of varying complexity and form can be found in the literature.

2.2.1.1 Mathematical model for Newtonian fluids

Mathematical formulation of the Newton´ s hypothesis is (Fig 2.4):

$$\tau = \mu \frac{du}{dy} \tag{2.1}$$

where τ is the shear stress parallel to the direction of the motion, μ is the constant of proportionality, also known as the dynamic viscosity and *du/dy* is the shear rate (rate, at which the velocity *U* is increasing in the direction normal to the direction of the motion).

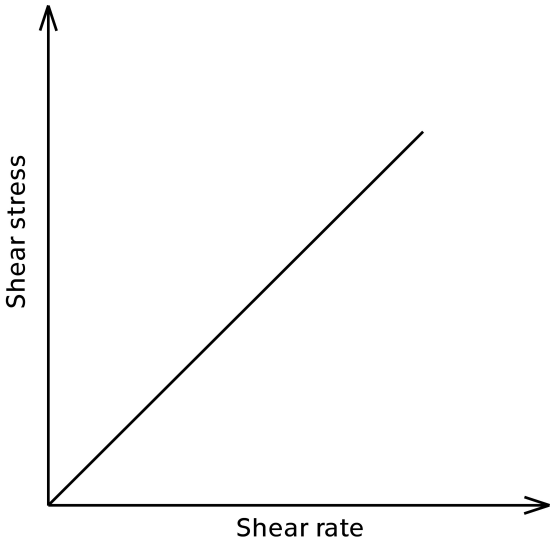

Figure 2. 4 - Characterisation of Newtonian fluid

2.2.1.2 Mathematical model for shear-thinning (thickening) behaviour

Only a perhaps most widely used model is described in this section, more complete description of mathematical models describing shear-thinning behaviour can be found in the literature (Bird, 1976; Bird et al., 1987; Carreau et al, 1997)

(i) Power-law or Ostwald de Waele fluid model

Power law (or Ostwald de Waele) rheological model offers the simplest representation of shear-thinning/thickening fluids and is expressed as (Fig 2.5):

$$\tau = K\left(\frac{du}{dy}\right)^n \tag{2.2}$$

Where K is coefficient of consistency and n is flow behaviour index.

A value of flow index determines the fluid behaviour:

$0 < n < 1$: the fluid exhibits shear-thinning properties

n = 1 the fluid shows Newtonian behaviour

$n > 1$: the fluid exhibits shear-thickening behaviour

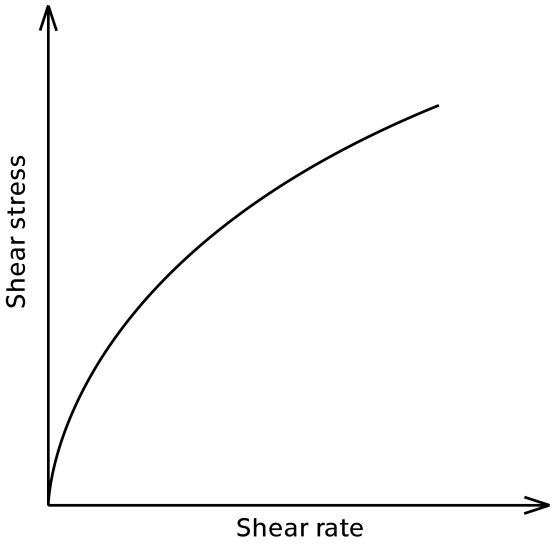

Figure 2. 5 - Power-law (Ostwald de Waele) rheological model

2.2.1.3 Mathematical models for viscoplastic behaviour

Over the years, many empirical expressions can be found in the literature describing fluids characterised as viscoplastic, as slurries of industrial interest often exhibit this kind of behaviour. Three commonly favoured models are described in this section.

(i) Bingham plastic fluid model

The proportionality between shear stress and velocity gradient is linear, but does not pass through the point of origin. Fluid behaves as a rigid elastic body until the yield stress is exceeded. Bingham plastic model offers the simplest equation describing the flow behaviour of a fluid with a yield stress, τ_y, and is written as (Fig 2.6):

$$\tau = \tau_y + \eta_B \frac{du}{dy} \tag{2.3}$$

where τ_y *is yield stress and* η_b is Bingham plastic viscosity.

Many practical examples fitting this mathematical description can be found, as this type of the non-Newtonian behaviour is quite common (suspensions of clay and water, sludge, toothpaste, chocolate...).

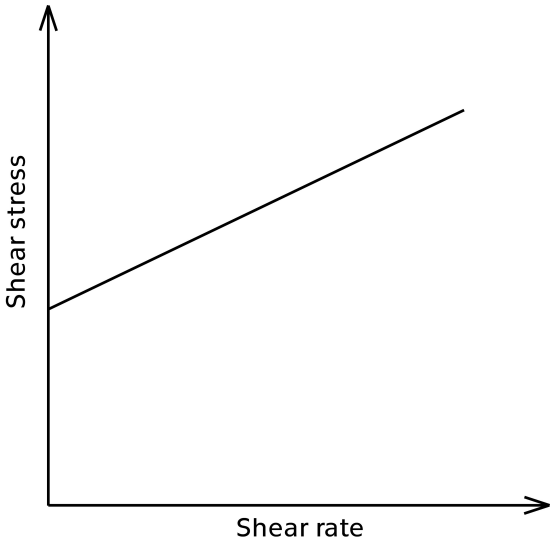

Figure 2. 6 – Bingham plastic rheological model

(ii) The Casson fluid model

This description is often favoured in food industry, as many food and biological materials, especially blood, are well described by this two-constant model as (Fig 2.7):

$$\tau^{\frac{1}{2}} = \tau_y + \mu_c^{\frac{1}{2}} \left(\frac{du}{dy} \right)^{\frac{1}{2}} \tag{2.4}$$

where μ_c is Casson plastic viscosity.

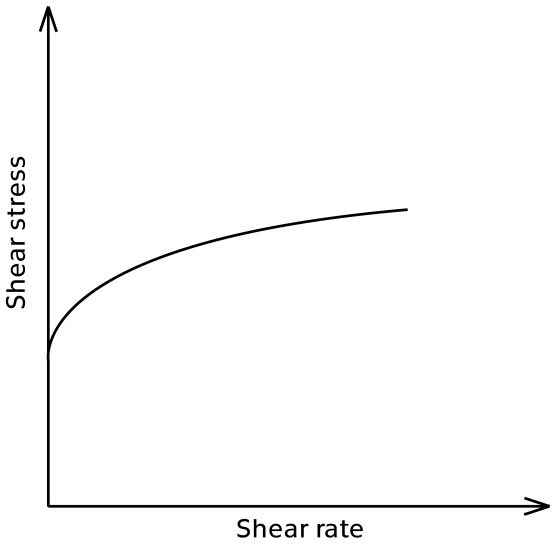

Figure 2. 7 – Casson rheological model

(iii) The Herschel-Bulkley fluid

The three constant Herschel-Bulkley fluid model is a simple generalization of the Bingham plastic model and maybe the most widely used due to the fact, that non-Newtonian slurry behaviour is very often best characterised by this model (Govier and Aziz. 1972; Hanks. 1979). The rheological equation is (Fig 2.8):

$$\tau = \tau_y + K\left(\frac{du}{dy}\right)^n \tag{2.5}$$

A value of flow index determines the fluid behaviour:

$0 < n < 1$: shear-thinning fluid – viscosity decreases with increasing strain rate

$n > 1$: shear-thickening fluid– viscosity increases with increasing strain rate

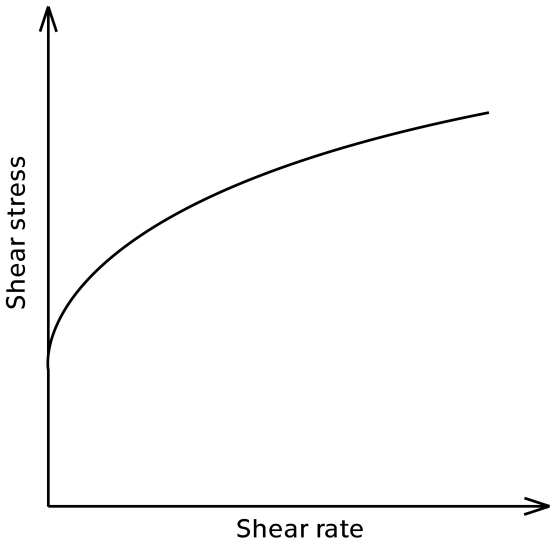

Figure 2. 8 - Herschel-Bulkley rheological model

The existence of yield stress and its implications was studied and discussed in literature (Barnes, 1999) and the comparative performance of several models, some of which are not discussed in this study, have been thoroughly evaluated in a paper review by Bird et al. (1983)

2.3 Viscometry

Viscometry is a field specialized in testing fluid samples for the purpose of establishing the relationship between shear stress and shear rate, known as rheogram. Subsequent identification of a suitable rheological model and actual

values of the rheological model constants, (eg. τ_y, K and n in case of Herschel-Bulkley model) based on the physical data from the tests. It is important to note however, that the rheological characterization of non-Newtonian fluids is far from being straightforward. Due to non-linear, dispersive, dissipative and thixotropic mechanical properties, even an apparently simple determination of a rheogram can be tricky.

The instruments used to measure the viscous properties are called viscometers and two main types of viscometers can be distinguished – rotational and tube.

2.3.1. Rotational viscometers

Rotational viscometers are more common, only a small sample of fluid is needed to perform the test, but they can be quite expensive. Various types of rotational viscometers are available (the concentric cylinder, the cone and plate, the parallel plate etc.), yet all of them follow the same principle. Fluid is sheared in a zone between the stationary - and rotating part, shear rate is determined from angular velocity and shear stress is found from simultaneous measurements of torque. Main advantages and disadvantages of various configurations are listed below

2.3.1.1 Cone and plate configuration

The main advantage of this configuration is that the shear rate is constant across the shearing gap (the cone angle is generally less than four degrees). A disadvantage is that this small angle can also produce large errors because of misalignment and eccentricities (Chhabra and Richardson, 1999). Also, the gap between cone and plate is generally very small and as a result, use this configuration is not suitable for fluids with particles, as they tend to get trapped in the gap and cause errors (Metzger, 1998)

2.3.1.2 Concentric cylinder configuration

There are variety of concentric cylinder measuring systems and only a very thin shearing gap needs to be used to acquire valid rheological data. Errors are induced by secondary flows, viscous heating, misalignment of geometry and end effect at the lower and of the rotating cylinder (Macosko, 1994).

2.3.1.3 Parallel plate configuration

This configuration is more suitable for measuring fluids with particles as the gap can be adjusted. It should be noted however, that the measuring gap should be at least five times the diameter of the largest particles (Metzger, 1998)

2.3.2. Tube viscometers

Alternatively, tube (also known as capillary) viscometers can be used to measure viscosity. Their major advantage in engineering practice is that a scale-up technique can be applied for an estimation of the pressure drop in an industrial pipe directly without intermediary of a rheological model (Wilson et al., 2006). They are also relatively cheap and simple. However, they are not as accurate as rotational viscometers and they are somewhat demanding in both sample size and free space in laboratory (due to the need of long capillaries for sake of accuracy). Also, while performing tests in a tube viscometer, it is essential to satisfy three conditions. Tested fluid must be incompressible, homogenous and maintain steady laminar flow regime.

2.4 Frictional head loss in pipe flows and effect of non-Newtonian viscosity

An important issue in the context of pipe flows is the rate of energy dissipation induced by dynamic processes in pipes. The energy loss due to overcoming viscous friction of the fluid and by occurrence of turbulent mixing is called a head loss. For a design and/or an optimization of a slurry pipeline, a reliable prediction of a relationship between the frictional head loss and independent design parameters is essential. Power consumption and consequently the entire economy of a hydrotransport line depends on information on energy losses.

2.4.1. Introduction

The shear stress distribution in a pipeline shown in Figure 2.9 can be obtained by considering a cylindrical element of length L in pipeline of diameter D, over

which a pressure difference ΔP exists. A force balance over the cylinder will yield the equation 2.6, in which τ_w is shear stress at wall:

$$\frac{\Delta P}{L} = \frac{4\tau_w}{D} \tag{2.6}$$

Note that this fundamental relationship is based only on a force balance and a condition, that the fluid is homogeneous. As the equation 2.6 does not rely on the viscous nature of the fluid, the linear distribution of shear stress is universal and thus applies to both Newtonian and non-Newtonian fluids.

The difference in viscous forces however impacts distributions of local viscosity, flow velocity and shear rate (Figure 2.9) over the pipeline cylinder.

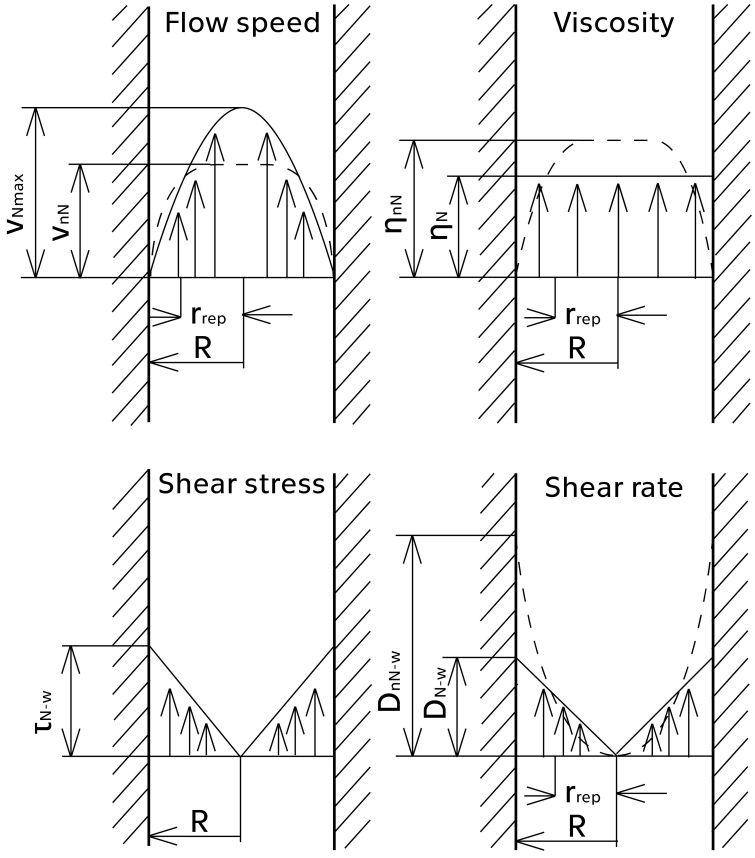

Figure 2. 9 – Distribution of local viscosity, flow velocity and shear rate over the pipeline cylinder (Matoušek, 2013)

While the viscosity in Newtonian flows stay the same regardless of the position, even though the shear rate varies with the position, the non-Newtonian viscosity (or in general rheological parameters) is influenced by the shear rate

distribution, thus creating a non-uniform profile. The velocity profile in Fig 2.9 shows the tendency of yield-pseudoplastic fluids to develop a plug flow, which as a consequence influence the distribution of shear rate. In order to develop plug flow, the fluid must exhibit a yield stress. At a certain position in the flow, the fluid develops a velocity gradient only if the yield stress is exceeded (Fig. 2.10).

Due to the interaction between the shear stress distribution and the yield stress, the higher the value of the yield stress, the thicker the plug flow which develops in a pipe.

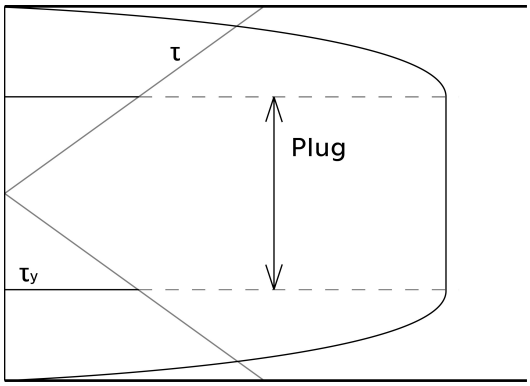

Figure 2. 10 - Plug in the centre of viscoplastic fluid flow (Matoušek, 2013)

In an analogy to the Newtonian turbulent pipe flow, it is assumed (Wilson and Thomas, 1985; Wilson, 1986; Thomas and Wilson, 1987), that momentum transport in the main flow (turbulent region) is inertial in nature and, as a result, is not directly affected by rheological properties, which leads to logarithmic velocity profile. In viscous sub-layer, velocity gradient is much steeper than that in logarithmic zone and therefore has an impact on mean velocity despite its small thickness. Within the sub-layer however, laminar conditions are present, and therefore different rheological properties have an effect in this region. It is assumed, that linear velocity profile remains within sub-layer (Fig. 2.11) for both Newtonian and non-Newtonian fluids, but due to the greater viscosity the sub-layer is thicker for non-Newtonians, and thus the logarithmic zone starts later.

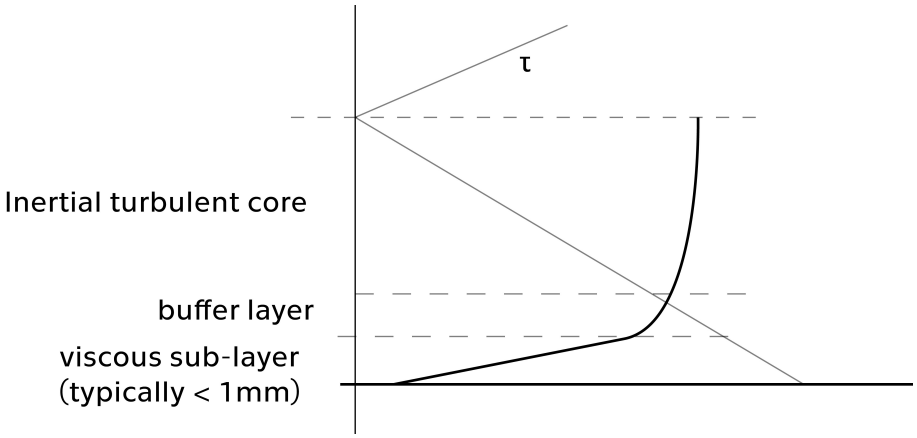

Figure 2. 11 - Velocity profile near wall in turbulence flow (Matoušek, 2013)

2.4.2. Flow regimes of non-settling slurries

2.4.1.1 Laminar flow of non-settling slurries

For laminar flow conditions, the relationship between mean velocity and shear stress at wall can be achieved by a relatively simple deduction. A general momentum equation can be written in the form of a force balance:

$$\Delta P \pi r^2 = \tau(r) 2\pi r L \tag{2.7}$$

In the momentum Equation 2.7, r is pipe radius and shear stress $\tau(r)$ can be specified further by a rheological model. Consequently, integration of the expanded momentum equation over the length and velocity produces a unique relationship between the mean flow velocity V_m and the wall shear stress τ_w, hence expressing the pressure gradient as:

$$\tau_w = \frac{\Delta P \cdot D}{4L} \tag{2.8}$$

The following chart shows the relationship between mean flow velocity and wall shear stress for some of the rheological models described in section 2.2.1:

Model	Laminar flow in a cylindrical pipe, $V_m = f(\tau_w)$
Newtonian	$V_m = \frac{\tau_w D}{8\mu}$
Power law	$V_m = \frac{D}{2}\left(\frac{n}{3n+1}\right)\left(\frac{\tau_w}{K}\right)^{1/n}$
Bingham plastic	$V_m = \frac{\tau_w D}{8\eta}\left(1-\frac{4}{3}\zeta+\frac{1}{3}\zeta^4\right),\ \zeta = \frac{\tau_y}{\tau_w}$
Casson model	$V_m = \frac{\tau_w 2D}{K}\left(1-\frac{16}{7}\sqrt{\zeta}+\frac{4\zeta}{3}-\frac{\zeta^4}{21}\right)$
Herschel Bulkley	$V_m = \frac{D}{2}\left(\frac{\tau_w}{K}\right)^{1/n}\left(\frac{\zeta^2}{a}(1-\zeta)^a+\frac{2\zeta}{b}(1-\zeta)^b+\frac{1}{c}(1-\zeta)^c\right)$ $a = 1+\frac{1}{n}\ b = 2+\frac{1}{n}\ c = 3+\frac{1}{n}$

The equations are implicit for τ_w (dP/dx), several authors however suggested simplified explicit solutions (e.g. Swamee and Aggarwal, 2011 or Chilton and Stainsby, 1998 for yield-pseudoplastic type fluids).

2.4.1.2 Laminar/Turbulent transition

The flow through a pipeline is considered to be laminar, when the flow velocity is below a specific critical value. Consecutively, if the flow velocity is above specific critical value, the flow is turbulent. This is shown in Fig. 2.12.

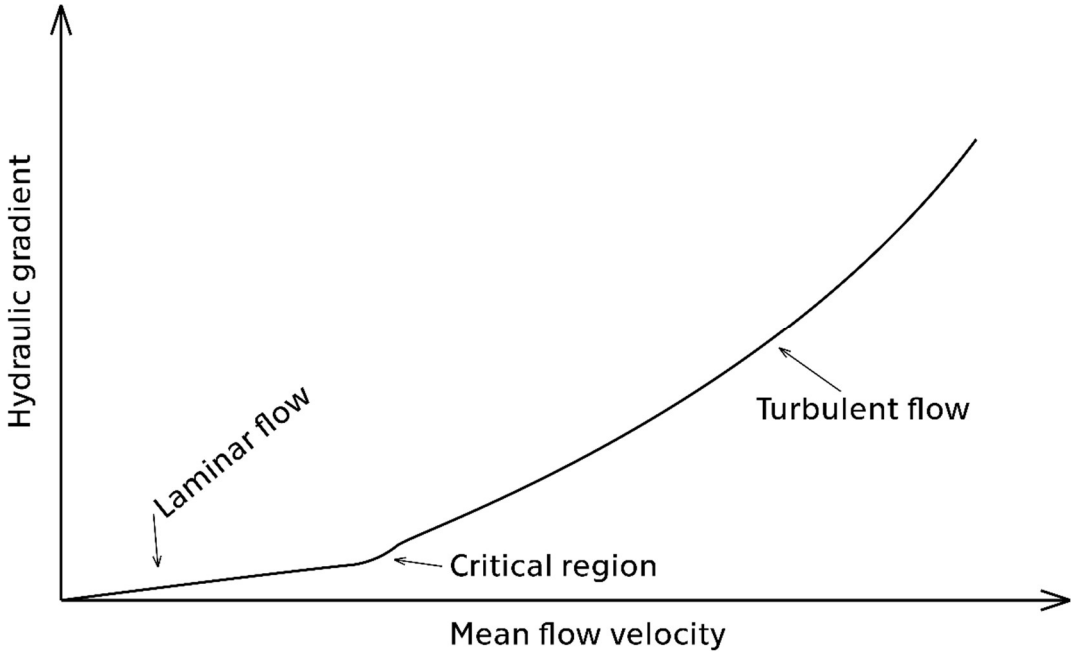

Figure 2. 12 – Development of flow regimes

As shown in the Fig. 2.12, the transition from laminar to turbulent flow regime results in a large increase in the flow resistance and in an abrupt change in the relation between energy loss and mean flow velocity. This change in the functional relationship is connected to fundamentally different flow patterns of the two regimes.

Generally accepted criterion for determination of the laminar/turbulent transition is a dimensionless group called Reynolds number, which is a ratio of the inertial to viscous forces. Usually accepted value of the Reynolds number at the lower boundary of the critical region is 2100 (Govier and Aziz, 1972). Unfortunately, great care must be taken, when predicting the transitional velocities. A large number of published work is available in literature, often with conflicting experimental evidence. For example, Heever et al. (2014) predicted transitional velocities using 3 different criteria with prediction errors ranging from 2.5 to 31% (both underpredicting and overpredicting) with no clear preference for any particular method. For most fluids however, it is probably an acceptable approximation to assume that the laminar flow conditions cease to prevail at Reynolds number above 2000-2500 (Chhabra and Richardson, 1999).

Some of the published approaches to determination of laminar/turbulent transition is described below.

(i) Metzner and Reed generalised Reynolds number

Metzner and Reed (1955) developed a generalised Reynolds number for correlating non-Newtonian pipe data. They proposed, that transition from laminar to turbulent flow regime begins at approximately the same Reynolds number as do Newtonian fluids. The generalised Metzner and Reed Reynolds number is defined as:

$$\mathrm{Re}_{MR} = \frac{8\rho V_m^2}{K'\left(\frac{8V_m}{D}\right)^{n'}} \tag{2.8}$$

where ρ is density of the fluid, K' is the apparent fluid consistency index and n' is apparent flow behaviour index.

Metzner and Reed derived their Reynolds number based on experiments with pseudoplastic fluids, for which the values of K' and n' were often constant. Unfortunately, experimental research shows that yield-pseudoplastic fluids cannot be characterised by constant values of K' and n' (Lazarus and Slatter, 1988). Therefore, values of K' and n' should be evaluated at each value of wall shear stress. Equations 2.9 and 2.10 show possible K' and n' expressions for yield-pseudoplastic fluids (Peker-Basara and Helvaci, 2008).

$$K' = \left(\frac{K^{1/n}}{4}\right)^{n'} \left(\frac{\tau_y}{r_{plug}/r}\right)^{1-n'(1/n)} \left\{\left(1-\left(r_{plug}/r\right)\right)^{1+1/n}\left[1+\frac{2\left(1-r_{plug}/r\right)\left(1+1/n\right)}{r_{plug}/r\left(2+1/n\right)}+\frac{\left(1-r_{plug}/r\right)^2\left(1+1/n\right)}{\left(r_{plug}/R\right)^2\left(3+1/n\right)}\right]\right\}^{-n'} \tag{2.9}$$

$$n' = \frac{\left(1-r_{plug}/r\right)+2\left(r_{plug}/r\right)\left(1-r_{plug}/r\right)\left(1+1/n\right)/\left(2+1/n\right)+\left(1-r_{plug}/r\right)^2\left(1+1/n\right)/\left(3+1/n\right)}{1/n+1-3\left(1-r_{plug}/r\right)\left[\left(r_{plug}/r\right)^2+2\left(r_{plug}/r\right)\left(1-r_{plug}/r\right)\left(1+1/n\right)/\left(2+1/n\right)+\left(1-\left(r_{plug}/r\right)\right)^2\left(1+1/n\right)/\left(3+1/n\right)\right]} \tag{2.10}$$

where r_{plug} is plug radius given by:

$$\frac{r_{plug}}{r} = \frac{\tau_y}{\tau_w} \tag{2.11}$$

(ii) Slatter approach

Slatter (1994) established a Reynolds number relation for yield-pseudoplastic fluids, defined as Re_3 in his work, placing an emphasis on the yield stress and a development of an unsheared concentric solid plug (as in Fig. 2.10) under laminar flow conditions:

$$\mathrm{Re}_S = \frac{8\rho V_{ann}^2}{\tau_y + K\left(\frac{8V_{ann}}{D_{shear}}\right)^n} \tag{2.12}$$

where V_{ann} is the mean velocity of the annulus (i.e. the area between unsheared concentric plug and pipe wall):

$$V_{ann} = \frac{V_m - \frac{D\left(\frac{1}{K}\right)^{\frac{1}{n}}}{2\tau_w}\left(\frac{n}{1+n}\right)\left(\frac{\tau_y}{\tau_w}\right)^2\left(\tau_w - \tau_y\right)^{\frac{1+n}{n}}}{\left(1-\frac{\tau_y}{\tau_w}\right)} \tag{2.13}$$

and D_{shear} is the sheared diameter, which represents the zone, at which the fluid is actually subjected to stress:

$$D_{shear} = D - D_{plug} = D\left(1-\frac{\tau_y}{\tau_w}\right) \tag{2.14}$$

Even though Slatter (1994) states that plug flow does not contribute to the inertial and viscous forces, without theoretical justification is this assumption an empiricism at best (Haldenwang et al., 2012).

(iii) Chilton and Stainsby correlation

Chilton and Stainsby (1998) presented their modification of the generalised Reynolds number. Proposed equation is supposed to be equivalent to that of Metzner and Reed (1955) in laminar flow regime, but physically more realistic in turbulent flow regime (Chilton and Stainsby, 1998). For Herschel-Bulkley fluids, the Reynolds number is expressed as:

$$\mathrm{Re}_{CS} = \frac{\rho V_m D}{\mu_w \left(\frac{3n+1}{4n}\right)\left(\frac{1}{1-a\zeta-b\zeta^2-c\zeta^3}\right)} \tag{2.15}$$

where ζ is given by:

$$\zeta = \frac{\tau_y}{\tau_w} = \frac{4L\tau_y}{D\Delta P} \tag{2.16}$$

and

$$a = \frac{1}{(2n+1)}; b = \frac{2n}{(n+1)(2n+1)}; c = \frac{2n^2}{(n+1)(2n+1)}; \mu_w = K^{1/n}\frac{\tau_w}{(\tau_w-\tau_y)^{1/n}} \tag{2.17}$$

(iv) Hanks stability criterion

Hanks (1963) proposed the following critical Reynolds number relation based on the stability criterion, which is very similar to that of Ryan and Johnson (1959). The critical Reynolds number for Herschel-Bulkley fluids is defined as:

$$\mathrm{Re}_{2k} = \frac{6464n}{(1+3n)^n}(2+n)^{\frac{2+n}{1+n}}\left[\frac{(1-c_{ok})^2}{1+3n} + \frac{2c_{ok}(1-c_{ok})}{1+2n} + \frac{c_{ok}^2}{1+n}\right]^{2-n}\frac{1}{(1-c_{ok})^n} \tag{2.18}$$

where c_{ok} is a critical ratio of tangential stresses ($c_{ok} = \tau_y/\tau_{ok}$), which is to be derived from the Hedström number:

$$He = \frac{3232}{n}(2+n)^{\frac{2+n}{1+n}}\left[\frac{c_{ok}}{(1-c_{ok})^{1+n}}\right]^{\frac{2-n}{n}}\left[\frac{1}{1-c_{ok}}\right]^n \tag{2.19}$$

and

$$He = \frac{\rho_m D^2}{\tau_y}\left(\frac{\tau_y}{K}\right)^{\frac{2}{n}} \tag{2.20}$$

For given mean velocity V_m, the Reynolds number value is calculated as:

$$Re = \frac{8\rho_m D^n V_m^{2-n}}{K\left(6+\frac{2}{n}\right)^n} \tag{2.21}$$

Experimental research of Slatter (1994) showed that for Herschel-Bulkley fluids the point of transition does not occur at the constant value of stability criterion, but increases with the value of Hedström number. Slatter (1997) investigated the effect of yield stress on the transition of yield pseudoplastic fluids and concluded that the Ryan and Johnson criterion didn't perform well for larger pipe diameters, even though it incorporates the effect of the yield stress.

(v) Swamee and Aggarwal correlation

Swamee and Aggarwal (2011) presented their own modification of the Reynolds number formula in their work on explicit friction factor equation for Herschel-Bulkley fluids based on curve fitting to the exact solution. The Reynolds number is defined as:

$$Re_{SA} = \frac{\rho_m D^n V_m^{2-n}}{8^{n-1} K} \left(\frac{4n}{1+3n} \right)^n \tag{2.22}$$

Compared to Reynolds number correlations above, advantage of this empirical formula lies in its simplicity, as the value of Reynolds number is a function of rheological parameters and mean flow velocity only. Laminar/turbulent transitional velocity can therefore be calculated explicitly, without the knowledge of wall shear stress at given mean velocity.

2.4.1.3 Turbulent flow of non-settling slurries

Non-Newtonian turbulent flow models for non-settling slurries can be divided into three categories. Firstly, there are models purely empirical, typical example would be approach of Bowen (1961). Secondly, there are models which are based on the presumption of similarity between Newtonian and non-Newtonian turbulence, such as those of Torrance (1963) or Wilson and Thomas (1985). The third category is formed by authors with semi-empirical approach, such as models of Dodge and Metzner (1959) or Kemblowski and Kolodziejski (1973). Note that before choosing a predictive model, a careful rheological study is recommended as the choice of the rheological model can significantly affect predictions in turbulent flow regime, especially for visco-plastic fluids (Hanks and Ricks, 1975; Heever, et al., 2014). As there are many turbulent flow

models available in the literature, only the frequently used models in pipeline practice are reviewed in this section.

(i) Torrance model

Torrance (1963) proposed a model for non-Newtonian turbulent flow of Herschel-Bulkley type fluid in pipelines using the same mixing length (and method of derivation) as would occur in Newtonian turbulent flows. In this model, the smooth wall turbulent velocity distribution is given by:

$$u^{+}=\frac{u}{V_{*}}=\frac{3,8}{n}+\frac{2,78}{n}\ln\left(1-\frac{\tau_{y}}{\tau_{w}}\right)+\frac{2,78}{n}\ln\left(\frac{V_{*}^{2-n}\rho y^{n}}{K}\right) \tag{2.23}$$

and the mean flow velocity in smooth pipe is then given by:

$$\frac{V_{m}}{V_{*}}=\frac{3,8}{n}+\frac{2,78}{n}\ln\left(1-\frac{\tau_{y}}{\tau_{w}}\right)+\frac{2,78}{n}\ln\left(\frac{V_{*}^{2-n}\rho\left(\frac{D}{2}\right)^{n}}{K}\right)-4,17 \tag{2.24}$$

where V_* is mean shear velocity, given by:

$$V_{*}=\sqrt{\frac{\tau_{w}}{\rho_{f}}} \tag{2.25}$$

where ρ_f is the fluid density. Similarly, for fully developed rough turbulent flow the mean velocity is given by:

$$\frac{V_{m}}{V_{*}}=\frac{2,5}{n}+\frac{2,78}{n}\ln\left(\frac{\frac{D}{2}}{k_{r}}\right)+8,5-\frac{3,75}{n} \tag{2.26}$$

where k_r is hydraulic roughness size. On partially rough wall turbulent flow, Torrance makes no comment.

Slatter (1994) compared predictions of Torrance (1963) model with turbulent flow data of a yield pseudoplastic material. At low shear rates, the Torrance model showed good agreement with the experimental results. Slatter et al. (1997) compared turbulent predictions of various turbulent techniques using

different materials. The average errors for the Torrance (1963) method were 11% for Bingham plastic, 35% for pseudoplastic and for 15% for yield-pseudoplastic. El-Nahhas et al. (2005) compared kaolin slurries experimental data to models of Torrance (1963), Wilson and Thomas (1985) and Slatter (1994). The Torrance prediction was in a close agreement with the prediction of Wilson and Thomas (1985), and both models were considered as being able to reliably predict the experimental data.

(ii) Wilson and Thomas model

Wilson and Thomas (1985) proposed an analysis which predicts the thickening of the viscous sub-layer (as in Fig 2.11) by a factor called the ratio A_r. This ratio is defined as the ratio of integrals of the non-Newtonian and Newtonian rheograms during identical shear conditions. For the Herschel-Bulkley type fluid, the area ratio can be expressed as:

$$A_r = 2\left[\frac{1+\frac{\tau_y}{\tau_w}n}{1+n}\right] \tag{2.27}$$

The mean velocity is given by:

$$\frac{V_m}{V_*} = \frac{V_N}{V_*} + 11{,}6(A_r - 1) - 2{,}5\ln A_r - \Omega \tag{2.28}$$

where V_N represents the mean velocity for the equivalent smooth-wall flow of a Newtonian fluid, i.e. flow with the same viscosity corresponding to the non-Newtonian value at $\tau = \tau_w$. The term Ω represents the effect of possible blunting of the velocity profile in the logarithmic (e.g. core) region of the flow, which would be caused by the yield stress and expressed as:

$$\Omega = -2{,}5\ln\left(1-\frac{\tau_y}{\tau_w}\right) - 2{,}5\frac{\tau_y}{\tau_w}\left(1+0{,}5\frac{\tau_y}{\tau_w}\right) \tag{2.29}$$

Work done by Slatter (1994) shows that at low velocities, the model predicts accurately turbulent flow experimental data, and that predictions of Wilson and Thomas (1985) model are almost identical to those of Torrance (1963) model.

Deviation from experimental data however occurs with increase of flow velocities. Slatter et al. (1997) compared Wilson and Thomas (1985) model predictions with experimental data of various rheologies. The analysis showed, that the method performed worst with yield-pseudoplastic rheology, having an average error of 27% and best with Bingham plastic rheology, having an average error of 11%. Chilton and Stainsby (1998) recommended the Wilson and Thomas (1985) model as the best predictive approach available for Herschel-Bulkley fluids in highly turbulent flows, which is in a direct contradiction with the findings of Slatter (1994). Chilton and Stainsby (1998) also commented on the models, which assume a negligible thickness of the viscous sub-layer. Those could not be valid for non-Newtonian flows. This should be especially true for fluids with a yield stress or with very low n values. Xu et al. (1993) published some cases, in which predictions of Wilson and Thomas model failed to fit the turbulent behaviour of slurries

(iii) Slatter model

Slatter (1999) proposed a new theoretical model for describing turbulent flows of non-Newtonian slurries assuming a similarity with the Newtonian turbulence. In this alternative theory it is assumed that a roughness effect is caused by the solid particles present in the carrier fluid. Roughness Reynolds number, Re_r, is then used as a condition for discernment of smooth and rough wall turbulent flow. For Herschel-Bulkley type fluid the roughness Reynolds number is expressed as:

$$\mathrm{Re}_r = \frac{8\rho V_*^2}{\tau_y + K\left[\frac{8V_*}{d_{85}}\right]^n} \tag{2.30}$$

where d_{85} is a particle diameter corresponding to the 85% particle. For smooth wall turbulent flow ($Re_r < 3{,}32$) the mean velocity is expressed as:

$$\frac{V_m}{V_*} = 2{,}5\ln\left(\frac{D}{2d_{85}}\right) + 2{,}5\ln\mathrm{Re}_r + 1{,}75 \tag{2.31}$$

And for fully developed rough wall turbulent flow ($Re_r > 3{,}32$) is:

$$\frac{V_m}{V_*} = 2{,}5\ln\left(\frac{D}{2d_{85}}\right) + 4{,}75 \tag{2.32}$$

For kaolin slurries, Slatter et al. (1997) show an average error of 6% when model predictions were fitted with experimental data. Results also show, that Slatted model predictions are more accurate than those of Torrance (1963), Wilson and Thomas (1985) and Chilton and Stainsby (1998). These results are supported by conclusions of El-Nahhas et al. (2005) and Vlasak and Chara (1999), which show, that Slatter (1994) model predicts the turbulent flow of kaolin slurries better than models of Torrance (1963) and Wilson and Thomas (1985).

2.4.3. Interaction between carrier fluid and solid particles

The interactions in solid/liquid suspensions (slurries) are complex, especially in turbulent flows. Depending on various aspects, such as particle size or intensity of the turbulence, slurry flow patterns may differ significantly (e.g. Matoušek, 2004). A settling slurry composed of small particles (approximately less than 40 μm) tends to behave as a homogenous matter. The particles are distributed uniformly throughout the entire cross section of a pipeline and a change in local concentration of solids with the local position (as the height above the pipe invert) is negligible. Basically, the fine particles interact with fluid so that they affect rheological properties of the carrier fluid. The small particles continue to express this homogeneous behaviour even when larger particle fractions are also present in the slurry. A slurry consisting of slightly coarser particles (e.g. fine sand of roughly 100 μm) exhibits a different behaviour. In case of turbulent flow, particles are distributed throughout the pipe cross section by turbulent diffusion, but the local concentration tends to decrease with the increasing height. This type of flow can be characterized as pseudo-homogenous flow. Even coarser particles (as those in the medium- and coarse-sand range, typically from 400 μm to 2 mm) cause that settling-slurry flow shifts to a heterogeneous behaviour, where the local concentration varies considerably across a pipe cross section. A certain proportion of solids is accumulated near the bottom of pipe while the rest is distributed across the upper part of the pipe cross section. If the accumulated particles form a

bed (sliding or stationary) at the bottom of the pipe, then the flow is considered stratified. If intensity of turbulence of carrier fluid is not capable of suspending any solid particle, then slurry flow is fully stratified.

The tendency of particles to settle under the influence of gravity and the tendency of carrier fluid to suspend particles has a major effect on the behaviour of the slurry flow. The settling tendency leads to an accumulation of particles in the lower section of pipeline and the amount of particles accumulated strongly depends on the velocity of slurry in pipeline. The higher the velocity, the greater the ability of the carrier fluid to suspend particles induced by work of turbulent eddies. At low velocity, particles tend to settle down and to be transported as a sliding bed while at very high velocity and thus high turbulence level, suspension may be almost homogenous.

2.4.3.1 Flow with a stationary bed

If the mean velocity of carrier fluid is low, the bed thickens. As the fluid above the bed tries to move the solids, they tend to roll and tumble. While coarser particles build up the bed, particles with the lowest settling velocity move as asymmetric flow pattern. As the velocity drops even further, coarser particles settle completely and finer particles continue to move by saltation and asymmetric suspension above the stationary bed. This situation may ultimately lead to a number of problems associated with blockage of pipeline.

2.4.3.2 Flow with a sliding bed

With low mean velocity and large number of coarse particles, most of the solids settle to the bottom of the pipe forming a bed. These grains are in virtually permanent contact and slide almost '*en bloc*'.

2.4.3.3 Heterogeneous suspension or asymmetric flow

With increasing velocity, turbulence is sufficient to lift more solids. All particles move in asymmetric pattern with the coarsest at the bottom of pipeline covered with superimposed layers of medium and fine sized particles.

2.4.4. Flows of complex slurries

The term complex slurry indicates that slurry is composed of solids covering a very broad range of particle sizes that overlaps more than one of the flow patterns - non-Newtonian, pseudo-homogenous, heterogeneous and fully-stratified. A typical complex slurry contains both very fine and very coarse particles and also exhibits a non-Newtonian behaviour. Typical examples are residual products ("tailings") from mining industry with normal average particle sizes of 20 to 100 μm or more. As current industrial and environmental interest is directed towards using less water or other carrier fluid, which means handling of tailing slurries at high solids concentration, reliable prediction models for flows of complex slurries need to be developed.

In literature, most models dealing with pipeline transport of solids covering a very broad range of particle sizes consider Newtonian fluid as a carrier (Sellgren et al., 2016; Visintainer et al., 2017). These models are inappropriate to use when carrier fluid exhibits non-Newtonian behaviour, but they can serve as a theoretical base when it comes to development of reliable and robust predictive models of frictional head loss of complex slurries flows in turbulent flow regime.

2.4.4.1 Laminar flow of settling slurries with non-Newtonian carrier and its predictive modelling

It has been well demonstrated in literature, that coarse particles, which would be under stationary conditions fully suspended in the carrier fluid due to the fact that submerged weight of the particles would not be enough to balance out the yield stress of the carrier fluid, still form the sliding bed during flow conditions, as the local viscosity of the sheared carrier fluid drops, allowing the coarse particles to settle down to the pipe invert (Cooke 2002, Pullum and Graham 2000).

If stratified mixture flow occurs in a pipeline, for the sake of modelling, such a flow can be simplified into the flow with a two-layer pattern of a particle-rich zone and a particle-lean zone. Various versions of layered model approaches

are available in the literature, when Newtonian fluid is considered as a carrier. However, only a few non-Newtonian carrier based models have been discussed so far. Pullum et al. (2004) presented a simple generic two-layer model for laminar and turbulent flow of power-law and viscoplastic carriers based on concept developed by Wilson (1976). This model uses empirical parameters and formulae based on comprehensive experimental database. Later, Rojas and Saez (2012) introduced and experimentally verified their version of two-layer model.

(i) Matoušek et al. two-layer model approach

According to the Matoušek et al. (2015) two-layer model, the behaviour of the flow is governed by the principle of force balance between driving and resisting forces acting on each layer in the flow.

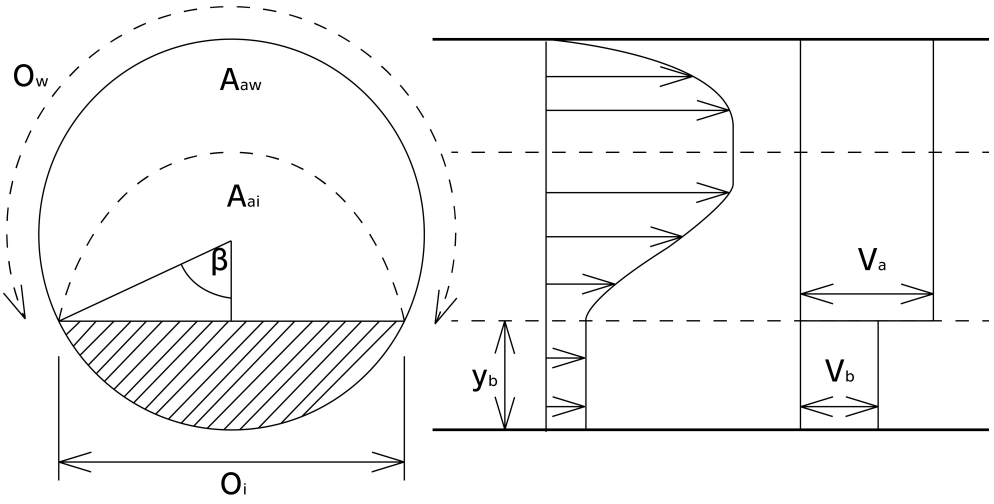

Figure 2. 13 - Schematic of two-layer model approach

An application of the mass conservation law to the two-layer pattern produces for slurry flow rates:

$$V_m = \frac{V_a A_a + V_b A_b}{A} \tag{2.33}$$

where A is area and subscript a stands for the upper layer and subscript b stands for the lower layer.

The solids flow rate can be written as:

$$C_{vd} A V_m = C_a A_a V_s + C_b A_b V_b \tag{2.34}$$

where C_{vd} is delivered concentration of solids.

Momentum balance for the upper layer can be expressed:

$$\Delta P A_a = \tau_a O_w L + \tau_i O_i L \tag{2.35}$$

and for the lower layer as:

$$\Delta P A_b + \tau_i O_i L = \left(\tau_{fb} + \tau_{sb}\right) O_b L \tag{2.36}$$

where O is perimeter, the subscript i stands for the interface and subscript b stands for the lower layer.

As the particles transmit their submerged weight to the pipeline wall, contact load solids exert resisting force against the flow driving forces. This resistance force is:

$$\mu_s F_N = \tau_{sb} O_b \tag{2.37}$$

where μ_s is coefficient of Coulombic sliding friction for the bed and F_N the total normal force, exerted by the normal intergranular stress against the pipeline wall, which can be obtained by integrating the normal stress over the pipeline perimeter O_b:

$$F_N = g\left(\rho_s - \rho_f\right) C_{vb} \frac{D^2}{2} \left(\sin\beta - \beta\cos\beta\right) \tag{2.38}$$

Viscous friction between the flowing carrier fluid and the flow boundary is described by the relevant boundary shear stress (wall shear stress τ_a, interfacial shear stress τ_i and under-bed carrier stress τ_{fb}). Matoušek et al. (2015) suggest following formulae for shear stresses in two-layer flow with viscoplastic carrier. The shear stress at the top of sliding bed below the shear layer is composed of the carrier shear stress and the grain shear stress:

$$\tau_i = \tau_{fi} + \tau_{si} \tag{2.39}$$

For laminar flow above stationary deposit, the interfacial shear stress τ_{fi} may be considered equal to the shear stress at pipe wall in the upper layer, τ_a (Pullum et al. 2004, Rojas and Saez 2012) since the shear stress is not a function

of the surface roughness, unlike in turbulent flows. However, if the bed slides (the interface moves while the pipe wall remains stationary) and a shear layer develops, then it seems appropriate to consider $\tau_{fi} \neq \tau_a$, with each stress being associated with a different hydraulic radius:

$$R_{hai} = A_{ai} / O_i \; and \; R_{haw} = A_{aw} / O_a \tag{2.40}$$

where A_{ai}, A_{aw} are sub-areas of the cross-sectional area of the upper layer associated with the interface and the pipe wall, respectively; O_i, O_a are perimeters of the interface and the pipe wall, respectively (Fig. 2.13).

The carrier component of the interfacial stress and wall shear stress takes the form:

$$\tau_{fi} = \frac{\lambda_{fi}}{8} \rho V_i^2 \; and \; \tau_a = \frac{\lambda_a}{8} \rho V_a^2 \tag{2.41}$$

where $V_i = V_a - V_b$ (V_a is the average velocity in the upper layer, V_b is the average velocity in the lower layer), and λ is Darcy friction factor, which is for laminar flow in a circular pipe given by $64/Re$. As Reynolds number is affected by rheological properties of the fluid, for Herschel-Bulkley carrier the Reynolds number takes the form of $Re = f(\tau_y, K, n, V_m, D, \rho)$. Numerous determinations of Reynolds number can be found in literature, for example the one proposed by Chilton and Stainsby (1998) can be used to calculate Reynolds number in the wall and the interface region. The shear stress exerted at the top of the sliding bed by colliding grains travelling in the shear layer is:

$$\tau_{si} = \frac{1}{2}(\rho_s - \rho_f) g H_{sh} C_b \tan\varphi' \tag{2.42}$$

in which $tan\,\varphi'$ is the coefficient of internal friction of colliding grains in the shear layer and H_{sh} is thickness of shear layer. The total shear stress at the pipe wall below the sliding bed is the sum of carrier stress (viscous friction) and grain stress (mechanical friction):

$$\tau_b = \tau_{fb} + \tau_{sb}$$

The carrier shear stress is a result of laminar shearing in between the pipe wall and the underside of the sliding bed. It can be assumed, that the region of

carrier shearing above the pipe wall is confined to a thin layer between the wall and the sliding bed. For the laminar flow of the Herschel-Bulkley carrier, a simple assumption is that the viscous shear stress at the pipe wall below the sliding bed is solved using the fluids constitutive equation with a strain rate given by V_b/d. Thus the under-bed carrier stress can be determined:

$$\tau_{fb} = \tau_y + K\left(\frac{V_b}{d}\right)^n \tag{2.43}$$

2.4.4.2 *Turbulent flow of complex slurries and its predictive modelling*

Since turbulence is dominated by inertial forces, prediction models for frictional head loss are based on the presumption that non-Newtonian turbulence is at least on macro-scale level similar to Newtonian turbulence (Pullum, 2007). Semi-empirical correlations available in the literature (focused on settling-slurry flow in Newtonian medium) are mostly based on a narrow size distribution model by Clift et al (1982) and further developed into a broad size distribution heterogeneous models (Wilson et al., 1990; Sellgren and Wilson, 2007; Sellgren et al., 2016; Visintainer et al., 2017). A comprehensive study on particle flow patterns and appropriate modelling approaches to heterogenenous and partially stratified flows in Newtonian medium was published by Matoušek et al. (2013) and Matoušek et al. (2014).

For complex slurries with broad spectrum of particle sizes in non-Newtonian medium, it is suggested to use a three-component model (Pullum et al. 2015), which is based on a presumption that particles moving through non-Newtonian fluids behave in a very similar manner to those moving through Newtonian fluids.

In the Pullum et al. (2015) model, the particle size distribution of the conveyed solids is split into three components of the model as shown in Fig. 2.14 and the value of total pressure gradient is given by a sum of pressure gradients from each component of the model:

$$\left(\frac{dp}{dx}\right)_{tot} = k_1\frac{dp}{dx_e} + k_2\frac{dp}{dx_h} + k_3\frac{dp}{dx_s} \tag{2.44}$$

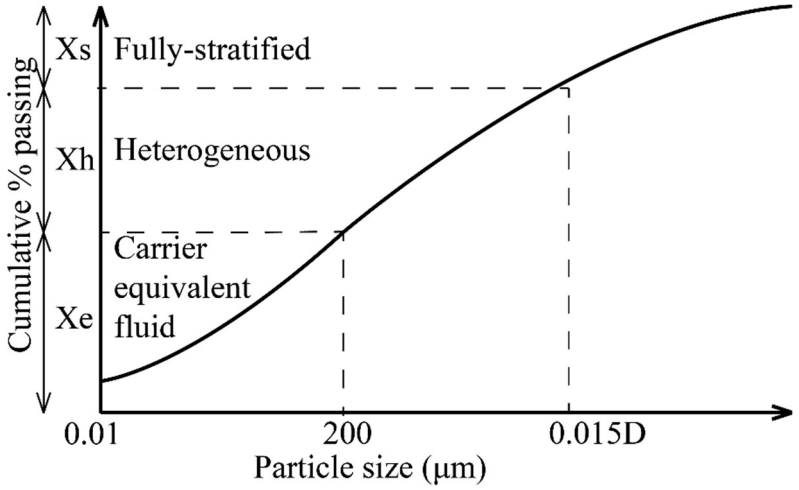

Figure 2. 14 – Subdvision of the particle size distribution in the three-component model (Pullum et al., 2015)

This approach assumes, that the interaction between particle fractions is somewhat negligible and therefore the resulting pressure gradient from each fraction may be combined independently. While in case of settling slurry flow with Newtonian carrier, it has been proven in the literature, that certain combinations of particle fractions may lead to a substantial reduction of pressure drop (Vlasák et al., 2011; Matoušek et al., 2018), no such pressure drop reduction behaviour have been reported for non-Newtonian slurry flows and due to the non-Newtonian nature of the carrier fluid, the particle interactions may have much lesser impact on flow properties when compared to Newtonian slurries.

Carrier fluid and the finest fraction of particles combine into a single equivalent-carrier fluid component, which exhibits a non-Newtonian behaviour. The mass fraction of carrier-equivalent fluid is denoted X_e and the remaining fractions are divided into two segments – heterogeneous X_h and fully-stratified X_s. The upper size of the X_e component is to be taken as 0.2 mm. It is suggested (Pullum et al., 2015), that each of the components is scaled by the coefficients k_1, k_2, k_3, to account for the non-Newtonian effect of the carrier and these are to be determined empirically.

The contributions to the overall pressure gradients from each fraction can be calculated as follows.

The equivalent fluid component is based on the underlying carrier fluids rheology and the density of the mixture of the fluid and the X_e-fraction of solids. The density and relative density of the equivalent fluid is:

$$\rho_e = \rho_c + X_e C_v \left(\rho_s - \rho_c\right) \tag{2.45}$$

or

$$S_e = S_c + X_e C_v \left(S_s - S_c\right) \tag{2.46}$$

where ρ_c is the actual carrier fluid density, ρ_s is the solids density and C_v is the total volumetric solids concentration. S_e, S_c, S_s are relative density equivalents. The resulting pressure gradient for the e-component is then given by:

$$\frac{dp}{dx_e} = \frac{dp}{dx_c}\left[1 + \left(1 - 0.25X_e\right) X_e C_v \left(S_s - S_c\right)\right] \tag{2.47}$$

The density of the heterogeneous portion of the slurry is:

$$\rho_h = \rho_c + \left(X_e + X_h\right) C_v \left(\rho_s - \rho_c\right) \tag{2.48}$$

or

$$S_h = S_c + \left(X_e + X_h\right) C_v \left(S_s - S_c\right) \tag{2.49}$$

The contribution to the pressure gradient from the heterogeneous portion of solids (X_h-component) is:

$$\frac{dp}{dx_h} = \rho_w g B X_h C_v \left(S_s - S_e\right)\left(\frac{V_{50}}{V_m}\right) \tag{2.50}$$

where B is derived from characteristic particle diameter d_h as follows:

$$d_h = \frac{200\mu m + \min\left(0.015D, d_{\max}\right)}{2} \tag{2.51}$$

where D is pipeline inner diameter and $B = 0.22$ when $d_h > 500$ μm (Pulum et al., 2015), otherwise:

$$B = 0.22 \cdot \frac{d_h - 200\mu m}{300\mu m} \tag{2.52}$$

The reference velocity V_{50} is written as:

$$V_{50} = 3.93 d_h^{0.35} \left(\frac{S_s - S_e}{1.65} \right)^{0.45} \tag{2.53}$$

Note, that in Equation 2.53 d_h is in mm, whereas V_{50} in m/s (Wilson et al., 1997). The contribution from the sliding bed to the friction head loss is approximated by:

$$\frac{dp}{dx_s} = \rho_w g X_s C_v \left(S_s - S_h \right) 0.3 \left(\frac{V_m}{0.55 V_{sm}} \right)^{-0.25} \tag{2.54}$$

where V_m is the mean velocity of mixture and V_{sm} is the deposition-limit velocity.

2.4.4.3 Deposition limit velocity

Determination of the deposition limit velocity is one of the most important and yet one of the most difficult problems associated with the design and operation of a pipeline system transporting settling slurries. Coarse settling slurries are transported at very different conditions (pipe size and geometry, solids contents in slurry etc.) and exhibit very different properties (slurry density, degree of stratification etc.). Examples include in-plant transfer lines, tailings disposal operations, dredging, deep sea mining, and long-distance pipelining (Spelay et al., 2016).

In slurry pipeline practice, the term "critical velocity" is often used to determine a threshold below which the flow of slurry should not drop in a pipe in order to avoid operational problems. In the literature, many names and definitions can be found for the so called critical velocity. Some authors refer to it as to velocity at which a stationary bed deposit starts sliding, other authors as to velocity at which the stationary bed or sliding bed disappears. Others consider the critical velocity as the velocity at which the hydraulic gradient is at a minimum on a pipe resistance curve for mixture at certain delivered concentration in a pipe of a certain size.

In this study the deposition limit velocity, V_{sm}, is considered as an average flow velocity at which grains first stop moving and start to develop a deposit at the bottom of a pipe.

The deposition limit velocity is sensitive to pipe diameter, to properties of both solids (size, density) and carrying liquid (density, viscosity), as well as to the concentration of transported solids. An estimation of deposition limit velocity in Newtonian slurries has been subject of numerous experimental studies and many predictive methods have been presented in the literature (for example Durand and Condolios, 1952; Durand, 1953; Miedema and Ramsdell, 2015; Wilson, 1979, 1986). In the slurry flows with non-Newtonian carrier fluid, to author´s knowledge, there is no reliable method available and literature background in this research area is very scarce. Pullum et al. (2015) states, that the deposition limit velocities obtained through the Wilson-GIW model described as VSCALC in Wilson et al. (1997) can be considerably lower than those calculated with a non-Newtonian two layer model, especially for low values of flow index n (Pullum et al., 2004). Poloski et al. (2009) published non-Newtonian slurry deposition method, predicted threshold velocities are different from the deposition limit velocity, however.

Below, only the Wilson-GIW method for determination of deposition limit velocity is described, as in the model of Wilson et al. (2006), where Equation 2.54 is presented, this method is recommended for the determination of the V_{sm}. It therefore seemed appropriate to analyse suitability of this method to predict the value of deposition limit velocity in non-Newtonian medium before moving on to more complex solutions, if needed. Results of this analysis are given in Chapter 5.3.

(i) Wilson-GIW model

Proposed correlations are fit functions of sliding-bed two-layer model calculations in turbulent flow regime of Newtonian liquid with coarse particles. In Wilson (1979), model results were originally given as a nomographic chart known as the demi-McDonald. Nowadays, Wilson (1992) sliding bed model fit functions presented below are often used for determination of V_{sm} in slurries with Newtonian carrier.

In this approach, the maximum deposition limit velocity, $V_{sm,max}$, can be estimated:

$$V_{sm,\max} = \frac{8.8\left(\frac{\mu_s\left(S_s - S_f\right)}{0.66}\right)^{0.55} D^{0.7} d^{1.75}}{d^2 + 0.11 D^{0.7}} \tag{2.55}$$

where particle diameter d is in mm and pipe diameter D is in m (Wilson, 1992). In order to account for the effect of solids concentration on the value of deposition limit velocity, further nomographs were developed to determine the V_{sm} from $V_{sm,max}$. The nomograph curves can be approximated by fit functions, and the actual value of V_{sm} can be calculated as follows:

$$\frac{V_{sm}}{V_{sm,\max}} = 6.75 C_r^{\frac{\ln(0.666)}{\ln(C_{rm})}} \left[1 - C_r^{\frac{\ln(0.666)}{\ln(C_{rm})}}\right]^2 \qquad \text{for} \qquad C_{rm} \le 0.33 \tag{2.56}$$

and

$$\frac{V_{sm}}{V_{sm,\max}} = 6.75(1 - C_r)^{2\frac{\ln(0.666)}{\ln(1-C_{rm})}} \left[1 - (1 - C_r)^{\frac{\ln(0.666)}{\ln(1-C_{rm})}}\right] \quad \text{for} \qquad C_{rm} > 0.33 \tag{2.57}$$

where C_r is a ratio of loose-poured bed concentration and delivered concentration of solids, and value of C_{rm} is given by:

$$C_{rm} = 0.16 D^{0.40} d^{-0.84} \left(\frac{S_s - S_f}{1.65}\right)^{-0.17} \tag{2.58}$$

in this fit, d is in mm and D is in m.

2.5 Conclusion

The literature review related to the flows of non-Newtonian slurries in pipelines has shown, that flows of homogeneous non-Newtonian slurries has been a subject of extensive investigation in recent years. Finding relevant data on flow of complex slurries proved to be difficult, however, as data focusing on this subject is very scarce.

2.5.1. Laminar flow of homogeneous non-Newtonian slurries and rheology

Several rheological models describing the dominant non-Newtonian characteristics of the fluid can be found in the literature. Mathematical formulae of five commonly used rheological models as well as formulae defining the value of mean flow velocity for each described rheological model, have been presented in this chapter.

2.5.2. Laminar/turbulent transition

Predicting non-Newtonian laminar/turbulent transition velocity is an ongoing problem. Several correlations for calculation of Reynolds number exist in the literature and experimental evidence often show conflicting conclusions. Some of the available criteria for predicting the laminar/turbulent transition have been selected and presented in this chapter and their performance against experimental data available in literature was reviewed.

2.5.3. Turbulent flow of homogeneous non-Newtonian slurries

Many turbulent flow correlations have been developed, some purely empirical, some with their own fundamental approach and behaviour assumptions. With several different types of rheological behaviour, it can be difficult to choose the right predictive model in order to ensure accurate predictions for specific non-Newtonian fluid. As most of the non-Newtonian slurries are best characterised by the Herschel-Bulkley rheological model (Govier and Aziz, 1972; Hanks, 1979), three frequently used predictive models appropriate for this kind of non-Newtonian fluid were presented in this section and their performance was discussed.

2.5.4. Flows of complex slurries

Literature review showed, that data on flow of complex slurries in pipes is very scarce. Laminar flow of complex slurries might be accurately modelled through a use of appropriate layered model, yet only a few non-Newtonian carrier based layered models are available in literature. One of these was selected to be

presented in this study. For turbulent flow of complex slurries, literature review showed that multi-component predictive model might be a reliable approach. Semi-empirical 3-component predictive model was presented in this section. Multi-component approach to predictive modelling of frictional losses in turbulent flows of complex slurries is approached in later sections of this work.

2.5.5. Deposition limit velocity in non-Newtonian fluids

Literature review showed, that there is no reliable method available and literature background in this area is very scarce. Subsequent part of this work is dedicated to address this issue and recommends a reliable method.

3. LABORATORY EXPERIMENTS

Series of experiments were conducted at the Water Engineering Laboratory of the Czech Technical University in Prague. Experimental conditions of these tests were set with the following objectives in mind:

(i) To do test work with yield-pseudoplastic carrier fluid covering various rheological properties

(ii) To do test work using different particle fractions (i.e. with particles sizes, that overlap more than one flow pattern)

(iii) To test over a wide range of flow velocities covering both laminar and turbulent flow regimes

(iv) To measure rheology of the carrier fluid accurately

(v) To accumulate a data base for calibration and validation of the model calculations described in sections 2.4.4.1 and 2.4.4.2

3.1 Experimental apparatus

A pipe loop (Fig. 3.1) was used to study the slurry flow behaviour. The loop was composed of pieces of a PE pipe (I.D. 51.4 mm, blank pipe in Fig. 3.1) and a piece of transparent acrylic pipe (I.D. 50.0 mm, grey pipe in Fig. 3.1). The total length of the loop was 22.96 m and its volume was 45.08 l. The length of the horizontal section was 6.20 m. The pump EBARA 3M 40-200/7,5 kW was driven by an electric motor with a variable frequency converter TECO GD100-011G-4 11 kW. Pump parameters were: power 7,5 kW, impeller diameter 200 mm, maximum flow 11.67 l/s, total head from 58 m to 44 m (valid for water for maximum flow).

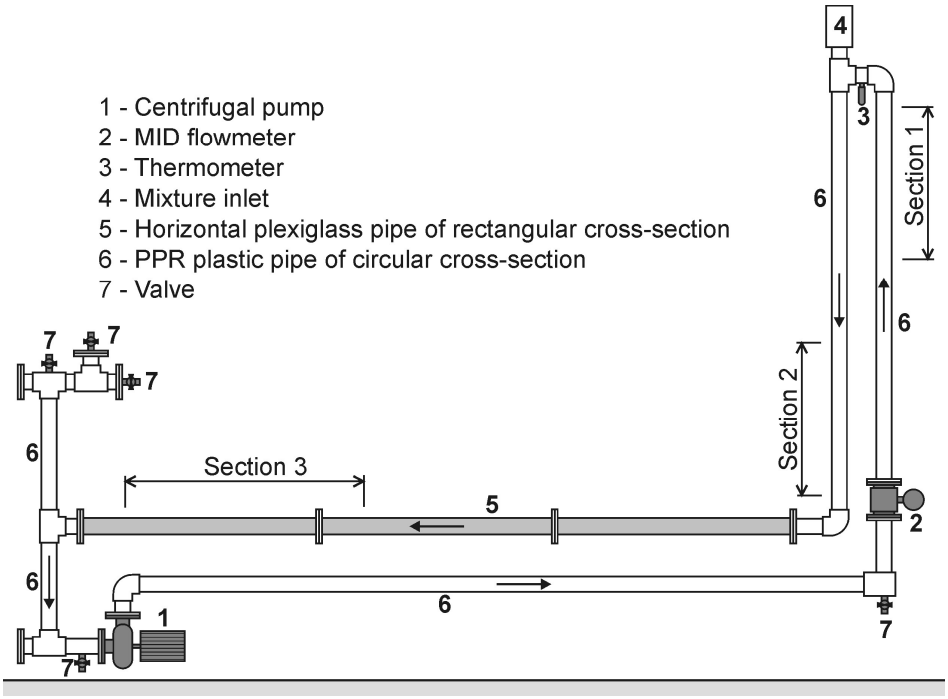

Figure 3. 1 - Test pipe loop in Water Engineering Laboratory

Differential pressures were measured over vertical Sections 1, 2 (1.3 m long) and the horizontal Section 3 (1 m long) using the differential pressure transducers Fischer Rosemount DP1151 (Sections 1 and 2) and the transducer Siemens Sitrans P DSIII (Section 3). An electromagnetic flow meter Krohne Optiflux 5000 was used to measure the flow rate in the vertical pipe mounted to the discharge outlet of the centrifugal pump. The temperature of the flowing medium was measured in the vertical invert pipe.

To monitor the distribution of solids in the horizontal flow, the pipe loop was equipped with a ERT (Electrical Resistance Tomography) setup. The setup contained 3 rings located at 3 different locations along the transparent acrylic horizontal pipe, each containing 16 electrodes. In past such equipment was used to measure a distribution of solid concentration in the pipe and its effect on particle diffusivity (Pěník et al., 2015).

3.2 Characterization of materials

Transport characteristics of flows of complex slurries were studied using a laboratory analogue in the form of different fractions of glass beads in a Carbopol carrier.

The finest particle fraction B134 (X_e - component) consisted of particles of sizes from 0.1 to 0.2 mm with the median size d_{50} = 0.18 mm and density ρ_e = 2452 kg/m3. The B7 (X_h - component) fraction was narrow graded (grain sizes from 400 to 750 microns) with d_{50} = 0.64 mm density ρ_h = 2423 kg/m3. The coarse fraction TK1.5 (X_s - component) was virtually monodisperse with d_{50} = 1.55 mm, the sieving test showed that all grains were finer than 1.61 mm and coarser than 1.49 mm with a density ρ_s = 2448 kg/m3. Carbopol (Ultrez 10 polymer) is an acidic powder, which after solution in water and neutralization process forms a transparent non-Newtonian fluid of yield-pseudoplastic type.

The rheology of fluids was determined in a rotational viscometer HAAKE VT 550.

3.3 Methodology and procedure

In a closed loop, a series of test runs were carried out with a slurry composing of a constant volume of solids introduced to the loop. The solids volume C_v was determined as the ratio of the known volume of particles introduced to the loop and the total volume of the loop. The test runs at different flow velocities included measurements of temperature, differential pressure in horizontal section and ERT images (set-up and post processing method described in Pěník et al., 2015; García Farrés 2018). Samples of carrier fluid were taken from the loop before and after each test series for rheological testing.

Differential pressure measurements were carried out using static pressure tappings located in the pipe walls of each test sections. Each tapping was fitted with an isolation pod, which collects any solids, that might enter the pressure tapping. Each isolation pod was connected to differential pressure transducer (DPT) by a tube with clear water. Linear regression was used as a calibration equation for processing of the transducer readings. The following procedure was adopted for calibrating the DPTs:

(i) Air and solids were flushed from all the lines
(ii) A differential head was set in a glass U-tube apparatus
(iii) This differential head was physically measured and the DPT output was logged at the same time

(iv) The calibration equation was obtained by linear approximation of at least two physically measured values of differential head

The following procedure was followed to run a test:

(i) Power was switched on, the carrier fluid and solid particles are loaded into the pipe loop.
(ii) The data logging programme was initialised
(iii) Air and solids were flushed from all pressure tapping tubes and DPTs
(iv) Calibration of the DPTs was checked and recalibrated, if needed
(v) The pump was set to a required speed and the data logging routine started. The magnetic flow meter and DPT outputs were logged for 60 to 90 seconds
(vi) Points (iii) – (v) were repeated at different pump speeds until maximum flow was reached and sufficient data has been collected

3.4 Test series overview

Five data sets are used in this study out of which three consist of new experimental data acquired by own laboratory experiments.

3.4.1. New experimental data

In the winter of 2019, series of experiments (referred to as Data set 2019) consisting of 26 test runs (22 test runs with particles, 4 test runs with clear Carbopol carrier fluid) were conducted in order to provide a comprehensive data base for analysis of the two-layer and three-component models described in sections 2.4.4.1 and 2.4.4.2 respectively. The test matrix of actual measured volumetric concentrations, fraction percentages and rheological parameters of the carrier fluid of the Data set 2019 are shown in Table 3.1.

Second test series conducted over the years 2017 and 2019 (referred to as Data set 2017/2019) was focused on laminar flow regime and occurrence of deposition limit velocity and consists of 8 test runs.

Third test series conducted over the years 2014 and 2015 (referred to as Data set 2014/2015) consists of 22 test runs and was used for the validation of the conclusions, that were based on analysis of Data sets 2019 and 2017/2019.

Detailed information about Data sets 2019 and 2017/2019 are presented in Appendix A along with the model predictions, Data set 2014/2015 is published elsewhere (Kesely, 2016)

Table 3.1 Test matrix showing actual measured fraction content, rheological parameters and volumetric concentration of solids of Data set 2019.

Test	1	2	3	4	5	6	7	8	9	10	11
X_e	0	0	0	1	1	1	0	0	0	0.6	0.5
X_h	1	1	1	0	0	0	0	0	0	0.4	0.5
X_s	0	0	0	0	0	0	1	1	1	0	0
τ_y [Pa]	2.04	1.88	1.87	1.7	0.8	0.2	0.5	0.2	0.1	1.6	0.6
K [Pa.s^n]	1.35	1.36	1.3	1.5	1	0.8	1.4	0.6	0.4	1.4	1.2
n	0.52	0.52	0.52	0.5	0.6	0.6	0.8	0.6	0.6	0.5	0.5
C_v	0.09	0.15	0.22	0.1	0.1	0.1	0.1	0.2	0.3	0.1	0.2
V_{sm} [m/s]							0.96	1.07	1.00		
Test	12	13	14	15	16	17	18	19	20	21	22
X_e	0.49	0	0	0	0.5	0.5	0.5	0.4	0.4	0.4	0.3
X_h	0.51	0.36	0.36	0.4	0	0	0	0.2	0.3	0.3	0.3
X_s	0	0.64	0.64	0.6	0.5	0.5	0.5	0.4	0.4	0.4	0.4
τ_y [Pa]s	0	1.07	1.01	0.2	1.1	0.8	0.3	5	3.1	2.4	1.2
K [Pa.s^n]	0.67	0.87	0.96	0.7	1.5	1.4	1.1	2.7	2.4	2.1	1.6
n	0.55	0.55	0.55	0.6	0.5	0.5	0.5	0.5	0.5	0.5	0.5
C_v	0.28	0.1	0.1	0.2	0.1	0.2	0.2	0.1	0.2	0.2	0.3
V_{sm} [m/s]		0.37	0.32	0.29	0.18	0.13	0.21	0.07	0.1	0.47	0.55

Fig. 3.2 shows the experimental results of Data set 2019 in a form of i_m-V_m diagram. The diagram clearly shows the graphical change in behaviour between laminar ant turbulent flow regimes. In a very rough approximation, the first point of turbulent flow regime can be from the i_m-V_m diagram determined as the first point of the curve, at which the friction loss gradient and mean flow velocity relation starts to rise rapidly.

The diagram also shows, that the influence of volumetric concentration of particles and rheological parameters of carrier fluid is much more significant in laminar flow regime, than in turbulent flow regime. These results very well agree with an assumption, that turbulence is dominated by inertial forces, therefore head loss in turbulent flow regime is less affected by the changes in viscosity of the fluid compared to laminar flow regime. Greater effect of volumetric concentration of solids on frictional loss gradient in laminar flow regime can also be explained by the structure of the laminar flow regime. Without hydrodynamic lift from turbulent eddies, the particles tend to flow as a sliding bed, therefore increasing the shear stress at wall and consequently, frictional loss gradient.

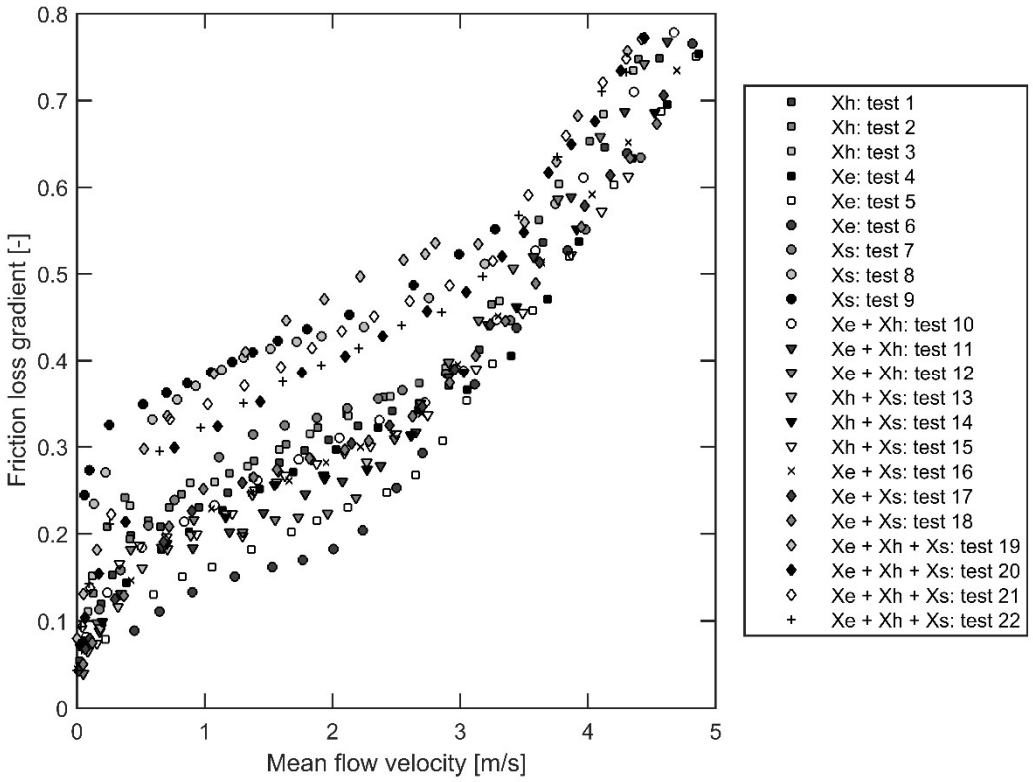

Figure 3. 2 – Flow curves - Data set 2019

3.4.2. CSIRO experimental database

CSIRO (Australia) graciously provided a part of their experimental database for the purpose of validation of this thesis results. Their experiments consist of a suspension comprising of sand particles in Carbopol (non-Newtonian) carrier

fluid. The database consists of 3 test runs with volumetric concentration, C_v, ranging from 10% to 30%. Characterisation of carrier fluid and solids is shown in Table 3.2, results of the sieving test for the sand particles is shown in Fig. 3.3.

Table 3.2 Test matrix showing material characteristics of Data set CSIRO

Pipe	Carrier fluid				Solids	
D [mm]	ρ_f [kg.m^{-3}]	τ_y[Pa]	K [Pa.s^n]	n	ρ_s[kg.m^{-3}]	d_{50}[mm]
44	1000	0.09	0.29	0.6	2650	0.16

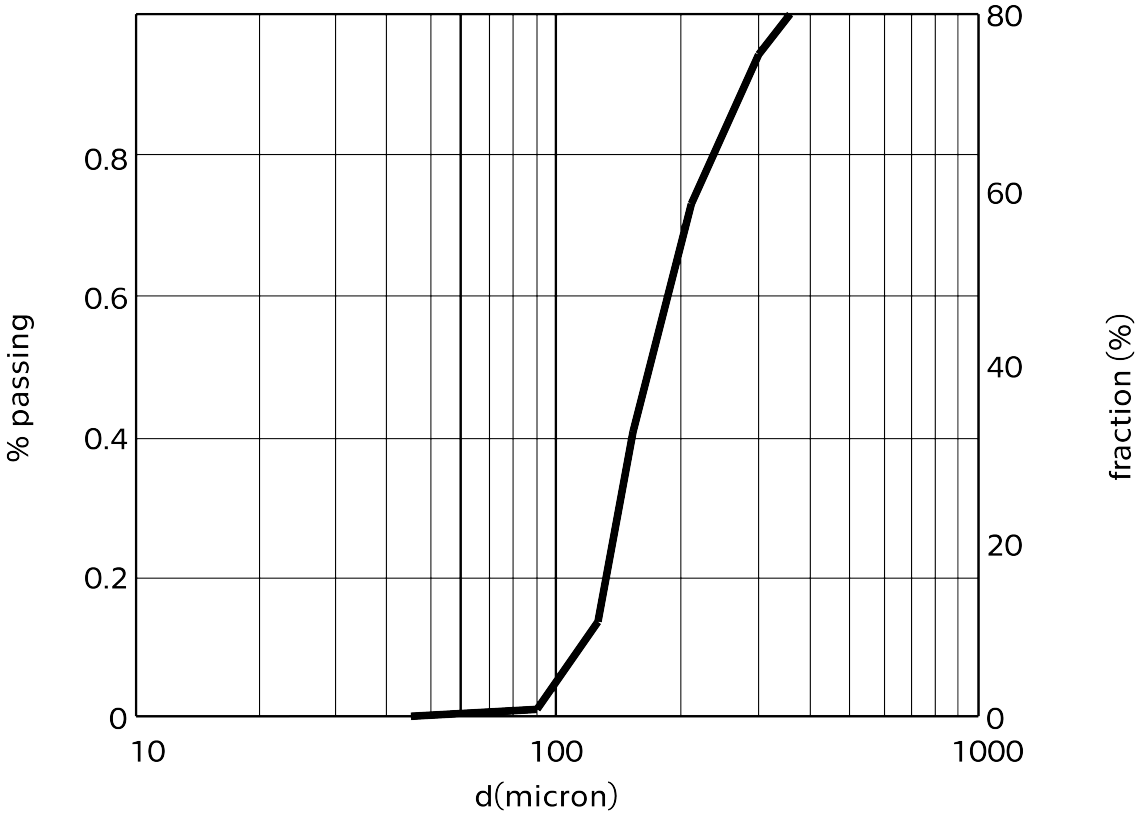

Figure 3. 3 – Grading curve - Data set CSIRO

Detailed information about Data set CSIRO is presented in Appendix A along with the model predictions.

3.4.3. GIW experimental database

GIW Industries, Inc. (USA) graciously provided their experimental data from the 2018 GIW Slurry Course for the purpose of validation of this thesis results. Their

experimental test series consist of suspensions of sand and gravel particles in kaolin (non-Newtonian) carrier fluid. The database consists of 3 test runs with 4.6% volumetric concentration of gravel and 15% volumetric concentration of sand. Characterisation of carrier fluid and solids is shown in Table 3.3, results of the sieving test for the GIW sand and gravel particles are shown in Tables 3.4 and 3.5, respectively.

Table 3.3 Test matrix showing material characteristics of Data set GIW

Pipe	Carrier fluid				Solids			
					GIW sand		GIW gravel	
D [mm]	$\rho_f[kg.m^{-3}]$	τ_y [Pa]	K [Pa.s^n]	n	$\rho_s[kg.m^{-3}]$	d_{50} [mm]	ρ_s [kg.m^{-3}]	$d_{50}[mm]$
78.87	1154	30	0.52	0.55	2633	0.6	2652	5.1

Table 3.4 Sieving test results of GIW sand – Data set GIW

Sieve Size	Mass Held	Total Mass Held	Total % Held	Total % Passed
(mm)	(g)	(g)	(%)	(%)
9.5	0.00	0.00	0.00	100.00
6.3	0.00	0.00	0.00	100.00
4.750	0.00	0.00	0.00	100.00
3.350	0.00	0.00	0.00	100.00
1.180	0.00	0.00	0.00	100.00
0.850	1.10	1.10	1.09	98.91
0.600	48.30	49.40	49.08	50.92
0.425	39.62	89.02	88.44	11.56
0.300	4.68	93.70	93.09	6.91
0.212	1.98	95.68	95.05	4.95
0.150	1.60	97.28	96.64	3.36
0.075	2.31	99.59	98.94	1.06
Pan	1.07	100.66	100.00	0.00

Table 3.5 Sieving test results of GIW gravel – Data set GIW

Sieve Size	Mass Held	Total Mass Held	Total % Held	Total % Passed
(mm)	(g)	(g)	(%)	(%)
9.5	5.78	5.78	2.19	97.81
6.3	68.48	74.26	28.11	71.89
4.750	72.32	146.58	55.49	44.51
3.350	76.02	222.60	84.27	15.73
1.180	38.12	260.72	98.70	1.30
0.850	1.27	261.99	99.18	0.82
0.600	0.57	262.56	99.39	0.61
0.425	0.40	262.96	99.55	0.45
0.300	0.29	263.25	99.66	0.34
0.212	0.21	263.46	99.74	0.26
0.150	0.12	263.58	99.78	0.22
0.075	0.20	263.78	99.86	0.14
Pan	0.38	264.16	100.00	0.00

Detailed information about Data set GIW is presented in Appendix A along with the model predictions.

3.5 Results and discussion

The experimental results are presented in Appendix A. Each pipe test is presented as a i_m-V_m diagram and a table giving a description of apparatus, material properties and a model performance of predictive model described in Chapter 5.

The experimental apparatus is described by inner diameter of pipeline D, roughness of pipe wall k_r and particle fractions present in the non-Newtonian mixture.

Slurry properties of data set 2019 are given by fraction content in non-Newtonian mixture X_e, X_h, X_s, yield stress τ_y, index of consistency K, flow behaviour index n, volumetric concentration of solids in the mixture C_v, measured laminar/turbulent transitional velocity $V_{ts,\ measuered}$, predicted laminar/turbulent transitional velocity $V_{ts,\ predicted}$ by method described in Chapter 5.2 and predicted value of deposition limit velocity for stratified fraction of particles by Matoušek et al. (2015) described in chapter 2.4.4.1.

The i_m-V_m diagram gives each data point graphically and in addition, the model of each component are plotted over the experimental data, providing a visual comparison of model predictions with experimental data. Model performance is also evaluated on the basis of the root-mean square error *RMSE*.

For Data set 2017/2019, slurry properties are defined by yield stress τ_y, index of consistency *K*, flow behaviour index *n*, coefficient of Coulombic sliding friction μ_c, ratio of bed layer height to that of inner diameter *y/D*, experimentally derived value of deposition limit velocity $V_{sm,,measured}$. Table also gives a theoretical prediction of deposition limit velocity $V_{sm,\ Xs,\ predicted}$ by Matoušek et al. (2015) layered model.

The i_m-V_m diagram gives graphical representation of data points in laminar flow regime.

4. ANALYSIS OF PULLUM ET AL. 2015 3-COMPONENT MODEL

The purpose of this chapter is to analyse the framework of Pullum et al. (2015) model presented in Chapter 2 in the light of experimental data obtained from the experiments described in Chapter 3. Based on this analysis, possible approaches to determination of model input parameters are discussed and modifications to model equations are presented. Since the total pressure drop is given by the sum of model components, the first step is the analysis of each component of the total head loss.

4.1 Analysis of components contribution to total pressure drop

To analyse the contribution of each component to the total pressure gradient, parameters equivalent to test runs 18 – 22 from Data set 2019 was used and scaling constants values were set to a constant of 1. Graphical representation of this analysis is displayed in Fig. 4.1. Examination of analysis results shows the diminishing contribution of particles to total pressure drop with rising mean velocity of the flow. This seems appropriate, as even the sliding bed formed by the coarse particles will be eroded at high velocities and the viscosity of the carrier fluid will be dominant flow resisting force. Fig. 4.1 also shows, that the contribution of each component contribution to the total pressure drop is a function of the solids volumetric concentration, rheological parameters, particle fractions combinations and mean velocity of the flow. Particles of X_h component exhibit lesser frictional losses then particles of X_s component, which is reasonable, as the particle-wall friction of the sliding bed is higher than particle/fluid friction in heterogeneous flow pattern. As the turbulent flow regime in non-Newtonian mixtures can be achieved rather high values of mean flow velocity, accurate determination of rheological parameters and calculation of the pressure drop from the carrier fluid alone is essential.

It has been proven in the literature however, that values of scaling constants need to be higher than 1 (Pullum et al., 2015; Kesely, 2016) for a proper prediction of the frictional losses induced by the particle fractions. Thus, resulting contributions from particles to total pressure drop will be higher and need to be taken into account.

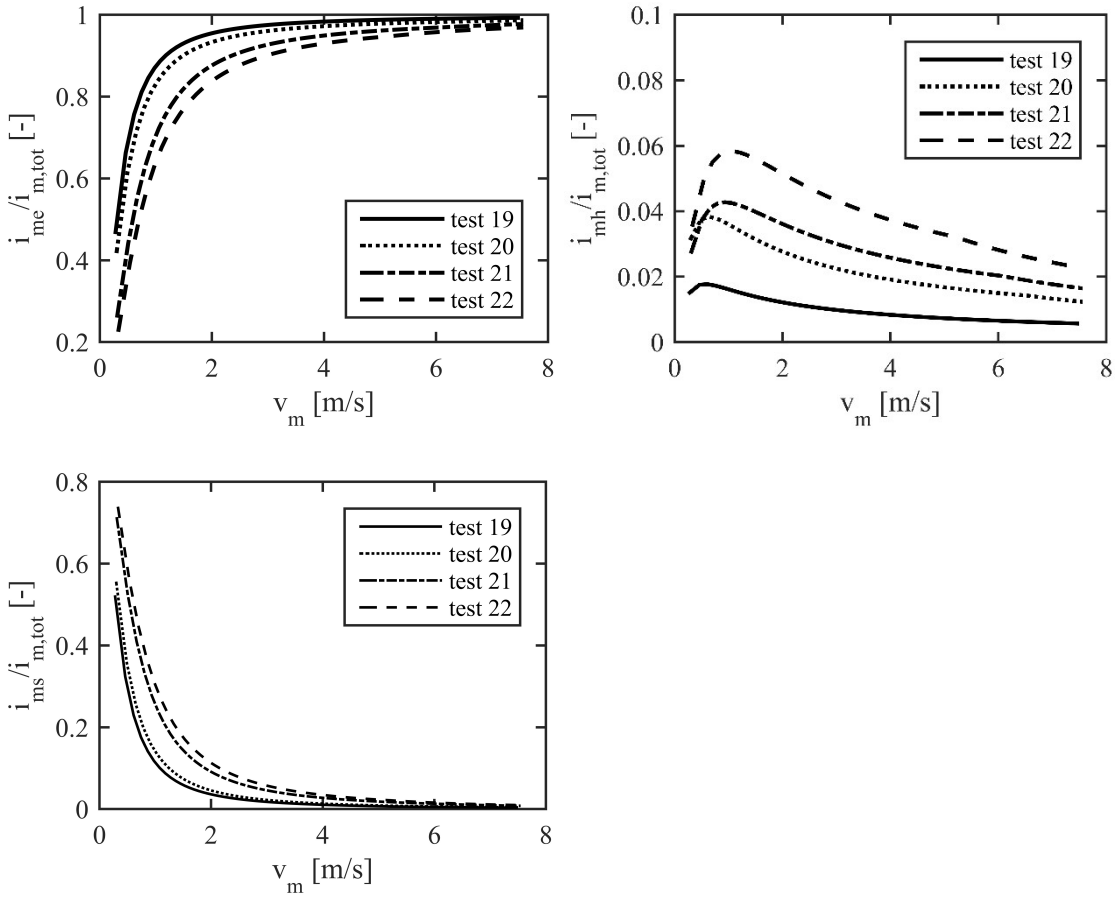

Figure 4. 1 - Graphical representation of X_e, X_h and X_s components contribution to the total pressure gradient

4.2 Sensitivity analysis of turbulent-flow models to rheological parameters

Analysis of the components contribution to total pressure drop in previous section 4.1 showed, that accurate calculation of carrier fluid pressure gradient is essential. As the models require rheological parameters, sensitivity of turbulent-flow models described in Chapter 2.4.1.3 to changes in rheology is investigated in order to get a sense of how accurate measurements of the fluids rheology is needed.

Base line values used for the analysis: ρ = 1000 kg/m^3; D = 50 mm; τ_y = 3.03 Pa; K = 1.56; n = 0.553; d_{85} = 100 μm; k_r = 0

The results of the sensitivity analysis can be seen in Figs. 4.2 – 4.10 and is summarized as an average deviation from the base line values after a percentile increase in value of each parameter in Table 4.1.

4.2.1 Sensitivity of the Torrance model

The sensitivity of the Torrance (1963) model to an increase in the rheological parameters is shown in Figs. 4.2 – 4.4.

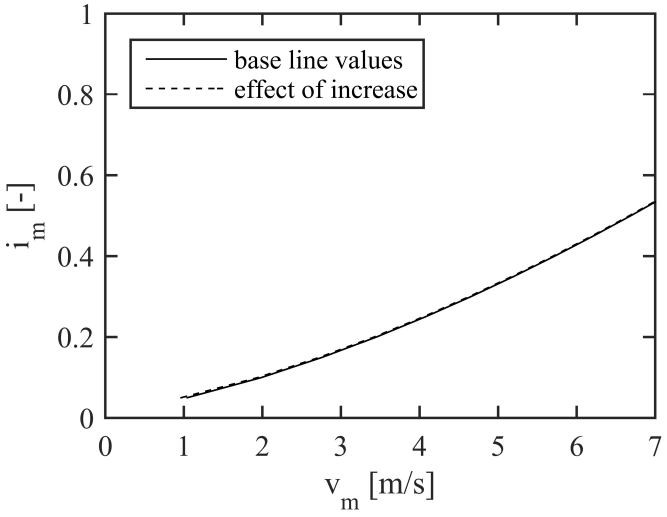

Figure 4. 2 - Sensitivity of the Torrance model to 40% increase in τ_y

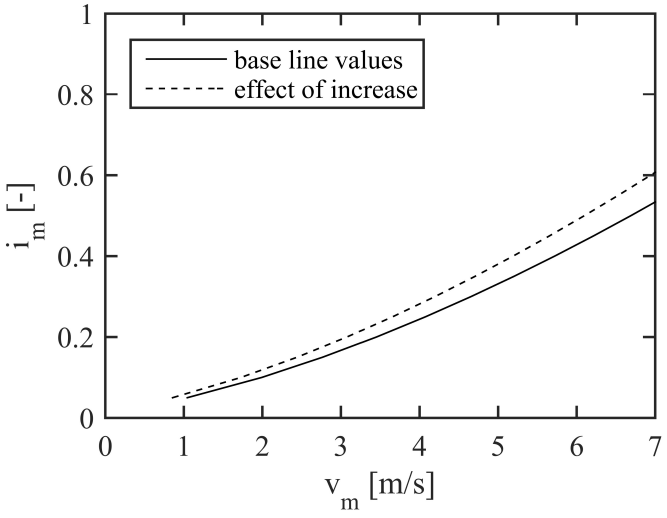

Figure 4. 3 - Sensitivity of the Torrance model to 40% increase in K

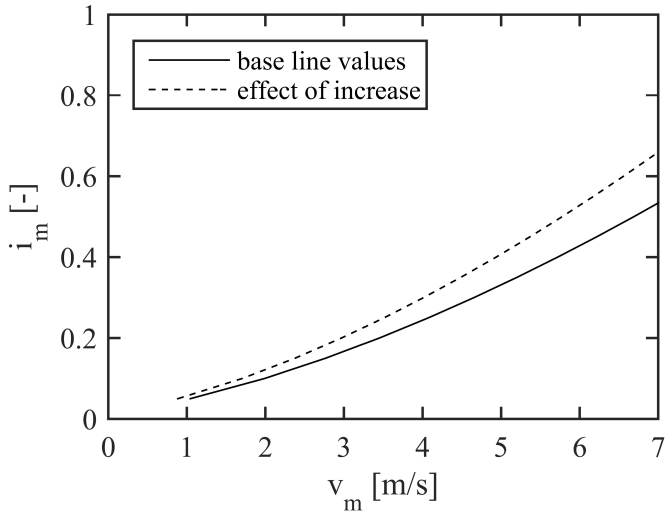

Figure 4. 4 - Sensitivity of the Torrance model to 10% increase in n

4.2.2 Sensitivity of the Wilson - Thomas model

The sensitivity of the Wilson-Thomas (1985) model to an increase in the rheological parameters is shown in Figs. 4.5 – 4.7.

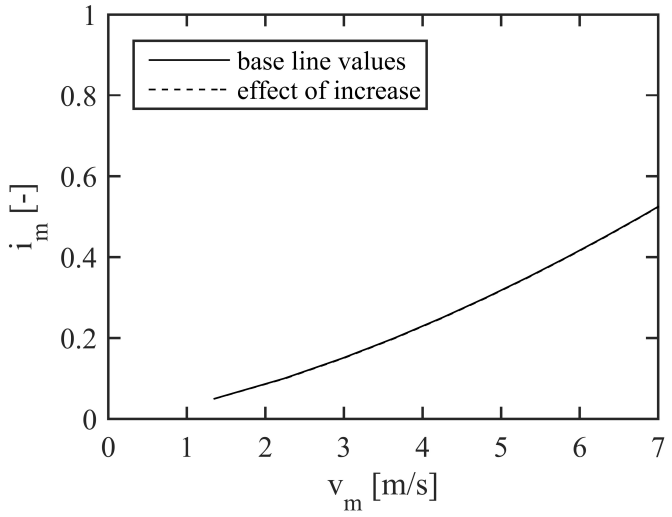

Figure 4. 5 - Sensitivity of the Wilson-Thomas model to 40% increase in τ_y

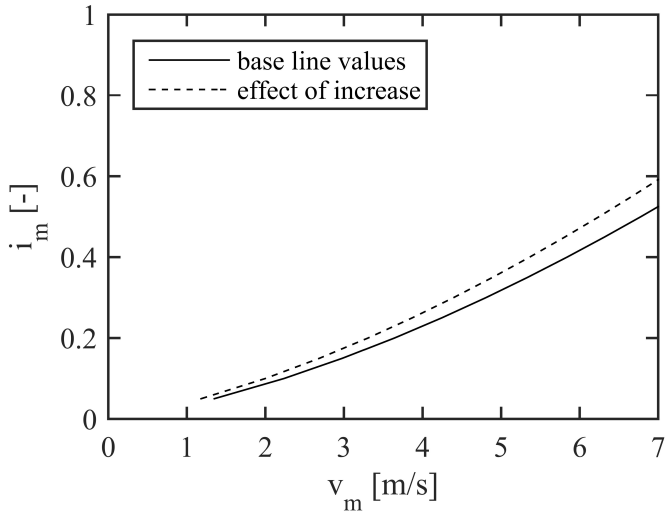

Figure 4. 6 - Sensitivity of the Wilson-Thomas model to 40% increase in K

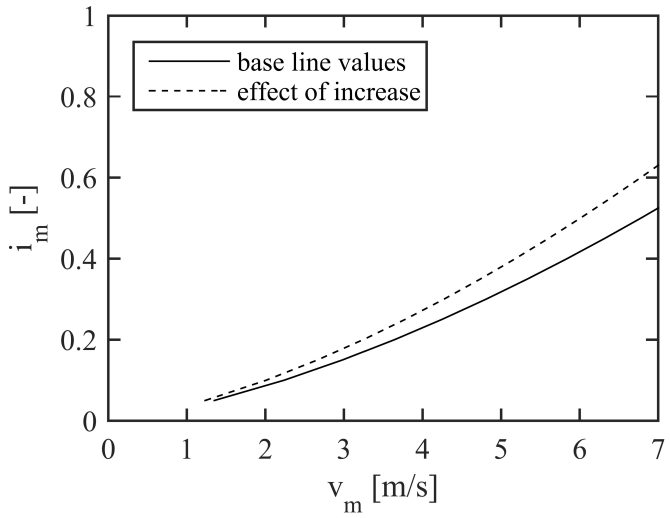

Figure 4. 7 - Sensitivity of the Wilson-Thomas model to 10% increase in n

4.2.3 Sensitivity of the Slatter model

The sensitivity of the Slatter (1999) model to an increase in the rheological parameters is shown in Figs. 4.8 – 4.10.

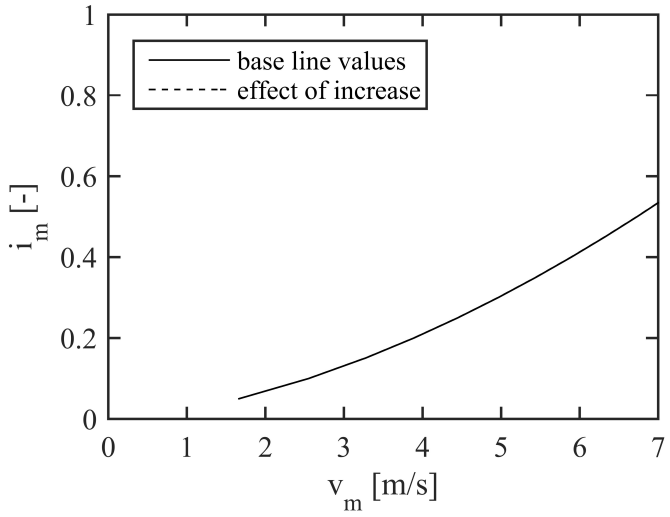

Figure 4. 8 - Sensitivity of the Slatter model to 40% increase in τ_y

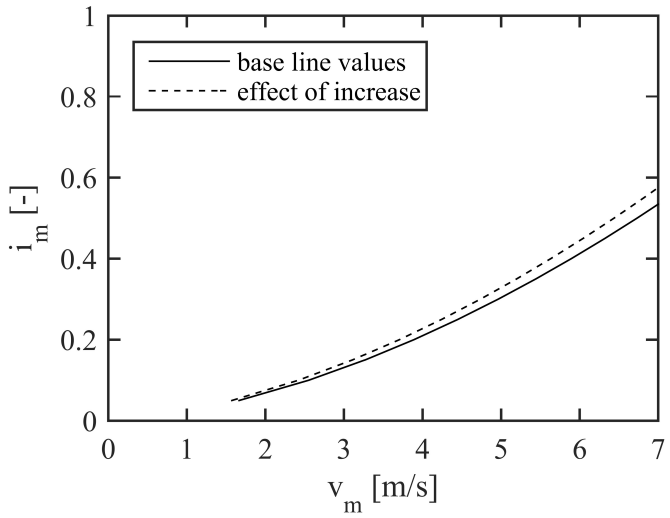

Figure 4. 9 - Sensitivity of the Slatter model to 40% increase in K

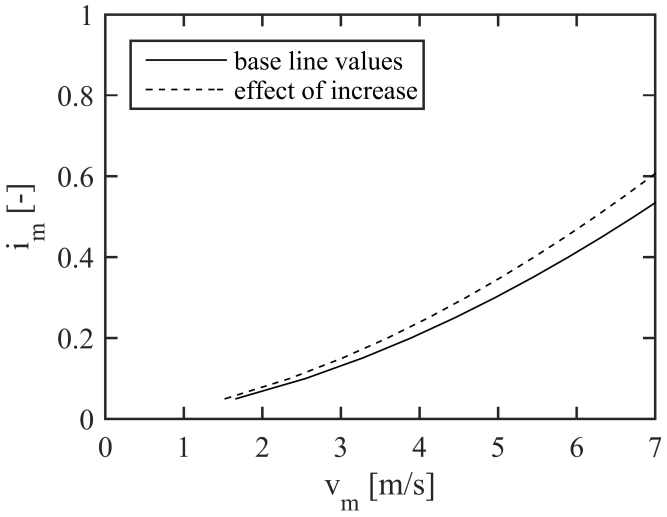

Figure 4. 10 - Sensitivity of the Slatter model to 10% increase in n

4.2.4 Discussion of the sensitivity of the turbulent-flow models

The models proved to be the most sensitive to a change in the value of parameter *n* and rather insensitive to the change in the value of yield stress τ_y. In the process of the rheological parameters determination, however, changes in the value of τ_y produce alterations in the values of parameters *K* and *n*, therefore all of the parameters are important and sensitivity of the models to the rheological parameters indicate the necessity of accurate measurements of the fluid rheology.

The models by Torrance (1963) and Wilson-Thomas (1985) show rather higher sensitivity to the rheological parameters than the model by Slatter (1999), but even though the dissipation of energy in turbulent flow is inertial in nature and as a result should not be directly affected by rheological properties (Wilson et al., 1992), the dependence on the rheological parameters can be reasonable, as chosen turbulent models rely on the laminar sub-layer existence in wall region of the pipeline.

Table 4.1 Matrix showing sensitivity of the models to rheological parameters.

Parameter	Increase in parameter [%]	Average dev. Torrance model [%]	Average dev. Wilson-Thomas model [%]	Average dev. Slatter model [%]
τ_y	40	0.57	0.12	0.02
K	40	8.92	7.78	3.3
n	10	13.68	11.29	6.3

4.3 Analysis of the scaling constant k_1

From Equation 2.47 it is evident, that the equivalent fluid component is a sum of the pressure gradients from the carrier fluid and from the contribution of very fine particles (if the modest particle fraction X_e is a part of the mixture). In Equation 2.44, however, equivalent fluid component is scaled by coefficient k_1, even if $X_e = 0$. As the pressure drop from the carrier fluid should be calculated using a suitable non-Newtonian turbulent model, it does not seem appropriate to further scale the predicted values of frictional losses and only the contribution to the pressure drop from the X_e-particles should be scaled. Therefore, when $X_e = 0$, the value of scaling coefficient k_1 should be equal to 1, and the following substitution of Equations 2.44 and 2.47 with Equations 4.1 and 4.2, respectively, should be used:

$$\left(\frac{dp}{dx}\right)_{tot} = \frac{dp}{dx_e} + k_2\frac{dp}{dx_h} + k_3\frac{dp}{dx_s} \tag{4.1}$$

$$\frac{dp}{dx_e} = \frac{dp}{dx_c} + k_1\frac{dp}{dx_c}\left[\left(1-0.25X_e\right)X_eC_v\left(S_s - S_c\right)\right] \tag{4.2}$$

4.4 Analysis of reference velocity V_{50}

By definition, the reference velocity, V_{50}, represents a value of the mean velocity V_m at which one half of the transported solid particles is suspended and the other half is in contact load, therefore it expresses the effect of particle suspension mechanisms, such as carrier turbulent diffusion and hydrodynamic lift. Equation 2.50 is considered to be valid for slurries with Newtonian carrier (it was calibrated for Newtonian slurries) and it should be noted, that the formula does not take the rheological parameters into account. The comparison of V_{50}

predictions with our experimental data of V_{ts} in Table 4.2 shows that a majority of calculated values of V_{50} by the original formula are still in the laminar flow regime and therefore fails its original purpose. In Table 4.2, values of V_{ts} were determined as the first points in the turbulent flow regime visually determined from the shape of the i-V_m curves (i.e. the point, at which the friction loss gradient starts to rise rapidly).

Table 4.2 Matrix comparing calculated values of V_{50} and experimental values of laminar/turbulent transition velocity V_{ts} *in m/s.*

Test	1	2	3	10	11	12	13	14	15	19	20	21	22
V_{ts}	2.91	2.91	2.88	3.03	2.38	2.19	2.27	2.62	2.75	3.5	3.05	3.25	3.17
V_{50}	2.71	2.71	2.71	2.62	2.58	2.5	2.71	2.71	2.71	2.66	2.63	2.59	2.56

Fig. 4.11 shows a picture of slurry flow with non-Newtonian carrier fluid and particle fraction TK15 at mean velocity of 1.61 m/s. Even though the flow is still laminar (laminar/turbulent transition for this run occurred at 2.1 m/s), the flow of particles is only partially stratified due to particle collisions with almost a non-existent sliding bed. This is confirmed by the ERT measurement of the concentration profile, which shows the highest concentration of solids about 0.32 (red line in Fig. 4.11). The value of maximum concentration should be around 0.55 for fully-stratified flow with the bed of round particles. While this flow structure can still be considered as contact load and therefore not contradicting the V_{50} definition, it raises a question of how to differentiate particles which are lifted due to carrier turbulent diffusion and hydrodynamic lift and those which are lifted due to the particle collisions.

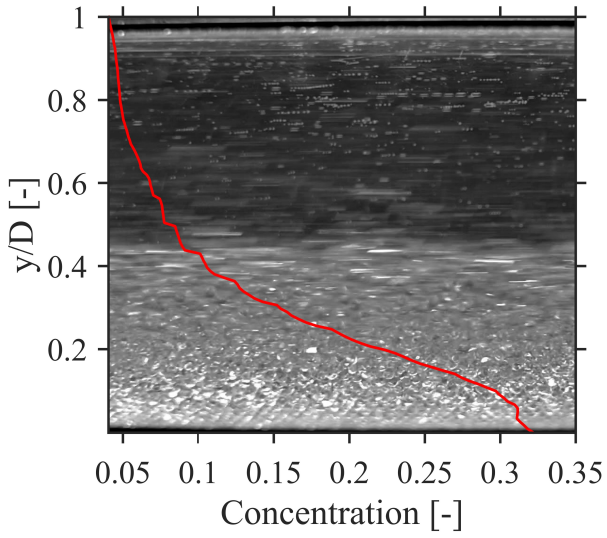

Figure 4. 11 - Laminar slurry flow with non-Newtonian carrier fluid at mean velocity = 1.61 m/s, Legend: red line = concentration profile obtained by ERT method (Pěník et al., 2015; García Farrés, 2018).

4.5 Conclusion

Framework of Pullum et al. (2015) component model was analysed in this chapter. Analysis of components contribution to total pressure drop showed, that accurate calculation of carrier fluid pressure gradient is essential, but contributions of individual particle fractions needs to be considered as well, as pressure drop induced by moving particles is not negligible.

Sensitivity analysis of turbulent-flow models for non-settling slurries show, that model predictions show rather high sensitivity to change in rheological parameters of the fluid, which indicates the necessity of accurate measurements of the fluid rheology.

The analysis of the reference velocity V_{50} shows, that recommended formula in Pullum et al. (2015) fails to accurately predict values of this reference velocity (Equation 2.53), as a majority of calculated values are still in the laminar flow regime. Moreover, the analysis of particle flow structure shows, that the bed layer becomes only partially stratified with rising values of mean velocity, while still in the laminar regime. This raises an inquiry of how to differentiate particles which are lifted due to carrier turbulent diffusion and hydrodynamic lift and

those which are lifted due to particle collisions, which is essential in order to predict the value of the reference velocity V_{50}.

5. NEW ANALYSIS

In this chapter, new approaches to the modelling of complex flow friction are presented. This work is believed to be new and to make a contribution to knowledge in the field.

New analysis is carried out with the following principle objectives:

(i) To develop a frictional head loss predictive model for flows of complex slurries, which does not rely on parameters that are not available to a process engineer in the basic engineering phase of a project

(ii) To analyse an effect of particles on the laminar/turbulent transition in non-Newtonian carrier fluid

(iii) To present a suitable approach to determination of deposition limit velocity for coarse particles in non-Newtonian carrier fluid

5.1 Modified approach to determine the pressure drop from the heterogeneous component

In the original formula (Equation 2.50) it is assumed, that the velocity V_{50} serves as a suitable reference velocity to evaluate turbulence-particle interactions. Due to the impracticality of V_{50} determination in non-Newtonian medium, it seems appropriate to propose an alternative reference velocity, which still holds the assumption mentioned above valid. By substituting the V_{50} in Equation 2.53 with the laminar/turbulent transition flow velocity, V_{ts}, the formula can be expressed as:

$$\frac{dp}{dx_h} = \rho_w g B X_h C_v \left(S_s - S_e\right)\left(\frac{V_{ts}}{V_m}\right)^M \tag{5.1}$$

For the exponent M, it is recommended to use the value of -1. In the original expression in Wilson et al. (1997), the exponent M is given by:

$$M = \left[\ln\left(\frac{d_{85}}{d_{50}}\right)\right]^{-1} \tag{5.2}$$

The value of M should not exceed 1.7 or fall below 0.25 (Wilson et al., 1997). As the Equation 5.2 (and related expression in Wilson et al., 1997) was calibrated for Newtonian slurries, it does not seem appropriate to use this expression for determination of the exponent value. $M = 1$ was calibrated so that the model predictions from the X_h - component fit the trend given by experimental data. Sensitivity analysis of the model predictions is shown in Fig. 5.1.

It should be noted, however, that the calibrated value of M = 1 is based on experimental data from laboratory analogue consisting of virtually monodisperse particles and without further data, its relevance to industrial slurries could not be validated.

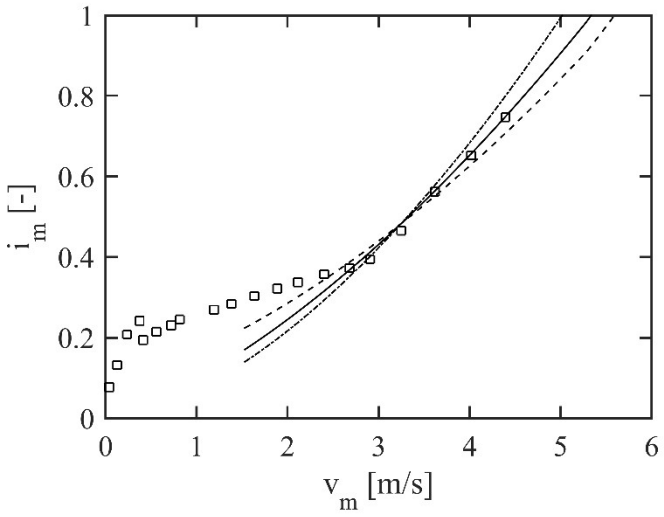

Figure 5. 1 - Sensitivity analysis of model X_h - component model predictions to value of exponent M, Legend: squares = experimental data (Test 2), dashed line: model predictions for M = 1.7, solid line: model predictions for M = 1, dotted line: model predictions for M = 0.25.

5.2 Laminar/Turbulent transition

Precise identification of the laminar/turbulent transition is one of the principle objectives in this chapter, as a V_{ts} value is needed in the newly proposed Equation 5.1 and it serves as a lower boundary for the applicability of 3-component model predictions.

Various approaches to laminar/turbulent transition described in the section 2.4.1.2 were analysed using the Data set 2019. The effects of particle fractions

on the resulting value of Reynolds number were studied. Figs. 5.2 and 5.3 along with Table 5.1 show calculated values of Reynolds number by several authors for the experimental V_{ts} values derived from the experimental i-V_m curve shape (as in Chapter 4.4). In Table 5.1, Re_{2k} and $V_{2k;Hanks}$ are based on Hanks (1963) stability criterion, and the values are calculated using Equations 2.18 and 2.21 respectively, presented in Chapter 2.4.1.2. Further laminar/turbulent transition data are presented in Appendix A along with the processed results.

Table 5.1 Reynolds number by several authors at the laminar/turbulent transition, V_{ts}, and results of Hanks (1963) stability criterion

Test run no.	Re_{SA} [-]	Re_{S} [-]	Re_{CS} [-]	Re_{MR} [-]	Re_{2k} [-]	$V_{2k;Hanks}$ [m/s]	V_{ts} [m/s]
23	1755	2174	1376	1613	2539	4.44	3.47
24	1763	2223	1177	1610	2527	4.42	3.48
25	1726	2139	1339	1571	2543	4.10	3.6
26	1757	2160	1388	1611	2533	4.32	3.37

Only test runs with clear non-Newtonian fluid (without particle fractions) are shown in Table 5.1. When approximated to the Newtonian fluids, where laminar/turbulent transition occurs roughly at Re = 2100, the correlation by Slatter (1994) is the most accurate, while Chilton and Stainsby (1998) Reynolds number gives the worst results, predicting the critical value of Re at about 1320. Hanks (1963) stability criterion shows only a slight scatter in the values of critical Reynolds number, Re_{2k}, but overpredicting the experimental value of V_{ts} by 24% in average. For used Carbopol fluids, all of the correlations show only a slight scatter from their specific critical value of Re, at which the laminar/turbulent transition occurs.

The graphical presentation in Figs. 5.2 and 5.3 shows the calculated values of Reynolds number plotted against the volumetric concentration of solids.

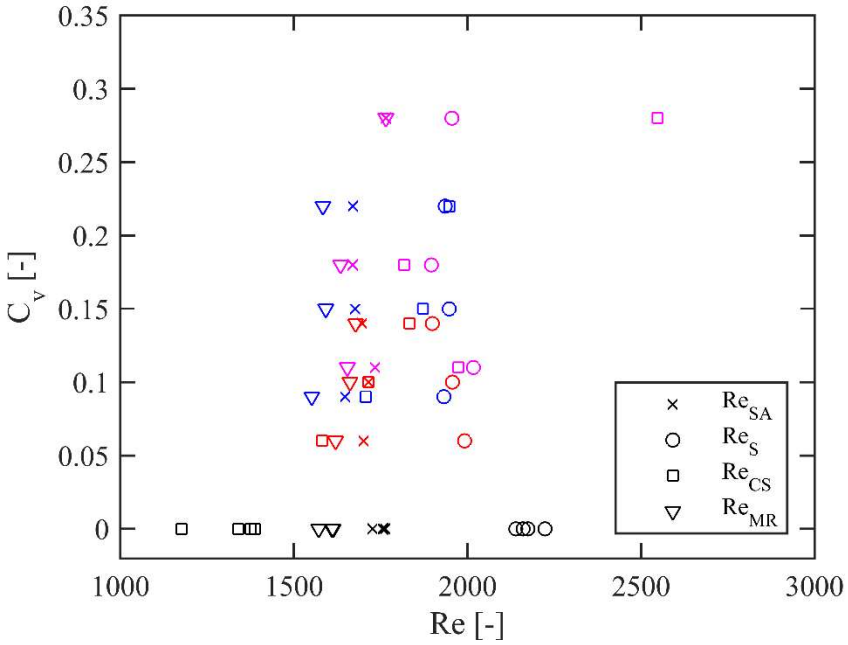

Figure 5. 2 - Critical Reynolds number vs volumetric concentration of solids. Legend: black markers – clear carrier fluid; red markers – X_e fraction; blue markers – X_h fraction; magenta markers – $X_e + X_h$ fractions – Data set 2019

The results of comparison presented in Fig 5.2 indicate almost negligible effect of C_v on the critical value of Re, when particles of X_e and X_h fraction are introduced to the non-Newtonian carrier fluid. Correlations by Metzner and Reed (1955) and Swamee and Aggarwal (2011) indicate practically no effect, while Slatter (1994) Reynolds number shows only a very mild decrease. Chilton and Stainsby (1998) method shows unreasonably high differences in the values of critical Reynolds number, ranging from 1176 to 2548.

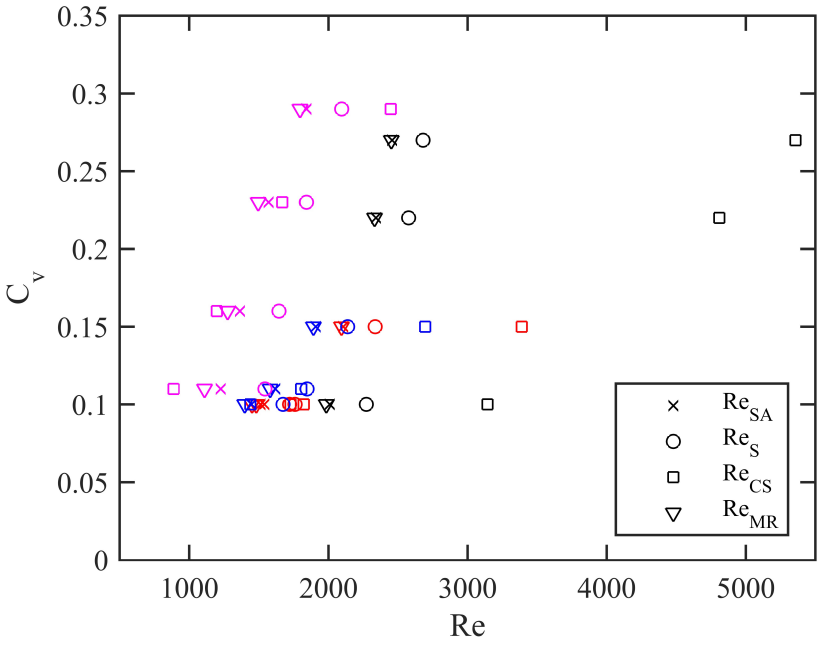

Figure 5. 3 - Critical Reynolds number vs volumetric concentration of solids. Legend: black markers X_s fraction; red markers – X_h + X_s fractions; blue markers – X_e + X_s fractions; magenta markers – X_e + X_h + X_s fractions – Data set 2019

Effect of particle concentration on the critical value of Reynolds number, can be clearly seen in Fig. 5.3, for the situation where the particles of X_s fraction are added in the mixture. While methods by Swamee and Aggarwal (2011), Metzner and Reed (1955) and Slatter (1994) show very similar trends and arguably the only difference is a somewhat constant offset of the critical values given by the specific models, the Chilton and Stainsby (1998) approach proves to be inadequate to predict the transition, as the critical values of Reynolds number range from 888 to 5357.

As Fig. 5.2 shows a negligible effect of X_e and X_h particles, it is assumed, that the increasing trend of critical *Re* values is connected with the volumetric concentration of the X_s fraction. The values of critical Reynolds number are plotted against the volumetric concentration of solids of the X_s fraction, $C_{v;Xs}$, in Fig. 5.4. In order to keep the results of this analysis generally applicable to several Reynolds number correlations, the value of critical Reynolds number is plotted as a ratio of actual value critical Reynolds number for a given mixture to the critical value of Reynolds number corresponding to the laminar/turbulent transition, denoted as *Re´* (for example, if for given slurry the actual value of

critical Reynolds number by Slatter (1994) is equal to 1700 and without interference of particles the laminar/turbulent transition is expected at Re_s = 2100, then the Re' = 1700/2100 = 0.8095).

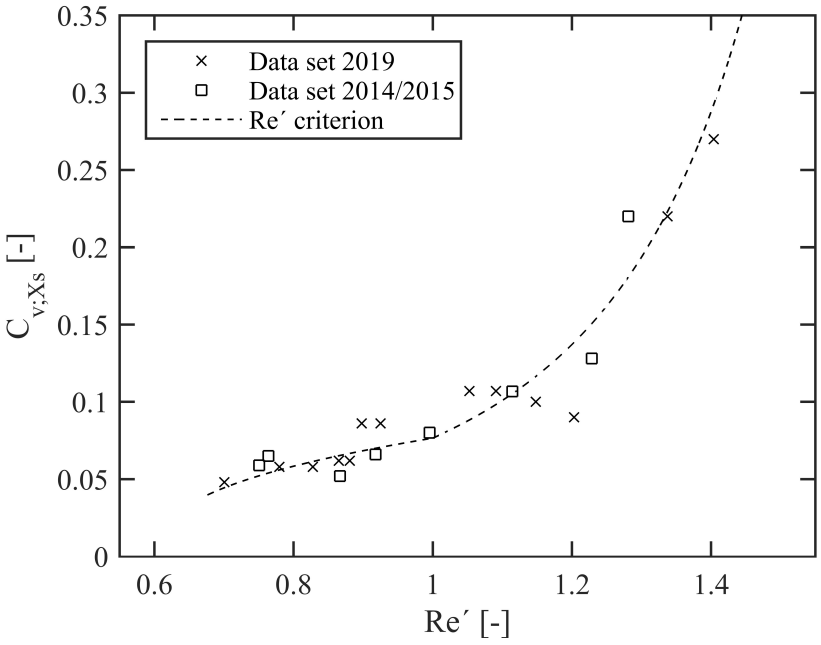

Figure 5. 4 - Critical Reynolds number vs X_s volumetric concentration of solids – Data sets 2019 and 2014/2015

The graphical presentation in Fig. 5.4 shows that low concentration of larger particles in the mixture results in earlier occurrence of laminar/turbulent transition, while volumetric concentrations of solids larger than 8% tends to stabilize the flow and therefore delays the laminar/turbulent transition. This effect is most likely connected to the existence of collisional layer of particles under laminar flow conditions described in section 4.4. For very small volumetric concentrations of coarse particles no compact sliding bed is formed in the flow as there are not enough particles in the cross section and the laminar flow is disturbed by the temporal cluster of colliding particles. In high volumetric concentrations of coarse grains, however, particles form a sliding bed, which actually stabilizes the flow and as a result, delays the occurrence of laminar/turbulent transition.

Based on the evidence in Fig 5.4, the effect of the particles of X_s fraction on the critical value of Reynolds number, which can be applied to several Reynolds number correlations, can be approximated:

$$Re' = 305.5 C_{v;Xs}^{2.587} + 0.6034 \qquad \text{when } Re' <= 1 \text{ a } C_{v;Xs} > 0.05 \tag{5.3}$$

and:

$$Re' = -0.405 C_{v;Xs}^{-0.367} + 2.0398 \qquad \text{when } Re' > 1 \tag{5.4}$$

Note, that experimental database used for this approximation ranged from $C_{v;Xs} = 0.06$ to $C_{v;Xs} = 0.29$. Presented approximation may be valid beyond those boundaries, but it is not validated by the experimental data.

5.3 Prediction of deposition limit velocity

As there is no recommended approach to V_{sm} determination by Pullum et al. (2015), a possibility of applying the Wilson-GIW method described in section 2.4.4.3 is tested (this approach is used in a four-component model for complex slurry flows with Newtonian carrier in e.g., Sellgren et al., 2016). The effect of the non-Newtonian behaviour can be implemented into calculations by using the equivalent viscosity, μ_{eq}, of the non-Newtonian fluid. The μ_{eq} can be calculated by relating the strain rate to V_m/D and the shear stress can be expressed directly from an appropriate rheological model (an approach previously used in Matoušek et al., 2015; Kesely and Matoušek, 2016, Kesely and Matoušek, 2017). For Herschel-Bulkley type fluid μ_{eq} can be then defined as:

$$\mu_{eq} = \frac{\tau_y + K\left(V_m / D\right)^n}{V_m / D} \tag{5.5}$$

Fig 5.5 shows a parity plot of the results. The prediction of V_{sm} calculated by the Wilson-GIW method using the equivalent viscosity proves to be very unsatisfactory, as the calculated values are considerably larger than the experimentally obtained values. The disagreement is not surprising, as the experimentally observed deposition limit velocity actually occurred in laminar flow regime and considerably below the critical laminar/turbulent transition velocity. Hence, the use of the Wilson-GIW method (originally for turbulent

Newtonian flows) to calculate V_{sm} proves to be inappropriate for the non-Newtonian flow conditions.

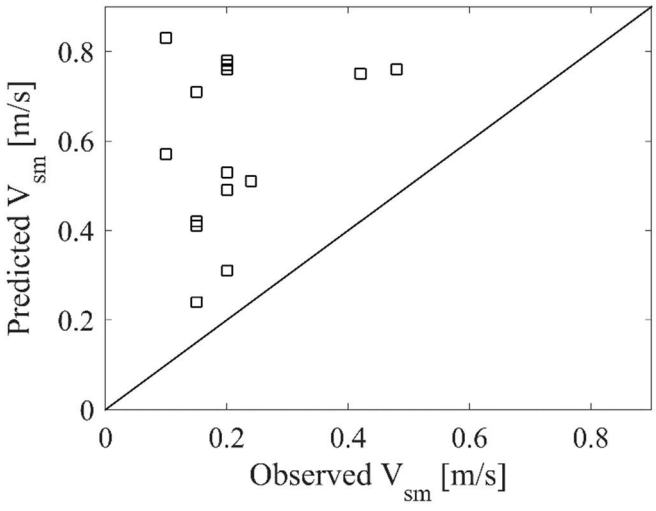

Figure 5. 5 – Parity plot comparing measured and predicted values of deposition limit velocity (Wilson-GIW method) – Data sets 2014/2015

As the semi-empirical Wilson-GIW formula gives unsatisfactory results, alternatively a capability of the two layer model approach by Matoušek et al. (2015) described in section 2.4.4.1 to predict the value of deposition limit velocity is analysed. For measured inputs (rheological parameters and density of the carrier fluid, solids diameter, density and delivered concentration of solids) together with some additional parameters (thickness of the bed, concentration of particles in bed and Coulombic friction coefficient) this layered model approach calculates a value of hydraulic gradient, delivered concentration and velocity of the stratified bed. Only a capability of the two-layer model to predict the value of deposition limit velocity is analysed, as a thorough analysis of model predictive abilities and sensitivity to input parameters is published elsewhere (Matoušek et al., 2015; Svoboda, 2018; Kesely et al., 2018).

In this study, the pressure gradient of carrier fluid was calculated using Swamee and Aggarwal (2011) method, the concentration in bed was estimated as 0.54 and Coulombic friction factor was set to a constant value of 0.33. Table 5.2 and Fig. 5.6 show a comparison between the measured and predicted values of the deposition limit velocity.

Table 5.2 Comparison of measured and predicted values of V_{sm} in m/s.

Test run no.	Data set 2017/2019								Data set GIW
	1	2	3	4	5	6	7	8	2
$V_{sm;\ measured}$	0.34	0.13	0.10	0.28	0.14	0.17	0.2	0.15	1.11
$V_{sm;\ predicted}$	0.39	0.1	0.09	0.38	0.08	0.11	0.13	0.21	1.20

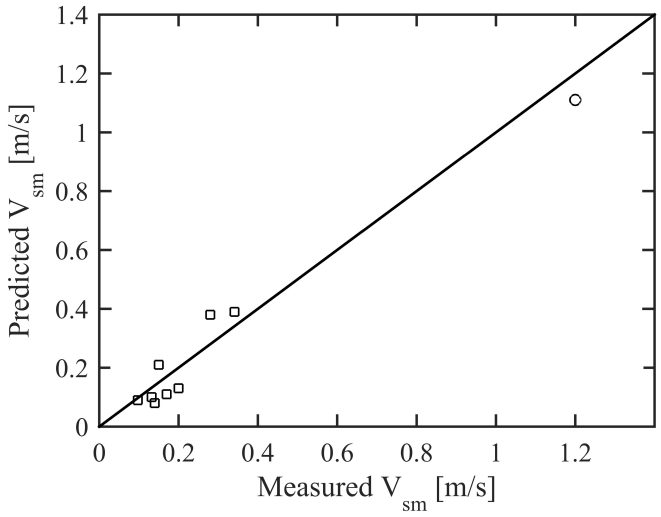

Figure 5. 6 – Parity plot comparing measured and predicted values of deposition limit velocity (Matoušek et al. 2015 method). Legend: black squares - Data set 2017/2019; black circles – Data set GIW

Reasonably accurate results can be seen in Fig. 5.6, when the predicted values of deposition limit velocity are compared with the experimental data. As a result, the layered model seems to be suitable to predict a value of deposition limit velocity although its predictions are very sensitive to input parameters (Svoboda, 2018; Kesely et al., 2018).

5.4 Experimental identification of scaling coefficients

In order to check the necessity to calibrate the scaling coefficients k_1, k_2, k_3, 3-component model predictions were subjected to a comparison with newly acquired experimental database from the Data set 2019. The frictional head loss from the turbulent flow of the carrier was calculated by the Slatter method (Slatter, 1999), as this method provides fairly accurate predictions for tested

Carbopol solutions (Kesely, 2016). Swamee and Aggarwal (2011) method was used to calculate the value of V_{ts}, with the critical value of Reynolds number set to 1750 and further approximated as in section 5.2. Matoušek et al. (2015) layered model was used to calculate the values of V_{sm} for the X_s component of the model (see Table 5.3).

Table 5.3 Matrix of predicted V_{sm} values

Test	7	8	9	13	14	15	16	17	18	19	20	21	22
V_{sm} [m/s]	0.89	1.45	1.73	0.29	0.25	0.20	0.14	0.55	1.00	0.10	0.10	0.40	0.50

A parity plot comparing the predicted pressure gradients with those observed, when scaling coefficients were set to $k_1 = k_2 = k_3 = 1$ are shown in Fig. 5.7.

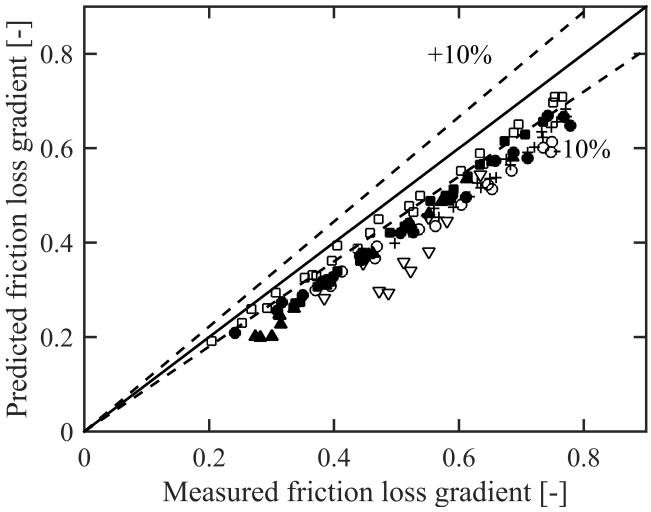

Figure 5. 7 – Parity plot comparing measured and predicted friction loss gradients – Data set 2019

Fig. 5.7. shows, that model predictions work fairly well with the alternative approach to V_{50} (equation 5.1) as the scatter of resulting data is relatively narrow. Model calculations however underpredict the experimental data, which indicates the necessity of the scaling coefficients calibration.

To calibrate the scaling coefficients, model predictions were fitted to the experimental data. Then, relations between these scaling coefficient values and salient parameters (such as volumetric concentration of solids, viscosity of

the carrier fluid, deposition limit velocity etc.) were studied. The study showed, that while the k_1 coefficient is best scaled by a constant value, the value of the coefficient k_2 seems to be a function of the volumetric concentration of solid (see Fig. 5.8) and the coefficient k_3 seems to be affected by the laminar/turbulent transition flow velocity V_{ts} (see Fig. 5.9). Expressing of the scaling coefficients k_2 and k_3 as functions improves the model predictions accuracy and is recommended over using an averaged constant value of the scaling coefficients k_2 and k_3, despite the fact, that using a constant value would be less complicated.

Based on the experimental investigation the values of the three scaling coefficients are best expressed as:

$$k_1 = 1.8 \tag{5.6}$$

$$k_2 = a \cdot \exp^{b \cdot Cv} \tag{5.7}$$

$$k_3 = x \cdot \exp^{y \cdot V_{ts}} \tag{5.8}$$

where $a = 9.124$, $b = -5.405$, $x = 2.940$, $y = 0.118$.

To determine the expression of the Equations 5.7 and 5.8, only the Data set 2019 was used, in Figs. 5.8 and 5.9, Data set 2104/2015 is shown only to confirm the given trend.

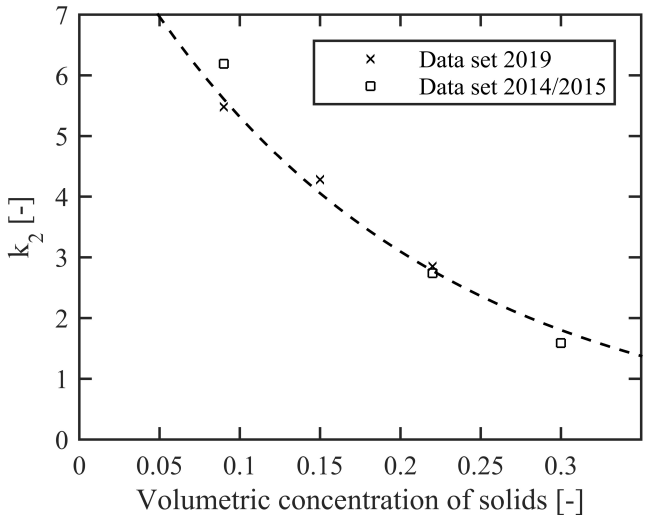

Figure 5. 8 – Effect of volumetric concentration of solids on the value of scaling coefficient k_2 *(Equation 5.7)*

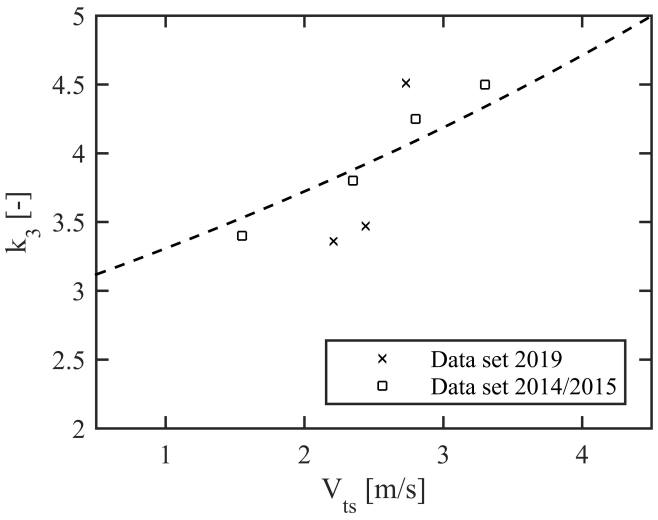

Figure 5. 9 – Effect of V_{ts} on the value of scaling coefficient k_3 *(Equation 5.8)*

5.5 Comparison of modified 3-component model predictions with experimental data

5.5.1. Results of model calibration

Figs. 5.10 – 5.12 show measured hydraulic gradient plotted against predicted hydraulic gradient for different fractions of particles (i.e. different components of the model) and their possible combinations. Comparison show very reasonable agreement with all data points within the 10% interval.

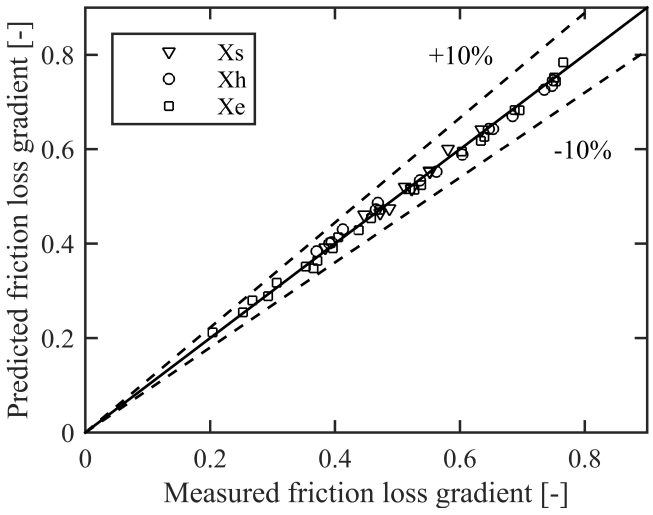

Figure 5. 10 – Parity plot comparing observed and predicted friction loss gradients when only one particle fraction was present in the slurry mixture – Data base 2019

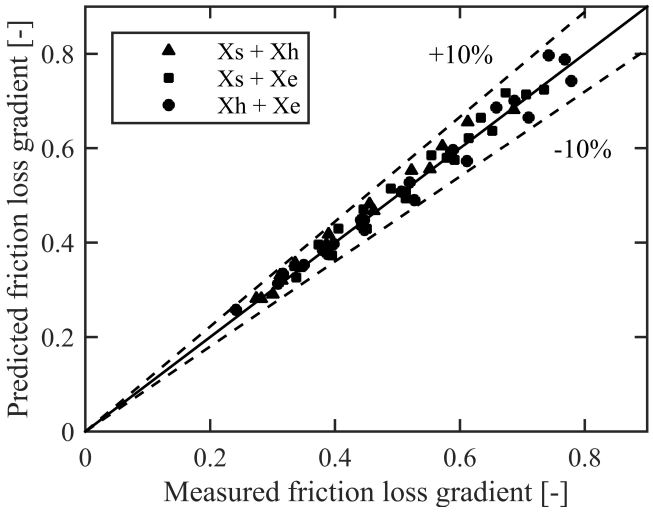

Figure 5. 11 – Parity plot comparing observed and predicted friction loss gradients when combinations of two particle fractions were present in the slurry mixture – Data base 2019

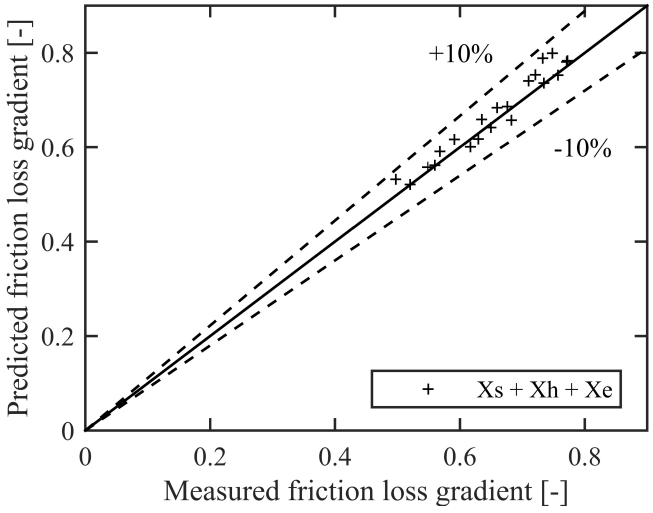

Figure 5. 12 – Parity plot comparing observed and predicted friction loss gradients when all three particle fractions were present in the slurry mixture – Data base 2019

5.5.2. Results of model validation

In order to validate the calibrated model, experimental results from Data bases 2014/2015, CSIRO and GIW were subjected to the comparison with model predictions. None of the data was used for the calibration of the model coefficients. Results of the comparison are shown in Figs. 5.13 – 5.17 for different combinations of fractions (components).

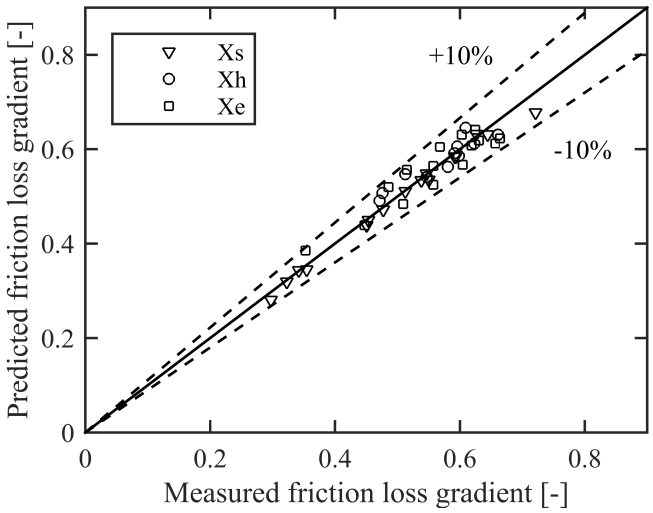

Figure 5. 13 – Parity plot comparing observed and predicted friction loss gradients when only one particle fraction was present in the slurry mixture – Data base 2014/2015

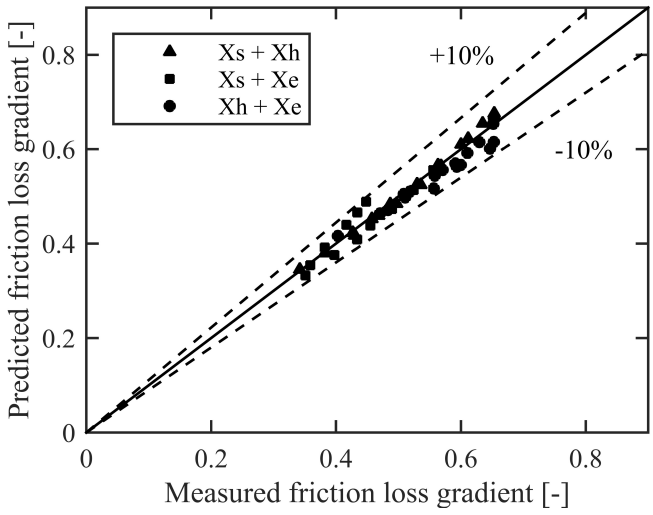

Figure 5. 14 – Parity plot comparing observed and predicted friction loss gradients when combinations of two particle fractions were present in the slurry mixture – Data base 2014/2015

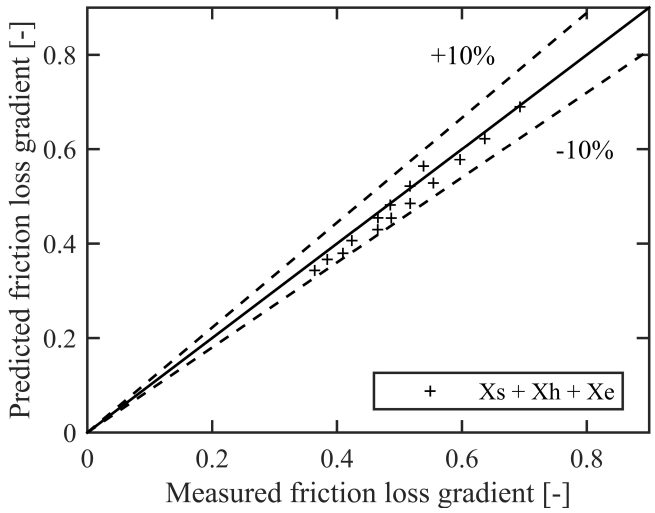

Figure 5. 15 – Parity plot comparing observed and predicted friction loss gradients when all three particle fractions were present in the slurry mixture – Data base 2014/2015

The comparison shows again a very reasonable agreement with all data points well within the 10% confidence interval and only a marginal deviation from the results with the new data set from 2019.

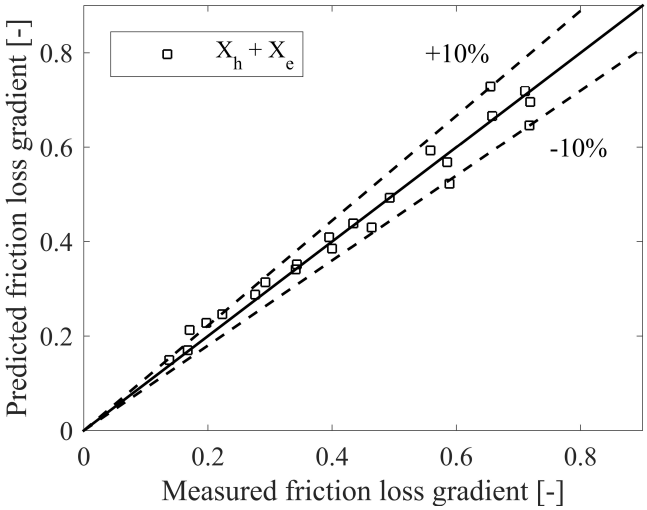

Figure 5. 16 – Parity plot comparing observed and predicted friction loss gradients when combination of X_h and X_e particle fractions were present in the slurry mixture – Data base CSIRO

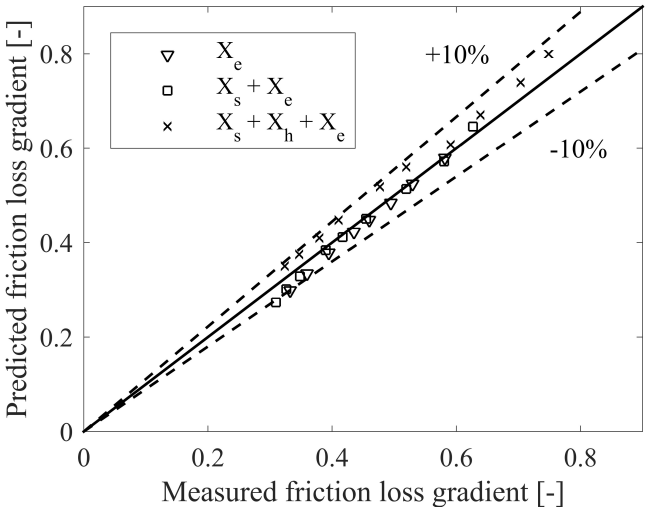

Figure 5. 17 – Parity plot comparing observed and predicted friction loss gradients for various combinations particle fractions were present in the slurry mixture – Data base GIW

5.6 Concluding comments

The study shows that predictive modelling of flow of complex slurries is far from being simple and straightforward and many variables need to be considered. Research subjects of non-Newtonian fluids and fluid/particle interactions are still not fully understood at this time. Therefore, the presented predictive approaches remain primarily empirical.

Without an exact theoretical analysis, it is important to provide robust predictive models, which accurately predict experimental data and therefore provide a reliable basis that meet the needs of engineering practice. The assumptions and correlations presented in this chapter will hopefully encourage a further research debate leading to better understanding of various aspects of complex flows.

6. SUMMARY, CONCLUSIONS AND RECOMMENDATIONS

The accurate predictions of frictional head loss in turbulent flows of complex slurries and determination of important design parameters (such as deposition limit velocity or laminar/turbulent transitional velocity) still remain a research field, that is not fully understood. This thesis describes a long-lasting research project, which has culminated in the presented modification of a 3-component model and it is believed to be fairly accurate, robust and reliable.

This component model approach assumes similarity between Newtonian and non-Newtonian turbulent flows. As a basis it uses well established, semi empirical formulae validated for a wide range of Newtonian systems in pipeline sizes ranging from laboratory to industrial scales.

6.1 Summary

Even though hydraulic transport has been considered a progressive technology in recent years, a present level of knowledge of complex slurry flows still does not fully satisfy needs of the engineering practice. This work seeks to provide a reliable complex-slurry turbulent-flow model, that reliably predicts frictional head loss, as well as it seeks to recommend the means as how to determine important design parameters, such as deposition limit velocity and laminar/turbulent transition.

The literature contains several approaches to a determination of laminar/turbulent transition. In this thesis, correlations of Reynolds number by Metzner and Reed (1955), Slatter (1994), Chilton and Stainsby (1998), Swamee and Aggarwal (2011), as well as stability criterion model by Hanks (1963) were investigated. The non-Newtonian turbulent flow models of Torrance (1963), Wilson and Thomas (1985) and Slatter (1999) were reviewed. The three-component predictive model for turbulent flows of complex slurries by Pullum et al. (2015) was analysed. Occurrence of deposition limit velocity and laminar/turbulent transition was studied, as the turbulent-flow predictive

modelling highlighted the problem of accurately predicting these design parameters.

Experimental pipe loop at Water Engineering Laboratory of the Czech Technical University in Prague was used to study complex slurry flow behaviour. Experimental data base containing three data sets was acquired. Reliable test techniques were developed in this facility and test data cover wide ranges of rheological properties of yield-pseudoplastic carrier fluid, particle fractions (3 fractions with d_{50} from 0.18 mm to 1.55 mm), volumetric concentrations (from 6% to 29%) and wide range of mean flow velocities covering both laminar and turbulent flow regimes (from 0 to 5 m/s). CSIRO (Australia) and GIW Industries, Inc. (USA) graciously provided parts of their experimental database for purposes of a validation of this thesis results.

Sensitivity analysis of the turbulent flow models to changes in rheological parameters proved that models are the most sensitive to a change in the value of flow index n and rather insensitive to the change in the value of yield stress τ_y. Note however, that in the procedure of the rheological characterization, changes in the value of τ_y produce alterations in the values of parameters K and n, therefore all three parameters are important. Turbulent flow models by Torrance (1963) and Wilson-Thomas (1985) show rather higher sensitivity to the rheological parameters than the model by Slatter (1999).

Analysis of the reference velocity V_{50} shows, that the original formula in Pullum et al. (2015) fails to accurately predict value of this reference velocity (Equation 2.53) in non-Newtonian fluids, as a majority of calculated values are still in the laminar flow regime. Moreover, an analysis of particle flow structure proves that particles in the bed layer become only partially stratified with rising mean flow velocity, while still in the laminar regime. This raises an inquiry of how to differentiate particles which are lifted due to carrier turbulent diffusion and hydrodynamic lift and those which are lifted due to particle collisions, which is essential in order to predict the value of reference velocity V_{50}.

The new analysis introduces five main parts. Modified formula for predicting the pressure drop from the heterogeneous fraction of solids is presented. In this

formula, laminar/turbulent transition velocity is used as a reference velocity instead of V_{50}. Effect of solid particles on laminar/turbulent transition is investigated using own experimental data. Deposition limit velocity for stratified fraction is modelled using the modified Wilson-GIW model (Wilson et al., 1992) and using a layered model (Matoušek et al., 2015). Predicted values of deposition limit velocity are compared to own experimental data as well as to CSIRO and GIW experimental data base. Scaling coefficients for component model are identified by analysis of own experimental data. The modified three-component model is compared to own, CSIRO and GIW experimental data, that were not previously used for calibration of the model equations.

The modified approach to determine the pressure drop from the heterogeneous component recommends substituting the velocity V_{50} with laminar/turbulent transitional velocity, V_{ts}. In the original formula, V_{50} serves as a reference to turbulence at specific velocity value. Using the laminar/turbulent transitional velocity leads to more accurate results, while holding the assumption mentioned above still valid.

Analysis of experimental data shows almost negligible effect of smaller particle fractions (X_e and X_h) on the critical value of Reynolds number. Effect of coarser particles (X_s) on laminar/turbulent transition is, however, evident. Low concentration of coarse particles in the mixture results in earlier occurrence of laminar/turbulent transition, while volumetric concentrations of solids larger than 8% tend to stabilize the flow and therefore delays the laminar/turbulent transition. Based on the experimental evidence, an approximation of the critical Reynolds number is presented.

Use of Wilson-GIW method (Wilson et al., 1992) for determination of deposition limit velocity proves to be inadequate, as the approach gives unsatisfactory results. This is not surprising, as the method is originally developed for turbulent Newtonian flows and observed deposition limit velocities in non-Newtonian fluid occurred in the laminar flow regime. Use of layered model (method by Matoušek et al., 2015) produced reasonably accurate results and seems to be

suitable for predicting the value of deposition limit velocity of coarse particles in non-Newtonian carrier fluid.

Experimental investigation showed some interesting relations between salient parameters and values of scaling coefficients. While the k_1 coefficient is best scaled by a constant value, the value of the coefficient k_2 is a function of the volumetric concentration of solids and the coefficient k_3 is affected by the laminar/turbulent transition flow velocity V_{ts}. Formulae for the scaling coefficients are presented.

Predictions of the modified 3-component model were validated by comparison with experimental data base, out of which none of the data was earlier used for the calibration of the model coefficients. Despite its somewhat open interpretation of flow characteristic behaviour (for example the assumption that the contribution from each fraction of particles to the total head loss may be combined independently, or that each fraction is fixed in specific flow pattern), the comparison of model predictions to experimental data show very reasonable agreement with all data points well within the 10% confidence interval. The proposed three-component model is computationally simple and represents an improvement to the previous version. Modified 3-component model calculations remain explicit, which gives the component model approach an advantage over more complex solutions like layered models, where the computational process is often implicit and can sometimes result in problems with convergence in computational process. Comparison of model predictions to experimental data confirms that it is suitable to use the model for predicting the frictional pressure loss in flows of complex slurries in pipelines.

6.2 Conclusions

A new analysis of complex slurry flows was developed and a procedure was recommended to predict frictional losses in turbulent flows of complex slurries in this thesis. The procedure is summarized in Appendix C.

The contribution of this thesis to knowledge in the field of complex slurries can be divided into four sections – evaluation of laminar/turbulent transition,

evaluation of deposition limit velocity, prediction of turbulent flow friction loss and exploration of experimental data.

6.2.1. Laminar/turbulent transition

(i) Correlations by Slatter (1994) predict the transitional velocity roughly at values of Re = 2150, correlations by Swamee and Aggarwal (2011) and Metzner and Reed (1955) predict somewhat lower values. Hanks (1963) stability criterion overpredicts the transitional velocity roughly by 24% and correlation by Chilton and Stainsby (1998) proves to be inadequate to predict the laminar/turbulent transition.

(ii) While laminar/turbulent transition does not seem to be affected by the fine and heterogeneous particles of X_e and X_h fractions, coarse particles of X_s fraction show strong influence.

(iii) Approximation of the effect of coarse particles on the critical Reynolds number value is presented based on the experimental evidence.

6.2.2. Deposition limit velocity

Use of the layered model (Matoušek et al., 2015) to predict the value of deposition limit velocity of coarse particles in non-Newtonian fluids of Herschel-Bulkley type proves to yield reasonably accurate results.

6.2.3. Turbulent flow predictive modelling

A computationally simple and robust 3-component model for predicting the frictional head loss is presented. The model does not rely on parameters that are not available to a process engineer in the basic engineering phase of the project, making it suitable to use in a design procedure.

6.2.4. Experimental work

Unique and extensive experimental data base covering wide ranges of slurry properties and flow conditions was established for the analysis and evaluation of presented results.

6.3 Future research recommendations

Results of this thesis are supported by data base acquired from measurements on experimental apparatus with relatively small inner diameters of pipes (DN44, DN50 and DN79). A larger data base obtained in larger pipes should be acquired to validate presented results in the future.

Conclusions of this thesis are based on a data base with particles of similar shape (round, well graded glass beads). The effect of particles of different shapes on laminar/turbulent transition and value of frictional head loss should be investigated.

Presented model predictions were tested on carrier fluid of Herschel-Bulkley type only. Possible effect on values of the scaling constants, when different type of carrier fluid is used, should be done.

Particles used during the experiments were virtually monodisperse and of the same material. Experimental data base should be extended with data covering wider size distribution and different materials. Comparison of model predictions to experimental data base provided by CSIRO and GIW Industries, Inc. show promising agreement (within 10% of confidence agreement), yet more extensive data base is needed in order to draw more general conclusions.

REFERENCES

Barnes, H. A., 1999: The yield stress – a review. J. non-Newtonian fluid mechanics, 81, pp. 133-178.

Bird, R. B, 1976: Useful non-Newtonian models. Annual review of fluid mechanics, pp. 13-34.

Bird, R. B., Dai, G. C., Yarusso, B. J., 1983: The rheology of viscoplastic materials. Reviews in Chemical Engineering, 1, pp. 1-70.

Bird, R. B., Armstrong, R. C., Hassager, O., 1987: Dynamics of polymeric liquids. 2nd edition, Fluid Dynamics, Vol.1, Wiley, New York.

Bowen, R., 1961: Designing turbulent flow systems. J. Chem. Eng, 68(15), pp. 143-150.

Carreau, P. J., Dekee, D., Chhabra, R. P. 1997: Rheology of polymeric systems: Principles and applications. Hanser, Munich, p. 520.

Chhabra, R. P., Richardson, J. F., 1999: Non-Newtonian flow in the process industries, Butterworth-Heinemann, Oxford, p. 436.

Chilton, R. A., Stainsby, R., 1998: Pressure loss equations for laminar and turbulent non-Newtonian pipe flow. Journal of Hydraulic Engineering, 124(5), pp. 522-529.

Clift, R., Wilson, K. C., Addie, G. R., 1982: A mechanistically-based method for scaling pipeline tests for settling slurries. In: Proc. Hydrotransport 8, Johannesburg, South Africa, pp. 91-101.

Cooke, R., 2002: Laminar flow settling: The potential for unexpected problems. In: Proc. 15th Int. Conf. on Slurry Handling and Pipeline Transport, pp. 121-133.

Dodge, D. W., Metzner, A. B., 1959: Turbulent flow of non-Newtonian systems. AIChE J., 5(2), pp. 189-204.

Durand, R., 1953: Basic relationships of the transportation of solids in pipes – experimental research. In: Proc. Minessota International Hydraulic Convention, pp. 89-103.

Durand, R., Condolios, E., 1952: Étude expérimentale du refoulement des matériaux en conduit. In: 2émes Journées de l´ Hydralique, pp. 29-55.

El-Nahhas, K., El-Hak, N. G., Rayan, M. A., El-Sawaf, I., 2005: Flow behaviour of non-Newtonian clay slurries. In: Proc. 16th Conference on the Hydraulic Transport of Solids, Santiago, pp. 47-59.

García Farrés, G., 2018: Development of a tool for a 2-phase flow electrical resistance tomography image reconstruction and analysis. MSc Thesis, Universitat Politècnica de Catalunya, p. 50.

Govier, G. W., Aziz, K., 1972: The flow of complex mixtures in pipes. E. Krieger Publishing Co., Malabar, Florida.

Haldenwang, R., Sutherland, A., Fester, V., Holm, R., Chhabra, R., 2012: Sludge pipeflow pressure drop prediction using composite power law friction factor-Reynolds number correlations based on different non-Newtonian Reynolds number. Water SA, 38(4), pp. 615-622.

Hanks, R. W., 1963: The laminar/turbulent transition for fluids with a yield stress, AIChE J., 9(3), pp. 306-309.

Hanks, R. W., 1979: The axial laminar flow of yield-pseudoplastic fluid in a concentric annulus. Ind. Eng. Chem. Process. Des. Dev, 18(3), pp. 488-493.

Hanks, R. W., Ricks, B. L., 1975: Transitional and turbulent pipeflow of pseudoplastic fluids. J. Hydronautics, 9(1), pp. 39-44.

Heever, E., Sutherland, A., Haldenwang, R., 2014: Influence of the rheological model used in pipe-flow prediction techniques for homogeneous non-Newtonian fluids. J Hydraul Eng, 140(12).

Kemblowski, Z., Kolodziejski, J., 1973: Flow resistances of non-Newtonian fluids in transitional and turbulent flow. J. Int. CHem. Eng, 13, pp. 265-279.

Kesely, M., 2016: Evaluation of settling velocity of coarse particles in visco-plastic fluid and frictional loss in complex slurry flow. MSc Thesis, CTU in Prague, 51 p.

Kesely, M., Matoušek V., 2016: Laminar settling of glass beads in visco-plastic liquids. Civil Engineering Journal, 25(1), pp. 1-9.

Kesely, M., Matoušek, V., 2017: Laboratory testing of pipe flows of bimodal complex slurries. In: Proc. T&S18, Prague, Czech Republic, pp. 161-168.

Kesely, M., Matoušek, V., Svoboda, L., 2018: Modelling of coarse-grained bed sliding in pipe flow of viscoplastic carrying liquid. In: Proc. 9th CHoPS, London, UK, 6 p.

Lazarus, J. H., Slatter, P. T., 1998: A method for the rheological characterisation of tube viscometer data. Journal of pipelines, 7, pp. 165-176.

Macosco, C. W., 1994: Rheology: Principles, Measurements and Applications. Wiley-VCH, New York, p. 568.

Matoušek, V., 2004: Dredge pumps and slurry transport. Lecture notes, Delft University of Technology.

Matoušek M., Krupička J., Picek T., 2013: Validation of transport and friction formula for upper plane bed by experiments in rectangular pipes. J. Hydrol. Hydromech., 61(2), pp. 120-125.

Matoušek, M., Krupička, J., Pěník, V., 2014: Distribution of medium-to-coarse glass beads in slurry pipe flow: evaluation of measured concentration profiles. Particul. Sci. Technol., 32(2), pp. 186-196.

Matoušek, V., Pěník, V., Pullum, L., Chryss, A., 2015: Experimental study of bed friction in stratified flow with viscoplastic carrier in pipe. In: Proc. T&S16, Delft, Netherlands, pp. 175-184.

Matoušek, V., Kesely, M., Visintainer, R., Furlan, J., Sellgren, A., 2018: Pipe friction of bimodal settling slurry flow, Proc. 9thCHoPS, London, UK, p. 6.

Metzger, T., 1998: A little course in rheology part 1. Physica, Messtechnik GmbH, Stuttgart, Germany, pp. 49-53.

Metzner, A. B., Reed, J. C., 1955: Flow of non-Newtonian fluids – correlation of laminar, transition and turbulent flow regions. AIChE, 1(4), pp. 434-440.

Miedema, S., Ramsdell, R., 2015: The limit deposit velocity model, new approach. J. Hydrol. Hydromech., 63, 4, pp. 273-286.

Pěník, V., Kesely, M., Matoušek, V., 2015: Coarse particle support in turbulent flow of visco-plastic carrier. In: Proc. EFM 2015, Prague, Czech Republic, pp. 588-592.

Poloski, A. P., Bonebrake, M. L., Casella, A. M., Johnson, M. D., MacFarlan, P. J., Toth, J. J., 2009: Deposition velocities of non-Newtonian slurries in pipelines: Complex simulant testing. Report PNNL-18316, Pacific Northwest National Laboratory, Richland, WA, USA, p. 162.

Pullum, L., 2007: Non-settling slurries part II – turbulent flows & scale up. Lecture slides, 30th Anniversary GIW Slurry Course, GIW Industries, Inc.

Pullum, L., Graham, L., 2000: The use of MRI to probe complex hybrid suspension flows. In. Proc. T&S10, Wroclav, Poland, pp. 421-433.

Pullum, L., Graham, L., Slatter, P., 2004: A non-Newtonian two layer model and its application to high density hydrotransport. In. Proc. Hydrotransport 16, Santiago, Chile, pp. 579-594.

Pullum, L., Chryss, A., Graham, L., Matoušek, V., Pěník, V., 2015: Modelling turbulent transport of solids in non-Newtonian carrier fluids applicable to tailing disposals. In: Proc. T&S16, Delft, Netherlands, pp. 229-239.

Ryan, N. W., Johnson, M. M., 1959: Transition from laminar to turbulent flow in pipes, AIChE, 5, pp. 433-435.

Rojas, M. R., Saez, A. E., 2012: Two-layer model for horizontal pipe flow of Newtonian and non-Newtonian settling dense slurries. Ind. Eng. Chem. Res, 51, pp. 7095-7103.

Sellgren, A., Wilson, K. C., 2007: Validation of a four-component pipeline friction-loss model. In: Proc. Hydrotransport 17, Cape Town, South Africa, pp. 193-204.

Sellgren, A., Visintainer, R., Furlan, J., Matoušek, V., 2016: Pump and pipeline performance when pumping slurries with different particle gradings. CJChE, 94(6), pp. 1025-1031.

Slatter, P. T., 1994: Transitional and turbulent flow of non-Newtonian slurries. PhD thesis, University of Cape Town, Cape Town, p. 314.

Slatter, P. T., 1997: The effect of the yield stress on the laminar/turbulent transition. In. Proc. T&S9, Cracow, pp. 547-561.

Slatter, P. T., 1999: The role of rheology in the pipelining of mineral slurries. Mineral Processing and Extractive Metallurgy, 20(1), pp. 281-300.

Slatter, P. T., Mollagee, M., Petersen, F. W., 1997: Non-Newtonian turbulence – a practical overview. In. Proc. T&S9, Cracow, pp. 83-95.

Spelay, R. B., Gillies, R. G., Hashemi, S. A., Sanders, R. S., 2016: Effect of pipe inclination on the deposition velocity of settling slurries. Can. J. Chem. Eng., 94, pp. 1032-1039.

Svoboda, L., 2018: Modelling of coarse slurry flow with non-Newtonian carrier in pipe using two-layer model. MSc thesis, Czech Technical University in Prague, Prague, p. 94.

Swamee, P. K., Aggarwal, N., 2011: Explicit equations for laminar flow of Herschel-Bulkley fluids. CJChE, 89(6), pp. 1426-1433.

Thomas, A. D., Wilson, K. C., 1987: New analysis of non-Newtonian turbulent flow- yield power law fluids. Can. J. Chem. Eng., 65, pp. 335-338.

Torrance, B., 1963: Friction factors for turbulent non-Newtonian fluid flow in circular pipes. The South African Mechanical Engineer, 13(4), pp. 89-92.

Visintainer, R., Furlan, J., McCall, G., Sellgren, A., Matoušek, V., 2017: Comprehensive loop testing of a broadly graded (4-component) slurry. In: Proc. Hydrotransport 20, Melbourne, Australia, pp. 307-323.

Vlasák, P., Chára, Z., 1999: Laminar and turbulent flow experiments with yield-power law slurries. Powder Technol., 104, pp. 200-206.

Vlasák, P., Chára, Z., Kysela, B., Sobota, J., 2011: Flow behaviour of coarse-grained slurries in pipes. In: Proc. 9th ISOPE, Maui, Hawaii, USA, pp. 158-164.

Wilson, K. C., 1976: A unified physically based analysis of solid-liquid pipeline flow. In: Proc. Hydrotransport 4, pp. 1-16.

Wilson, K. C., 1979: Deposition-limit nomograms for particles of various densities in pipeline flow. In: Proc. Hydrotransport 6, pp. 1-12.

Wilson, K. C., 1986: Effect of solids concentration on deposit velocity. Journal of Pipelines, 5, 4, pp. 251-257.

Wilson, K. C., 1992: Influence of particle properties on solids effect. In. Proc. 10th Int. Kol. Massenguttransport durch Rohrleitungen, Univ. GH Paderborn, Meschede, Germany, A.

Wilson, K. C., Thomas, A. D., 1985: A new analysis of the turbulent flow of non-Newtonian fluids. CJChe, 63(4), pp. 539-546.

Wilson, K. C., Clift, R., Addie, G.R., Maffett, J., 1990: Effect of broad particle grading on slurry stratification ratio and scale-up. Pow-tech. 61, pp. 165-172.

Wilson, K. C., Addie, G. R., Sellgren, A., Clift, R., 1997: Slurry transport using centrifugal pumps, 2nd edition, Blackie Academic & Professional, London, p. 432.

Wilson, K. C., Addie, G. R., Sellgren, A., Clift, R., 2006: Slurry transport using centrifugal pumps, 3rd edition, Springer, USA, p. 442.

Xu, J., Gillies, R., Small, M., Shook, C. A., 1993: Laminar and turbulent flow of kaolin slurries. In. Proc. Hydrotransport 12, BHR Group, p. 595.

NOMENCLATURE

a	constant	[-]
A	area	[m^2]
B	parameter	[-]
A_r	area ratio	[-]
b	constant	[-]
c_{ok}	critical ratio of tangential stresses	[-]
C_r	particle concentrations ratio	[-]
C_v	volumetric concentration	[-]
C_{vd}	delivered concentration	[-]
D	pipe inner diameter	[m]
d	particle diameter	[m]
dp/dx	pressure gradient	[$Pa \cdot m^{-1}$]
du/dy	strain rate	[s^{-1}]
F_N	total normal force	[N]
g	gravitational acceleration	[$m \cdot s^{-2}$]
He	Hedström number	[-]
H_{sh}	shear layer thickness	[m]
i_m	hydraulic gradient	[-]
K	coefficient of consistency	[$Pa.s^n$]
$K´$	apparent fluid consistency index	[-]
k	scaling coefficient	[-]
k_r	hydraulic roughness size	[m]
L	length	[m]
M	exponent	[-]
n	flow index	[-]

$n´$	apparent flow index	[-]
O	perimeter	[m]
ΔP	pressure difference	[Pa]
r	pipe radius	[m]
Re	Reynolds number	[-]
$Re´$	apparent Reynolds number	[-]
Re_p	particle Reynolds number	[-]
S	relative density	[-]
U	velocity	[m·s^{-1}]
u^+	dimensionless velocity	[-]
V	flow velocity	[m·s^{-1}]
V_{50}	reference velocity	[m·s^{-1}]
V_{sm}	deposition limit velocity	[m·s^{-1}]
V_{ts}	laminar/turbulent transition velocity	[m·s^{-1}]
V_*	shear velocity	[m·s^{-1}]
x	constant	[-]
X	mass fraction	[-]
y	constant	[m^{-1}·s]
Y	length	[m]

Greek letters

β	angle	[°]
ζ	yield to wall shield stress ratio	[-]
η_B	Bingham plastic viscosity	[Pa·s]
λ	Darcy-Weisbach friction factor	[-]
μ	dynamic viscosity	[Pa·s]
μ_c	Casson plastic viscosity	[Pa·s]
μ_s	coefficient of Coulombic sliding friction	[-]

ρ	density	[kg·m^{-3}]
τ	shear stress	[Pa]
$\bar{\tau}$	surficial shear stress	[Pa]
Ω	velocity function	[-]

Index

a	upper layer
ann	*annulus*
b	lower layer
c	carrier
CS	Chilton and Stainsby
e	equivalent carrier fluid
eq	equivalent
f	fluid
h	heterogeneous
i	interface
m	mean
max	maximum
MR	Metzner and Reed
N	Newtonian
p	pseudo-homogeneous
r	roughness
s	solids/stratified
S	Slatter
SA	Swamee and Aggarwal
shear	sheared

tot	total
w	wall
y	yield
50	50 percentile of the particle passing
85	85 percentile of the particle passing

Appendix A – Detailed pipeline test results

Data set 2019	
Test run no.	1
APPARATUS	
D [m]	0.05
material	B7
pipe roughness	0
SLURRY PROPETIES	
X_e	0
X_h	1
X_s	0
τ_y [Pa]	2.04
K	1.35
n [Pa.s^n]	0.52
C_v	0.09
$V_{ts,\,measured}$ [m/s]	2.91
$V_{ts,\,predicted}$ [m/s]	2.9
$V_{sm,\,Xs,\,predicted}$ [m/s]	-
MODEL PERFORMANCE	
RMSE	0.0070

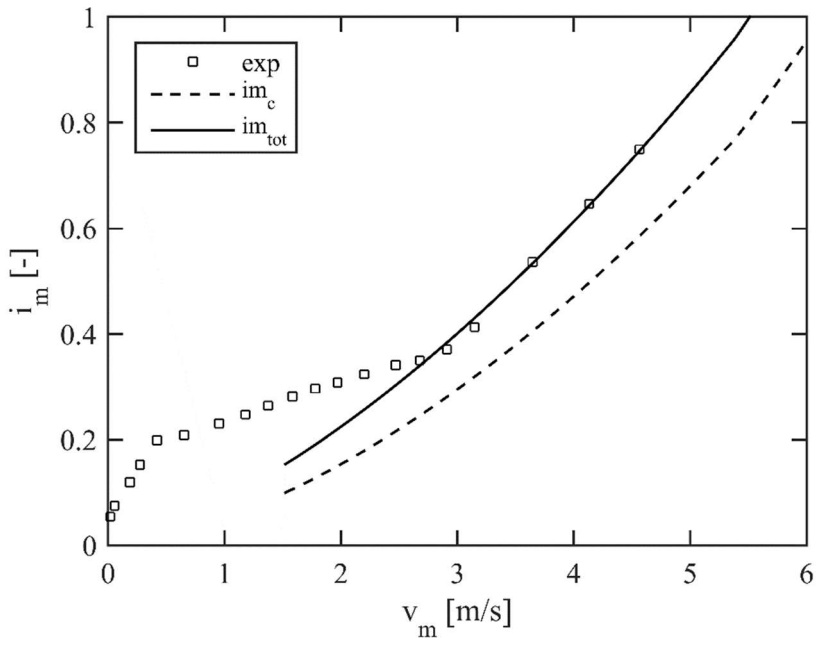

Data set 2019	
Test run no.	2
APPARATUS	
D [m]	0.05
material	B7
pipe roughness	0
SLURRY PROPETIES	
X_e	0
X_h	1
X_s	0
τ_y [Pa]	1.88
K	1.36
n [Pa.s^n]	0.52
C_v	0.15
$V_{ts,\,measured}$ [m/s]	2.79
$V_{ts,\,predicted}$ [m/s]	2.87
$V_{sm,\,Xs,\,predicted}$ [m/s]	-
MODEL PERFORMANCE	
RMSE	0.0069

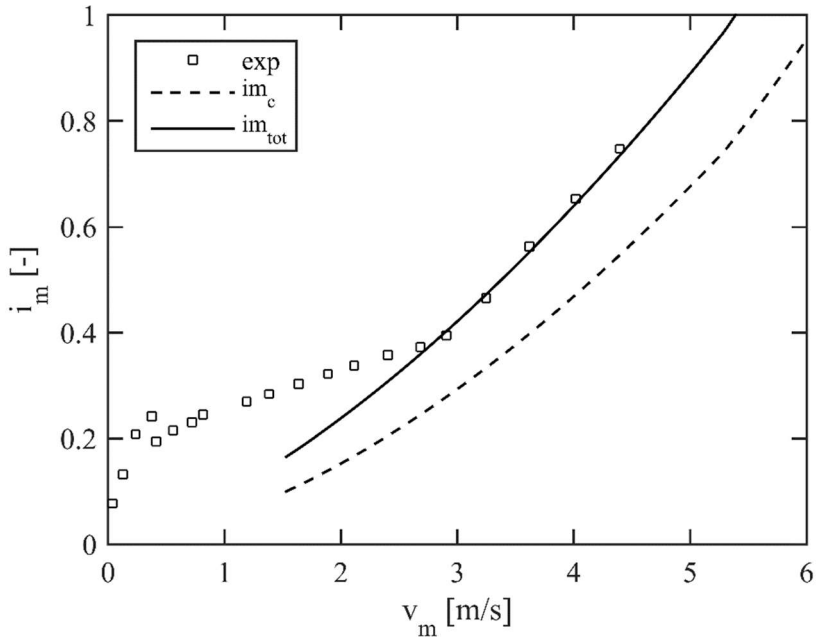

Data set 2019	
Test run no.	3
APPARATUS	
D [m]	0.05
material	B7
pipe roughness	0
SLURRY PROPETIES	
X_e	0
X_h	1
X_s	0
τ_y [Pa]	1.87
K	1.3
n [Pa.s^n]	0.52
C_v	0.22
$V_{ts,\,measured}$ [m/s]	2.68
$V_{ts,\,predicted}$ [m/s]	2.77
$V_{sm,\,Xs,\,predicted}$ [m/s]	-
MODEL PERFORMANCE	
RMSE	0.0096

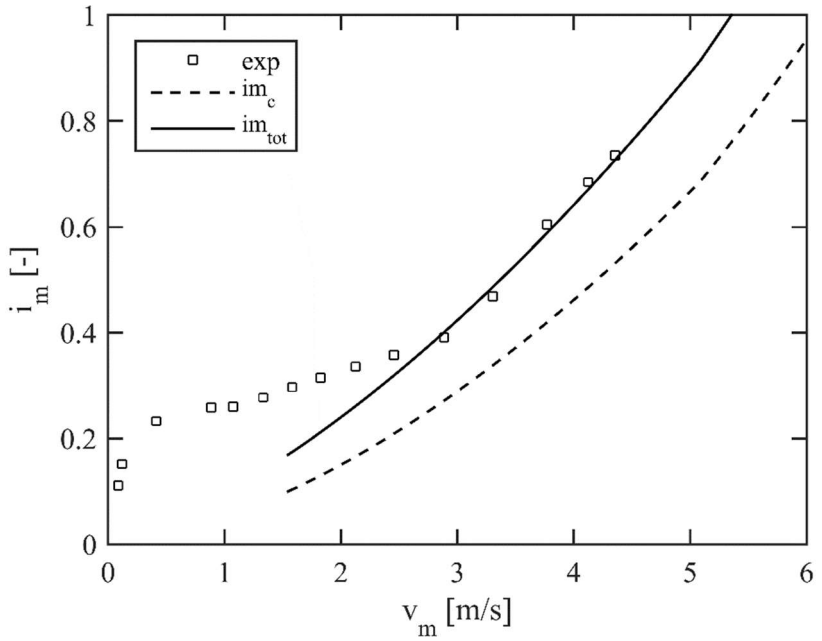

Data set 2019	
Test run no.	4
APPARATUS	
D [m]	0.05
material	B134
pipe roughness	0
SLURRY PROPETIES	
X_e	1
X_h	0
X_s	0
τ_y [Pa]	1.69
K	1.54
n [Pa.s^n]	0.52
C_v	0.06
$V_{ts,\,measured}$ [m/s]	3.168
$V_{ts,\,predicted}$ [m/s]	3.12
$V_{sm,\,Xs,\,predicted}$ [m/s]	-
MODEL PERFORMANCE	
RMSE	0.0088

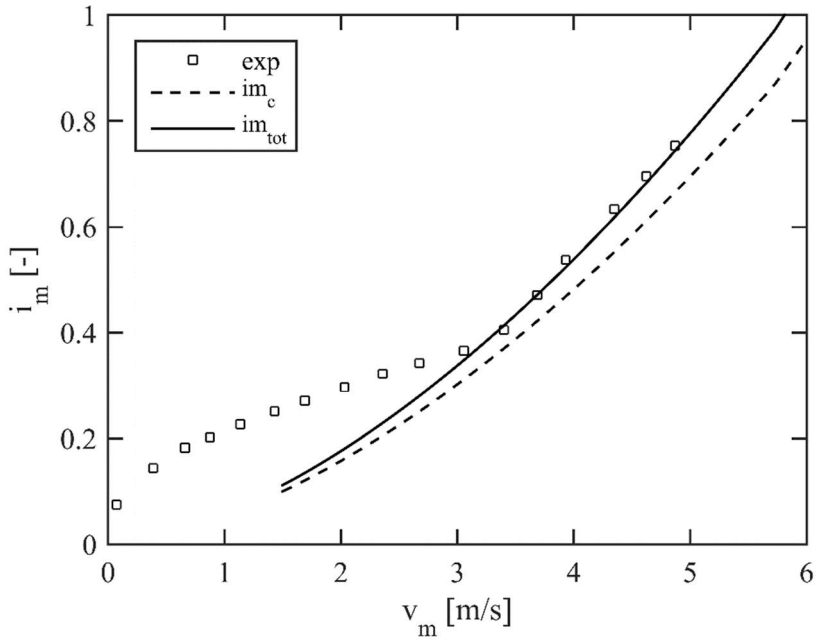

Data set 2019	
Test run no.	5
APPARATUS	
D [m]	0.05
material	B134
pipe roughness	0
SLURRY PROPETIES	
X_e	1
X_h	0
X_s	0
τ_y [Pa]	0.78
K	0.98
n [Pa.s^n]	0.55
C_v	0.1
$V_{ts,\,measured}$ [m/s]	2.55
$V_{ts,\,predicted}$ [m/s]	2.54
$V_{sm,\,Xs,\,predicted}$ [m/s]	-
MODEL PERFORMANCE	
RMSE	0.0048

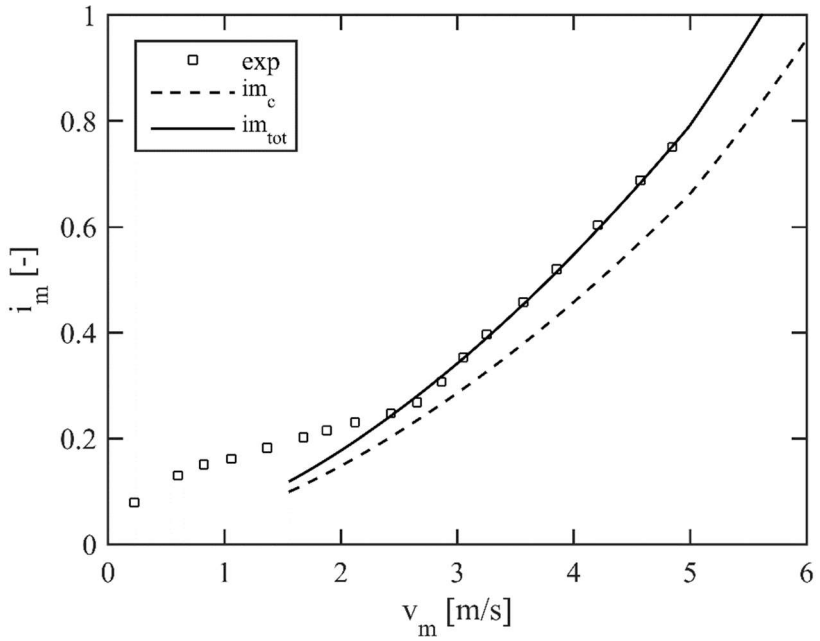

Data set 2019	
Test run no.	6
APPARATUS	
D [m]	0.05
material	B134
pipe roughness	0
SLURRY PROPETIES	
X_e	1
X_h	0
X_s	0
τ_y [Pa]	0.21
K	0.77
n [Pa.s^n]	0.55
C_v	0.14
$V_{ts,\,measured}$ [m/s]	1.92
$V_{ts,\,predicted}$ [m/s]	2.15
$V_{sm,\,Xs,\,predicted}$ [m/s]	-
MODEL PERFORMANCE	
RMSE	0.0076

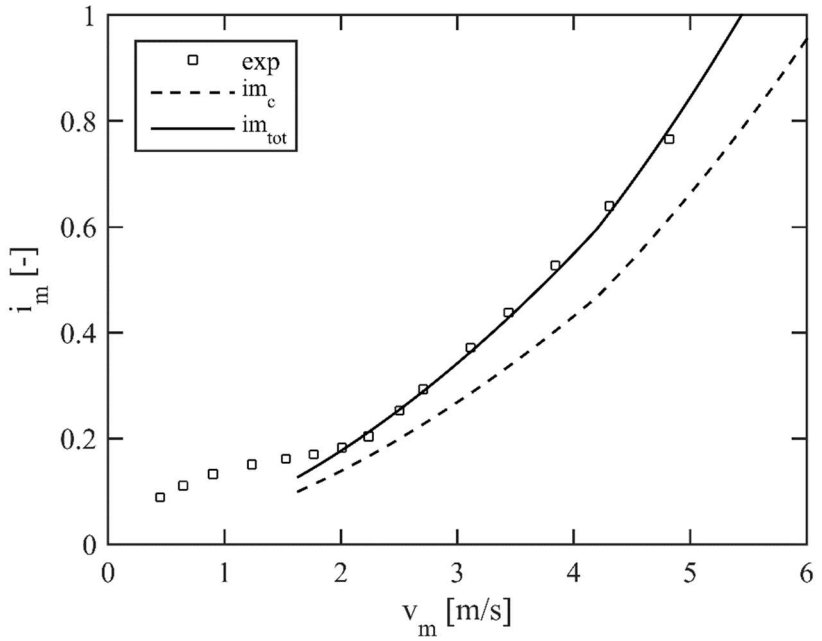

Data set 2019	
Test run no.	7
APPARATUS	
D [m]	0.05
material	TK15
pipe roughness	0
SLURRY PROPETIES	
X_e	0
X_h	0
X_s	1
τ_y [Pa]	0.46
K	1.43
n [Pa.s^n]	0.8
C_v	0.1
$V_{ts,\,measured}$ [m/s]	2.6
$V_{ts,\,predicted}$ [m/s]	2.68
$V_{sm,\,Xs,\,predicted}$ [m/s]	0.89
MODEL PERFORMANCE	
RMSE	0.0048

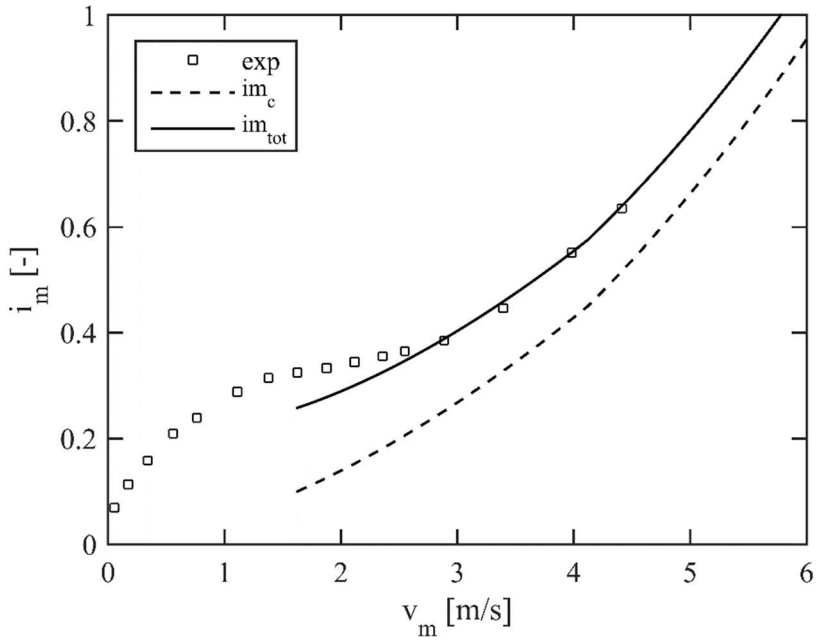

Data set 2019	
Test run no.	8
APPARATUS	
D [m]	0.05
material	TK15
pipe roughness	0
SLURRY PROPETIES	
X_e	0
X_h	0
X_s	1
τ_y [Pa]	0.18
K	0.6
n [Pa.s^n]	0.57
C_v	0.22
$V_{ts,\,measured}$ [m/s]	2.44
$V_{ts,\,predicted}$ [m/s]	2.44
$V_{sm,\,Xs,\,predicted}$ [m/s]	1.45
MODEL PERFORMANCE	
RMSE	0.0092

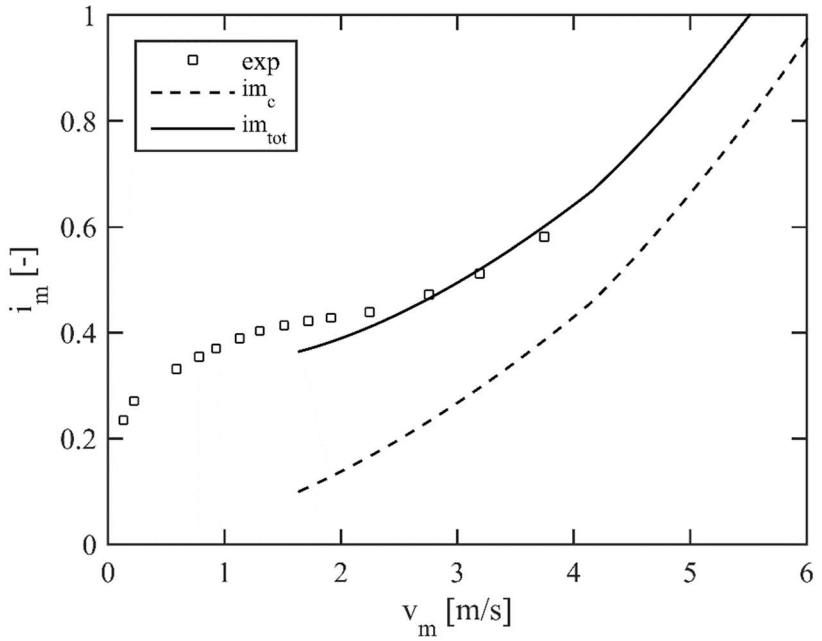

Data set 2019	
Test run no.	9
APPARATUS	
D [m]	0.05
material	TK15
pipe roughness	0
SLURRY PROPETIES	
X_e	0
X_h	0
X_s	1
τ_y [Pa]	0.08
K	0.39
n [Pa.s^n]	0.62
C_v	0.27
$V_{ts,\,measured}$ [m/s]	2.21
$V_{ts,\,predicted}$ [m/s]	2.19
$V_{sm,\,Xs,\,predicted}$ [m/s]	1.73
MODEL PERFORMANCE	
RMSE	0.0064

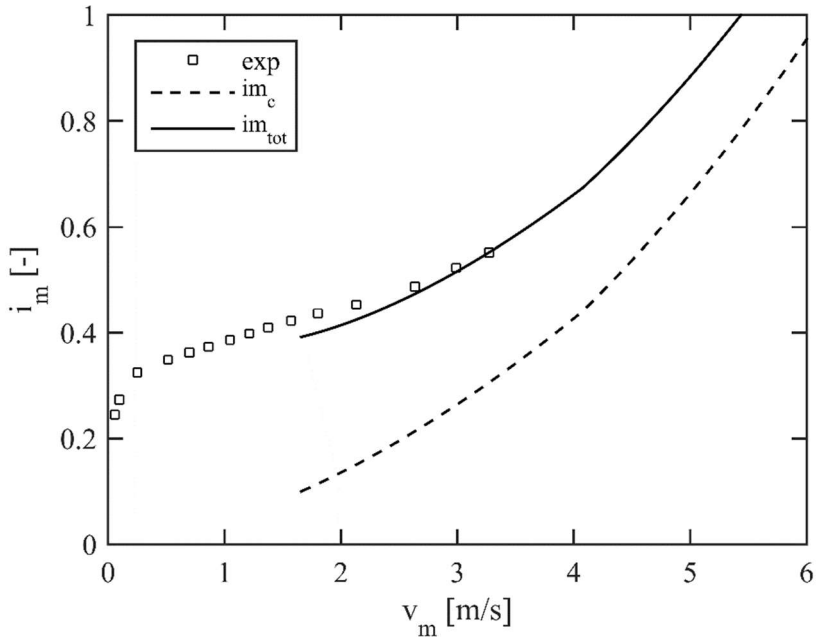

Data set 2019	
Test run no.	10
APPARATUS	
D [m]	0.05
material	B134; B7
pipe roughness	0
SLURRY PROPETIES	
X_e	0.61
X_h	0.39
X_s	0
τ_y [Pa]	1.59
K	1.42
n [Pa.s^n]	0.51
C_v	0.11
$V_{ts,\,measured}$ [m/s]	2.73
$V_{ts,\,predicted}$ [m/s]	2.75
$V_{sm,\,Xs,\,predicted}$ [m/s]	-
MODEL PERFORMANCE	
RMSE	0.0237

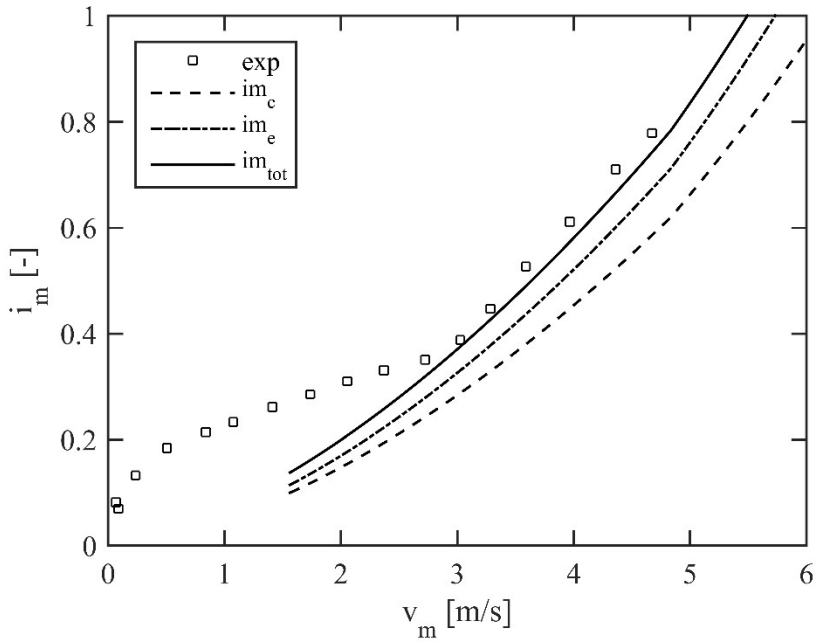

Data set 2019	
Test run no.	11
APPARATUS	
D [m]	0.05
material	B134; B7
pipe roughness	0
SLURRY PROPETIES	
X_e	0.54
X_h	0.46
X_s	0
τ_y [Pa]	0.57
K	1.18
n [Pa.s^n]	0.52
C_v	0.18
$V_{ts,\,measured}$ [m/s]	2.5
$V_{ts,\,predicted}$ [m/s]	2.59
$V_{sm,\,Xs,\,predicted}$ [m/s]	-
MODEL PERFORMANCE	
RMSE	0.0086

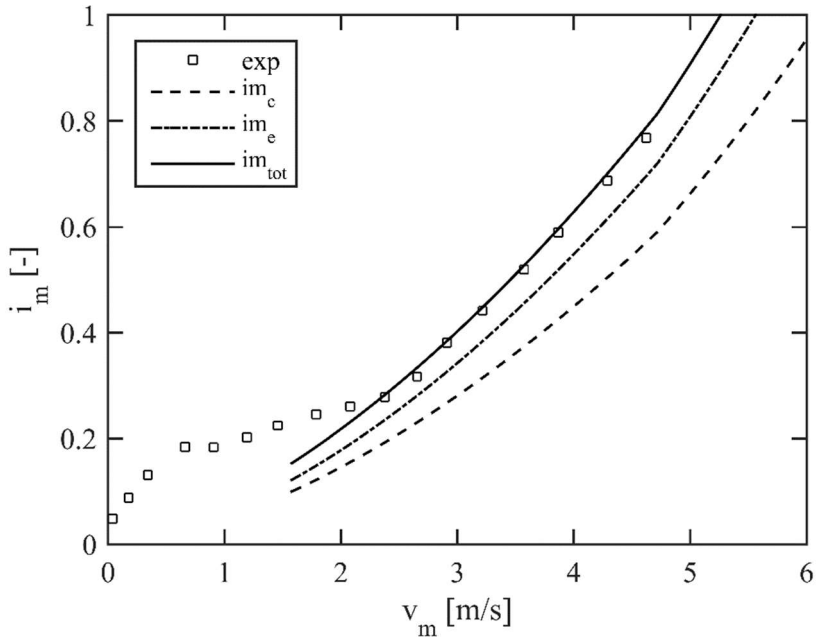

Data set 2019	
Test run no.	12
APPARATUS	
D [m]	0.05
material	B134; B7
pipe roughness	0
SLURRY PROPETIES	
X_e	0.49
X_h	0.51
X_s	0
τ_y [Pa]	0
K	0.67
n [Pa.s^n]	0.55
C_v	0.28
$V_{ts,\,measured}$ [m/s]	2.2
$V_{ts,\,predicted}$ [m/s]	1.96
$V_{sm,\,Xs,\,predicted}$ [m/s]	-
MODEL PERFORMANCE	
RMSE	0.0151

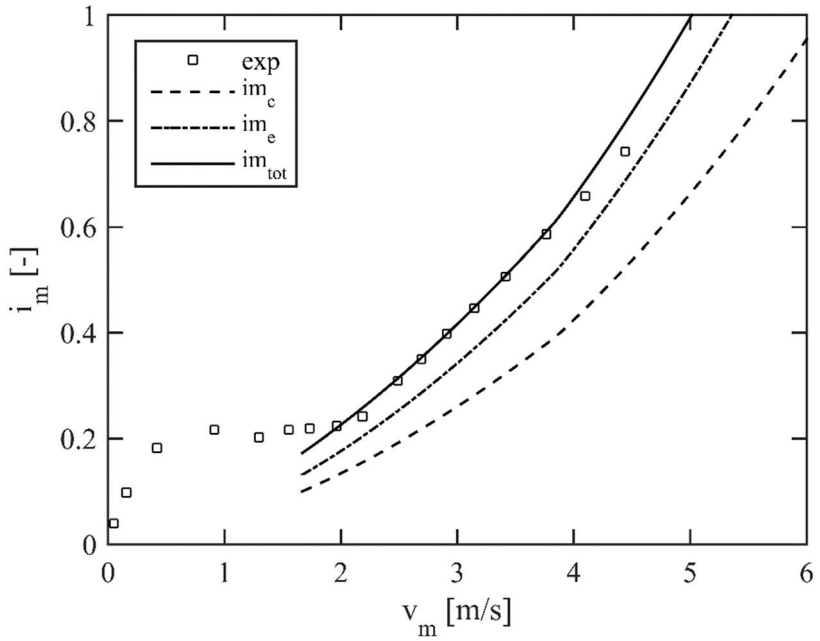

Data set 2019	
Test run no.	13
APPARATUS	
D [m]	0.05
material	B7; TK15
pipe roughness	0
SLURRY PROPETIES	
X_e	0
X_h	0.36
X_s	0.64
τ_y [Pa]	1.07
K	0.87
n [Pa.s^n]	0.55
C_v	0.1
$V_{ts,\,measured}$ [m/s]	2.13
$V_{ts,\,predicted}$ [m/s]	2.11
$V_{sm,\,Xs,\,predicted}$ [m/s]	0.29
MODEL PERFORMANCE	
RMSE	0.0086

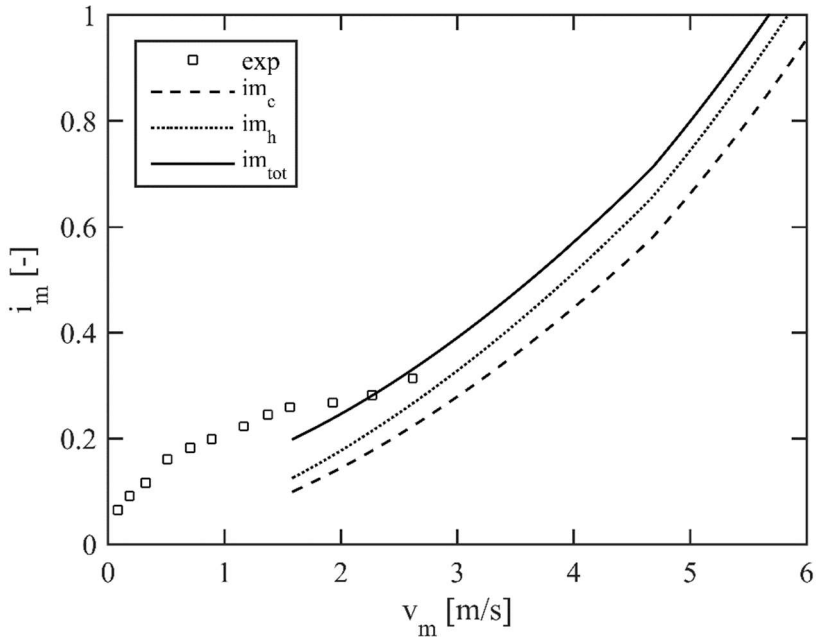

Data set 2019	
Test run no.	14
APPARATUS	
D [m]	0.05
material	B7; TK15
pipe roughness	0
SLURRY PROPETIES	
X_e	0
X_h	0.36
X_s	0.64
τ_y [Pa]	1.01
K	0.96
n [Pa.s^n]	0.55
C_v	0.1
$V_{ts,\,measured}$ [m/s]	2.27
$V_{ts,\,predicted}$ [m/s]	2.23
$V_{sm,\,Xs,\,predicted}$ [m/s]	0.25
MODEL PERFORMANCE	
RMSE	0.0069

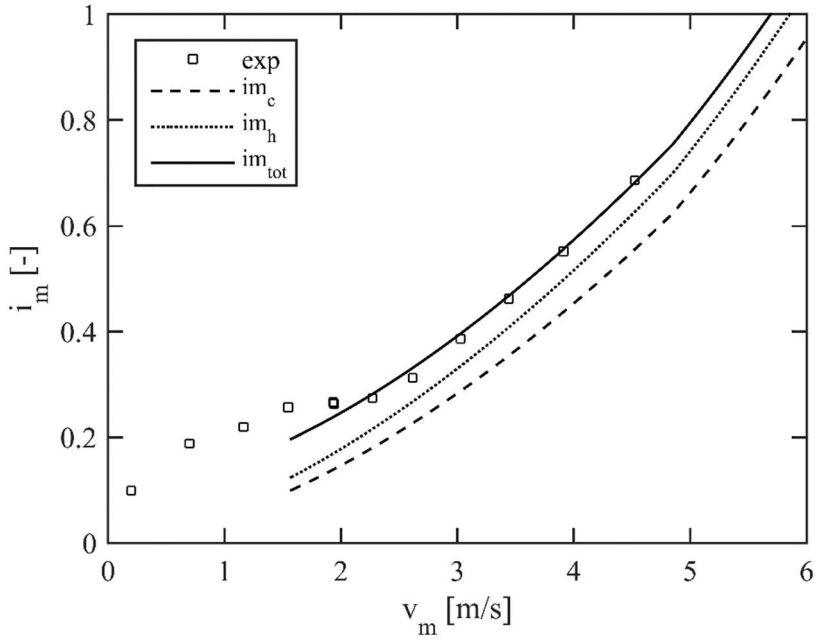

Data set 2019	
Test run no.	15
APPARATUS	
D [m]	0.05
material	B7; TK15
pipe roughness	0
SLURRY PROPETIES	
X_e	0
X_h	0.41
X_s	0.59
τ_y [Pa]	0.16
K	0.7
n [Pa.s^n]	0.55
C_v	0.15
$V_{ts,\,measured}$ [m/s]	2.3
$V_{ts,\,predicted}$ [m/s]	2.1
$V_{sm,\,Xs,\,predicted}$ [m/s]	0.25
MODEL PERFORMANCE	
RMSE	0.0225

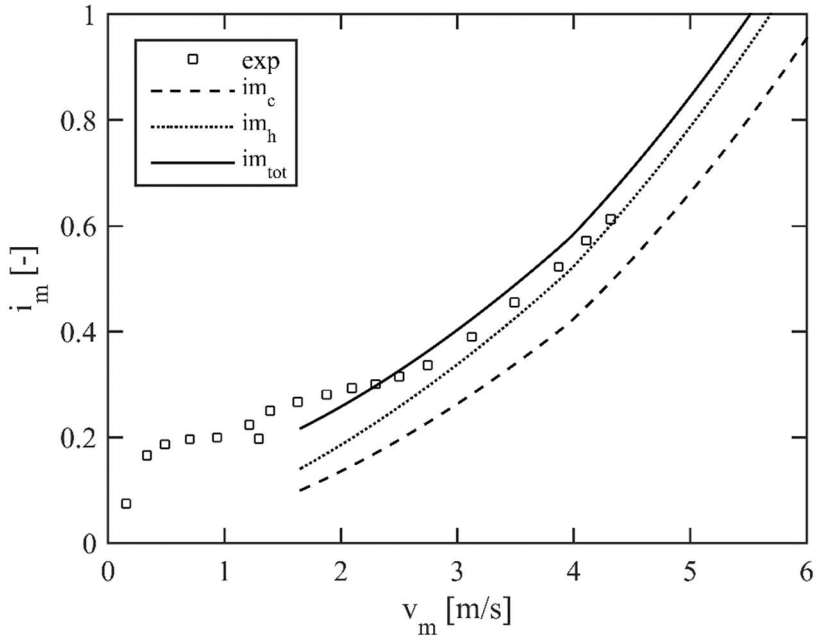

Data set 2019	
Test run no.	16
APPARATUS	
D [m]	0.05
material	B134; TK15
pipe roughness	0
SLURRY PROPETIES	
X_e	0.52
X_h	0
X_s	0.48
τ_y [Pa]	1.09
K	1.54
n [Pa.s^n]	0.51
C_v	0.12
$V_{ts,\,measured}$ [m/s]	2.6
$V_{ts,\,predicted}$ [m/s]	2.38
$V_{sm,\,Xs,\,predicted}$ [m/s]	0.14
MODEL PERFORMANCE	
RMSE	0.0122

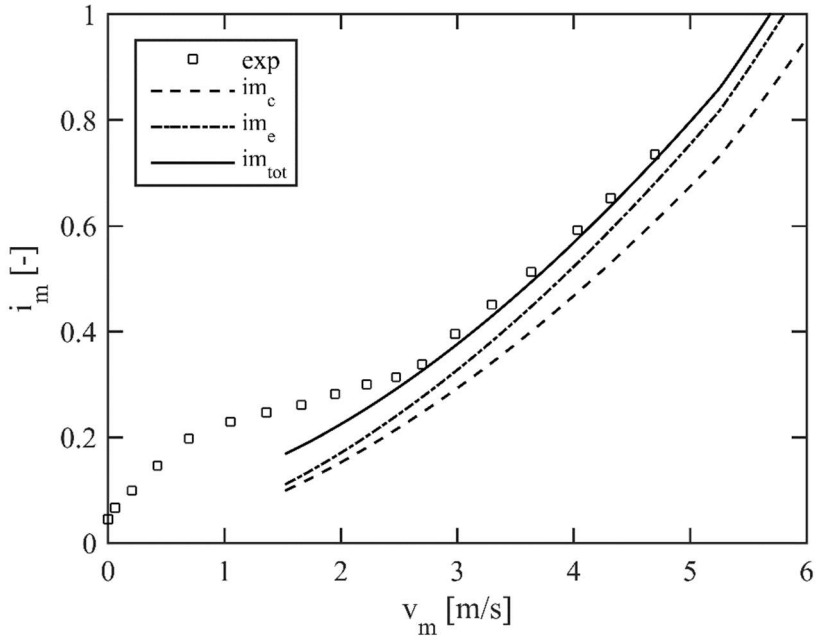

Data set 2019	
Test run no.	17
APPARATUS	
D [m]	0.05
material	B134; TK15
pipe roughness	0
SLURRY PROPETIES	
X_e	0.49
X_h	0
X_s	0.51
τ_y [Pa]	0.77
K	1.44
n [Pa.s^n]	0.51
C_v	0.17
$V_{ts,\,measured}$ [m/s]	2.68
$V_{ts,\,predicted}$ [m/s]	2.4
$V_{sm,\,Xs,\,predicted}$ [m/s]	0.55
MODEL PERFORMANCE	
RMSE	0.016

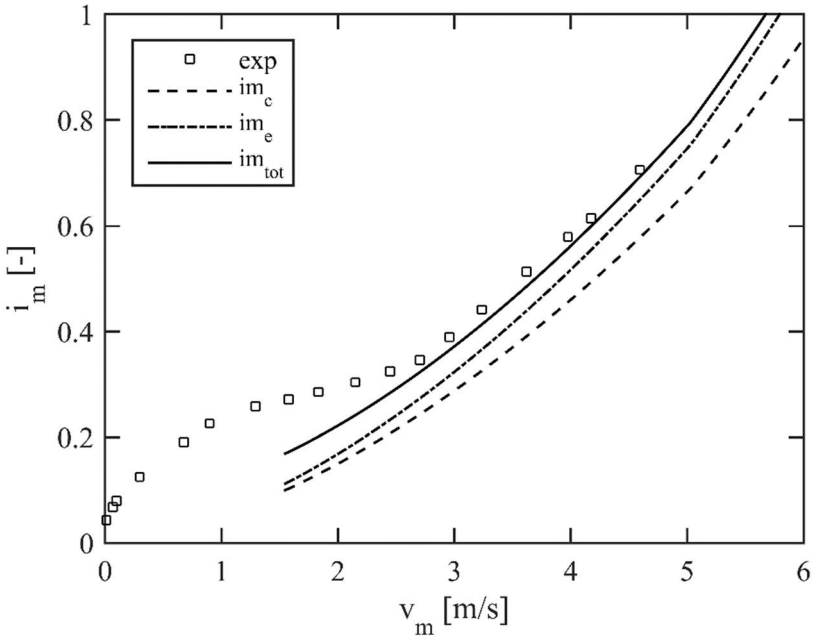

Data set 2019	
Test run no.	18
APPARATUS	
D [m]	0.05
material	B134; TK15
pipe roughness	0
SLURRY PROPETIES	
X_e	0.48
X_h	0
X_s	0.52
τ_y [Pa]	0.28
K	1.06
n [Pa.s^n]	0.52
C_v	0.21
$V_{ts,\,measured}$ [m/s]	2.55
$V_{ts,\,predicted}$ [m/s]	2.42
$V_{sm,\,Xs,\,predicted}$ [m/s]	0.95
MODEL PERFORMANCE	
RMSE	0.0068

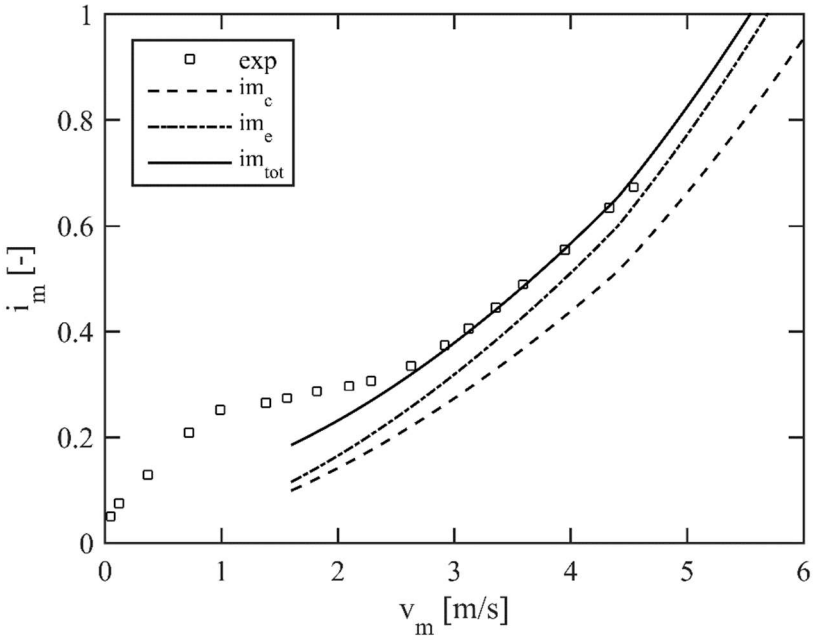

Data set 2019	
Test run no.	19
APPARATUS	
D [m]	0.05
material	B134; B7;TK15
pipe roughness	0
SLURRY PROPETIES	
X_e	0.38
X_h	0.19
X_s	0.43
τ_y [Pa]	5.02
K	2.67
n [Pa.s^n]	0.51
C_v	0.11
$V_{ts,\,measured}$ [m/s]	3.41
$V_{ts,\,predicted}$ [m/s]	3.47
$V_{sm,\,Xs,\,predicted}$ [m/s]	0.05
MODEL PERFORMANCE	
RMSE	0.0094

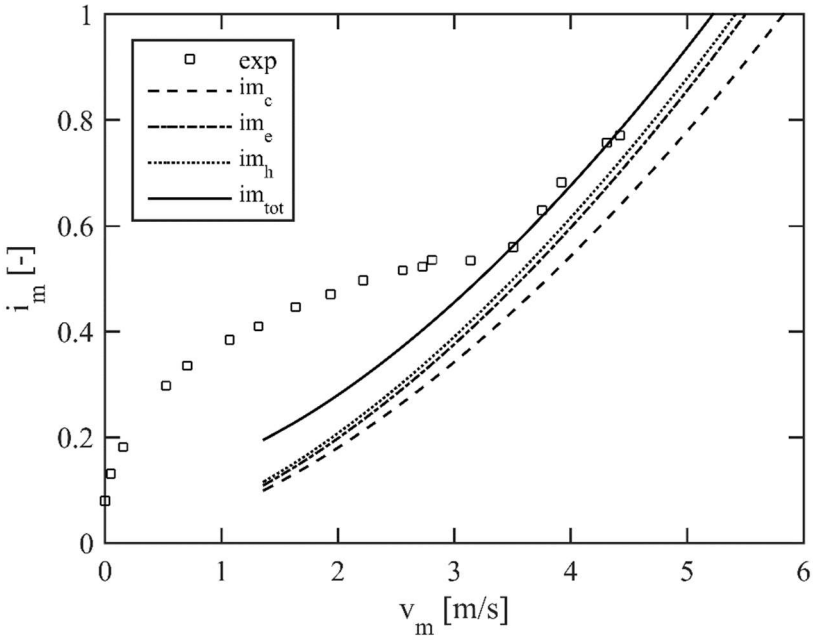

Data set 2019	
Test run no.	20
APPARATUS	
D [m]	0.05
material	B134; B7;TK15
pipe roughness	0
SLURRY PROPETIES	
X_e	0.39
X_h	0.26
X_s	0.35
τ_y [Pa]	3.1
K	2.36
n [Pa.s^n]	0.5
C_v	0.16
$V_{ts,\,measured}$ [m/s]	3.18
$V_{ts,\,predicted}$ [m/s]	3.19
$V_{sm,\,Xs,\,predicted}$ [m/s]	0.07
MODEL PERFORMANCE	
RMSE	0.0067

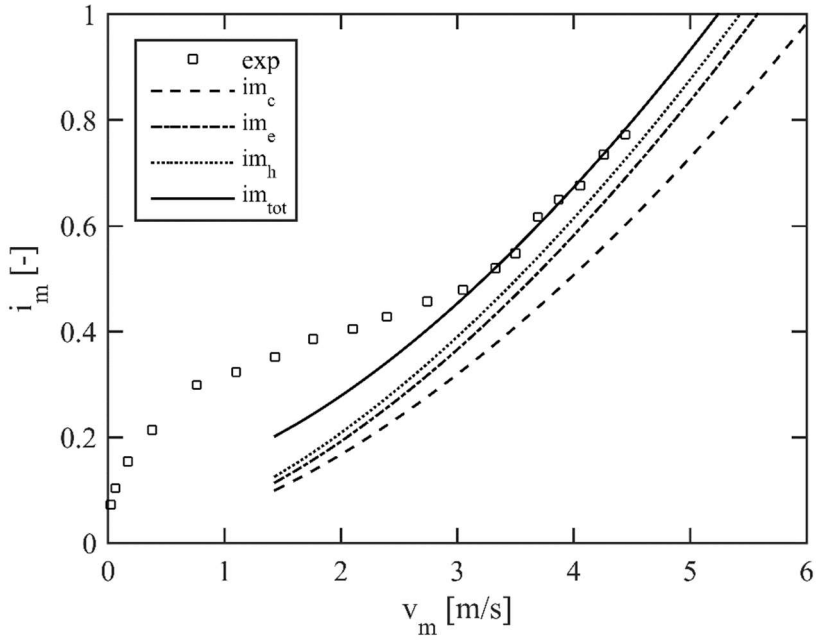

Data set 2019	
Test run no.	21
APPARATUS	
D [m]	0.05
material	B134; B7;TK15
pipe roughness	0
SLURRY PROPETIES	
X_e	0.35
X_h	0.28
X_s	0.37
τ_y [Pa]	2.41
K	2.13
n [Pa.s^n]	0.5
C_v	0.23
$V_{ts,\,measured}$ [m/s]	3.26
$V_{ts,\,predicted}$ [m/s]	3.59
$V_{sm,\,Xs,\,predicted}$ [m/s]	0.38
MODEL PERFORMANCE	
RMSE	0.0247

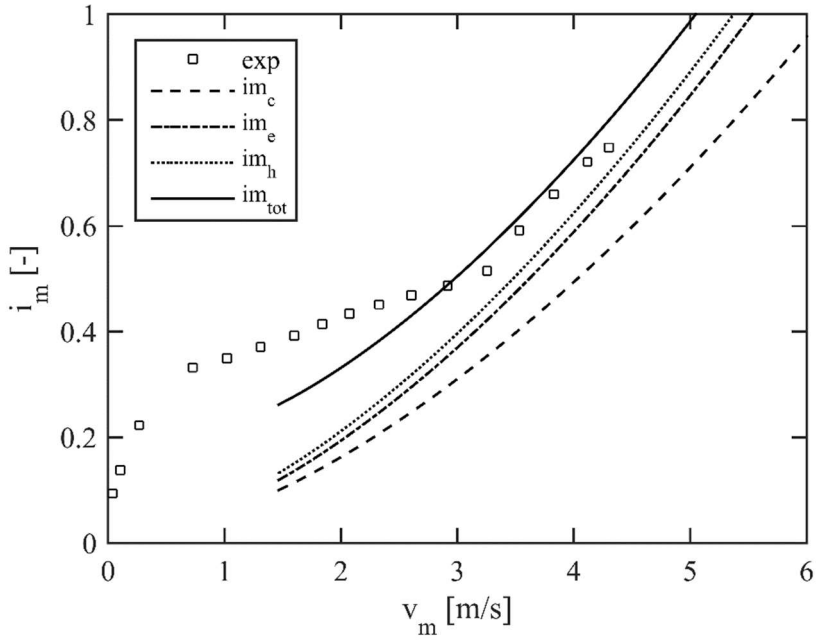

Data set 2019	
Test run no.	22
APPARATUS	
D [m]	0.05
material	B134; B7;TK15
pipe roughness	0
SLURRY PROPETIES	
X_e	0.34
X_h	0.29
X_s	0.37
τ_y [Pa]	1.15
K	1.56
n [Pa.s^n]	0.51
C_v	0.29
$V_{ts,\,measured}$ [m/s]	3.05
$V_{ts,\,predicted}$ [m/s]	3.19
$V_{sm,\,Xs,\,predicted}$ [m/s]	0.47
MODEL PERFORMANCE	
RMSE	0.0253

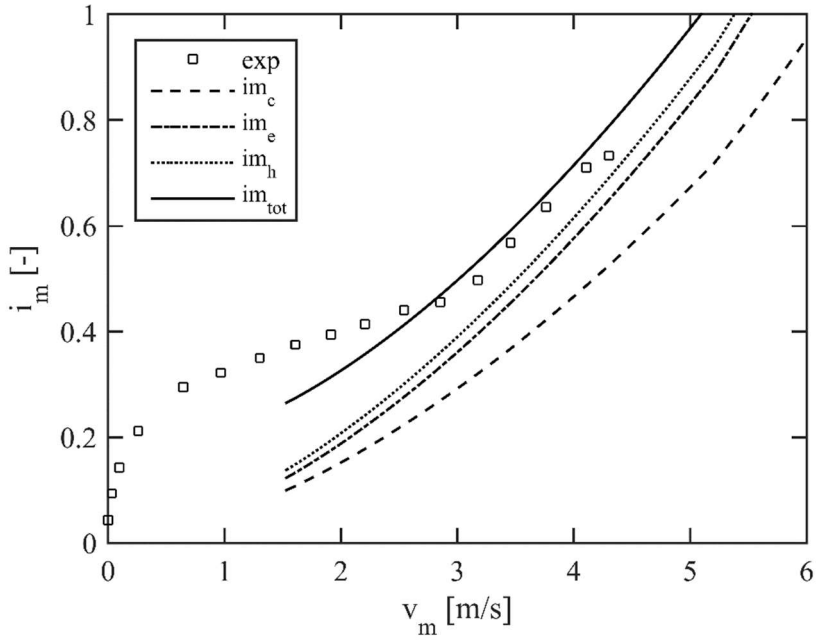

Data set 2019	
Test run no.	23
APPARATUS	
D [m]	0.05
material	-
pipe roughness	0
SLURRY PROPETIES	
X_e	0
X_h	0
X_s	0
τ_y [Pa]	3.03
K	1.56
n [Pa.s^n]	0.53
C_v	0
$V_{ts,\,measured}$ [m/s]	3.15
$V_{ts,\,predicted}$ [m/s]	3.23
$V_{sm,\,Xs,\,predicted}$ [m/s]	-
MODEL PERFORMANCE	
RMSE	0.0079

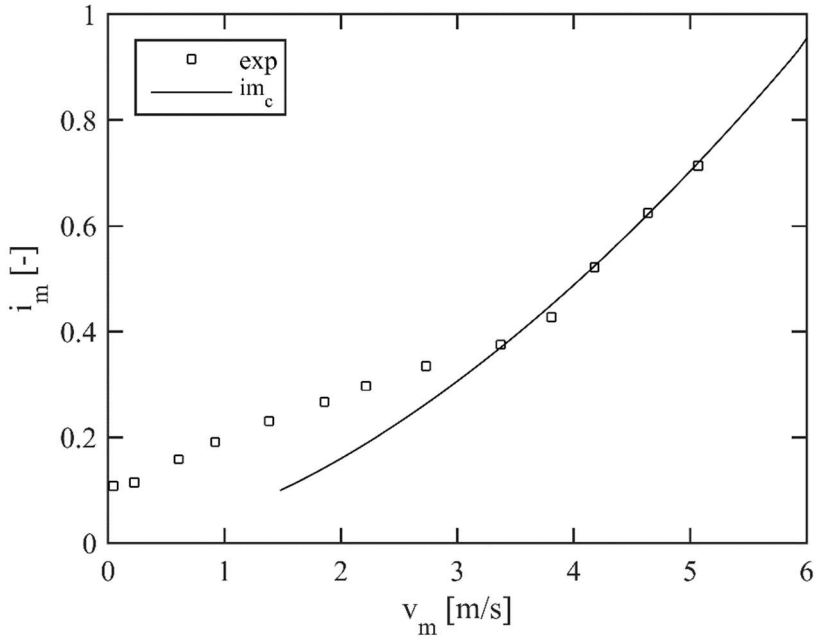

Data set 2019	
Test run no.	24
APPARATUS	
D [m]	0.05
material	-
pipe roughness	0
SLURRY PROPETIES	
X_e	0
X_h	0
X_s	0
τ_y [Pa]	3.18
K	1.71
n [Pa.s^n]	0.53
C_v	0
$V_{ts,\,measured}$ [m/s]	3.37
$V_{ts,\,predicted}$ [m/s]	3.44
$V_{sm,\,Xs,\,predicted}$ [m/s]	-
MODEL PERFORMANCE	
RMSE	0.0095

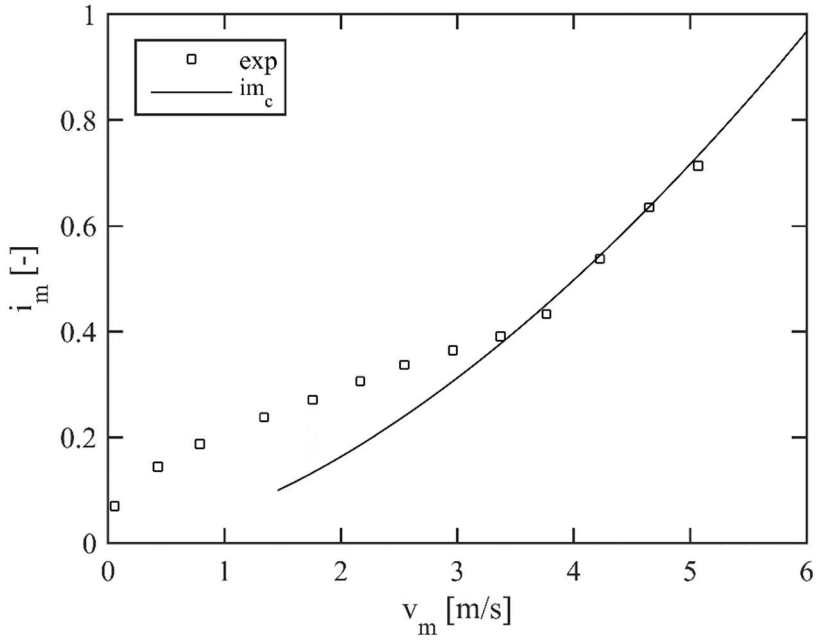

Data set 2019	
Test run no.	25
APPARATUS	
D [m]	0.05
material	-
pipe roughness	0
SLURRY PROPETIES	
X_e	0
X_h	0
X_s	0
τ_y [Pa]	3.33
K	1.96
n [Pa.s^n]	0.51
C_v	0
$V_{ts,\,measured}$ [m/s]	3.47
$V_{ts,\,predicted}$ [m/s]	3.47
$V_{sm,\,Xs,\,predicted}$ [m/s]	-
MODEL PERFORMANCE	
RMSE	0.0101

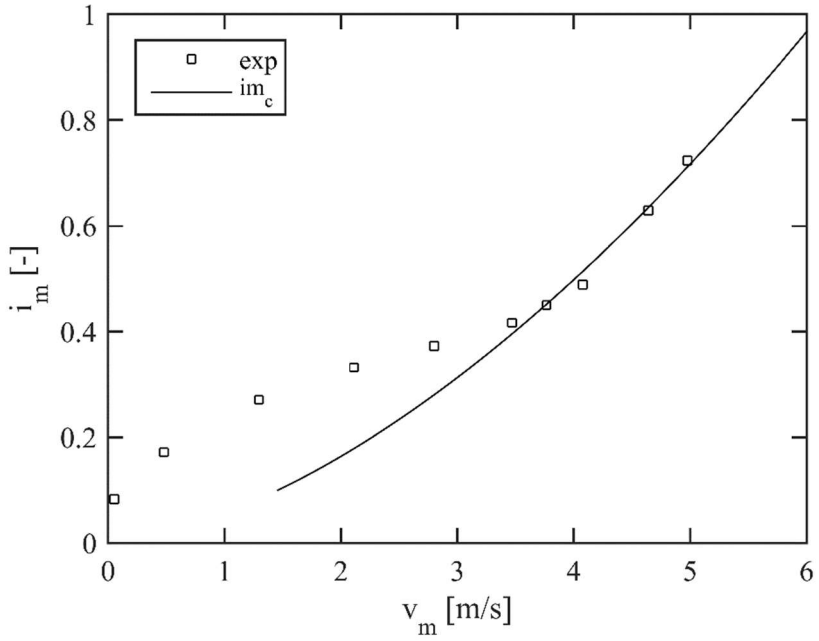

Data set 2019	
Test run no.	26
APPARATUS	
D [m]	0.05
material	-
pipe roughness	0
SLURRY PROPETIES	
X_e	0
X_h	0
X_s	0
τ_y [Pa]	3.074
K	2.01
n [Pa.s^n]	0.51
C_v	0
$V_{ts,\,measured}$ [m/s]	3.48
$V_{ts,\,predicted}$ [m/s]	3.53
$V_{sm,\,Xs,\,predicted}$ [m/s]	-
MODEL PERFORMANCE	
RMSE	0.0135

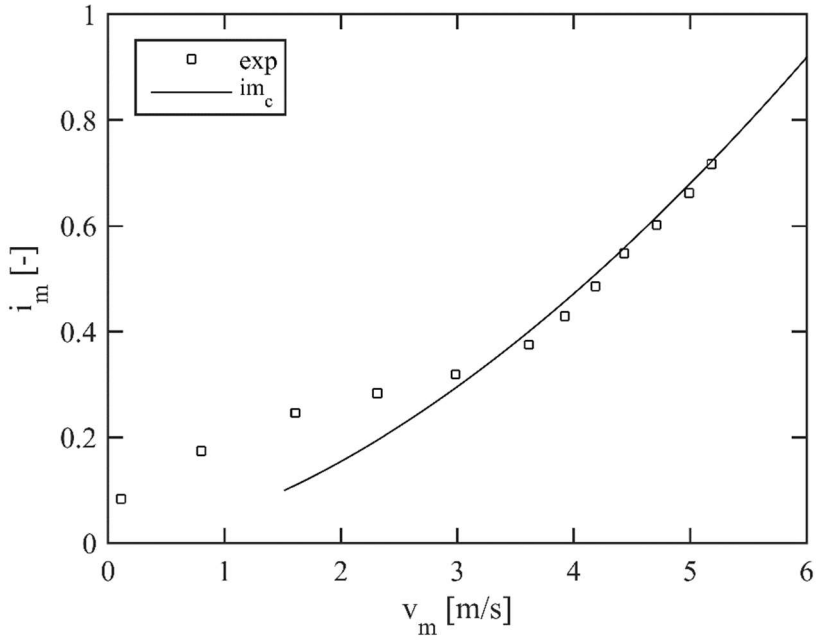

Data set GIW	
Test run no.	1
APPARATUS	
D [m]	0.07887
material	Kaolin
pipe roughness *[m]*	0.00000197
SLURRY PROPETIES	
X_e	0
X_h	0
X_s	0
τ_y [Pa]	30
K	0.52
n [Pa.s^n]	0.55
C_v	0
$V_{ts,\,measured}$ [m/s]	4.4
$V_{ts,\,predicted}$ [m/s]	4.45
$V_{sm,\,Xs,\,predicted}$ [m/s]	-
MODEL PERFORMANCE	
RMSE	0.0129

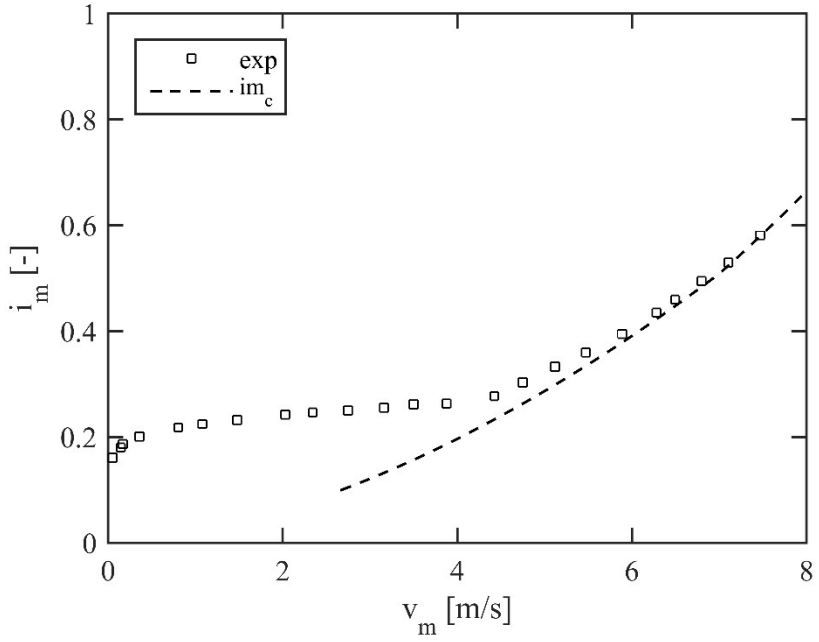

Data set GIW	
Test run no.	2
APPARATUS	
D [m]	0.07887
material	Kaolin; GIW Gravel
pipe roughness *[m]*	0.00000197
SLURRY PROPETIES	
X_e	0
X_h	0
X_s	1
τ_y [Pa]	30
K	0.52
n [Pa.s^n]	0.55
C_v	0.046
$V_{ts,\,measured}$ [m/s]	4.2
$V_{ts,\,predicted}$ [m/s]	3.87
$V_{sm,\,Xs,\,predicted}$ [m/s]	1.11
MODEL PERFORMANCE	
RMSE	0.0126

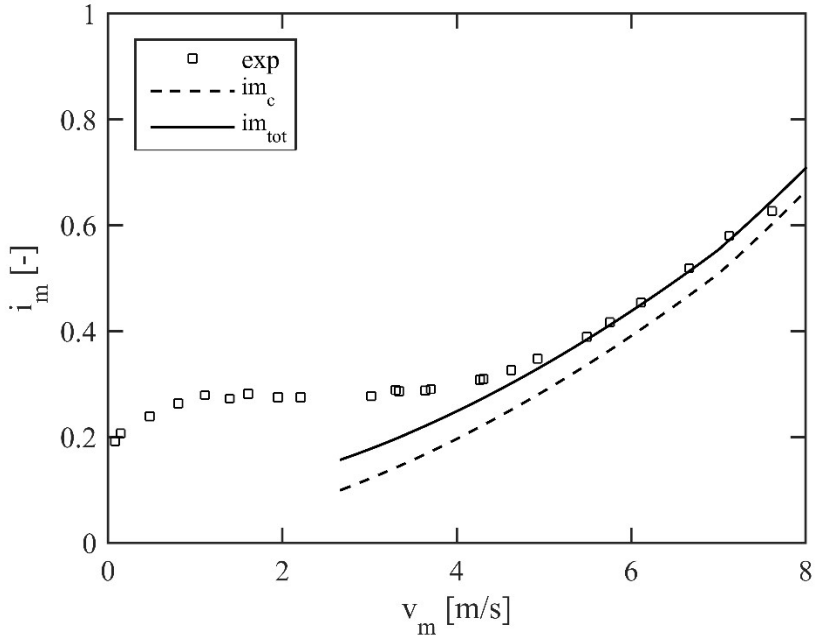

Data set GIW	
Test run no.	3
APPARATUS	
D [m]	0.07887
material	Kaolin; GIW Gravel; GIW Sand
pipe roughness *[m]*	0.00000197
SLURRY PROPETIES	
X_e	0
X_h	0.765
X_s	0.235
τ_y [Pa]	30
K	0.52
n [Pa.s^n]	0.55
C_v	0.196
$V_{ts,\,measured}$ [m/s]	3.8
$V_{ts,\,predicted}$ [m/s]	3.87
$V_{sm,\,Xs,\,predicted}$ [m/s]	1.11
MODEL PERFORMANCE	
RMSE	0.0248

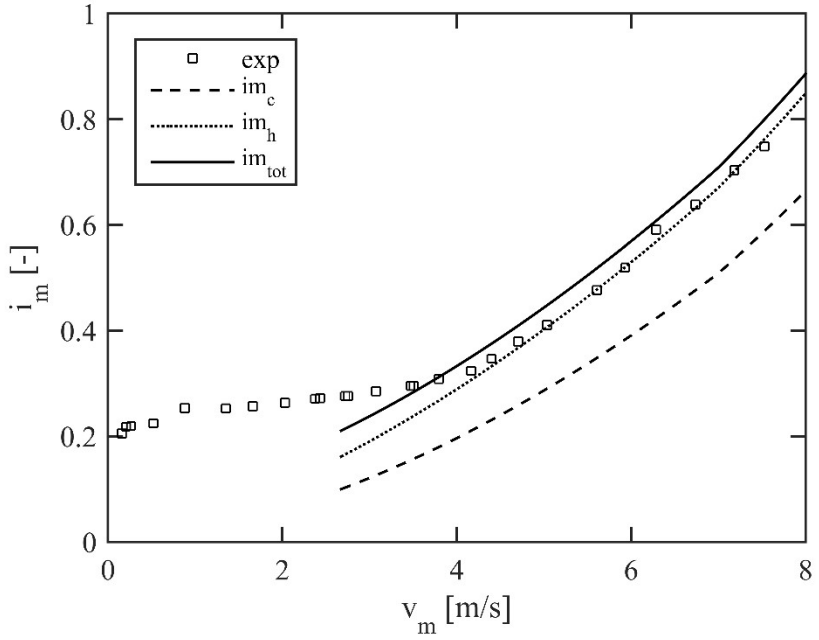

Data set CSIRO	
Test run no.	1
APPARATUS	
D [m]	0.044
material	Sand
pipe roughness	0
SLURRY PROPETIES	
X_e	0.67
X_h	0.33
X_s	0
τ_y [Pa]	0.09
K	0.29
n [Pa.s^n]	0.60
C_v	0.1
$V_{ts,\,measured}$ [m/s]	2
$V_{ts,\,predicted}$ [m/s]	1.39
$V_{sm,\,Xs,\,predicted}$ [m/s]	-
MODEL PERFORMANCE	
RMSE	0.0136

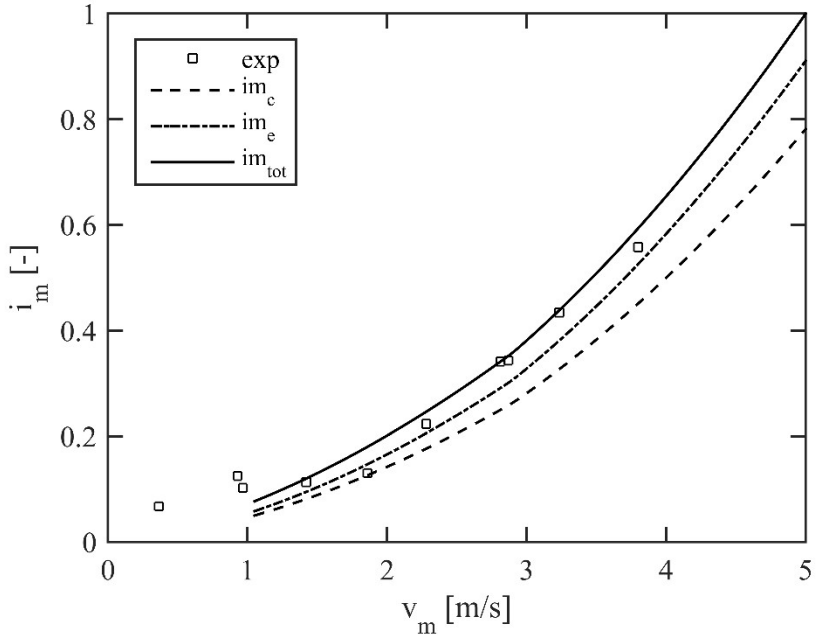

Data set CSIRO	
Test run no.	2
APPARATUS	
D [m]	0.044
material	Sand
pipe roughness	0
SLURRY PROPETIES	
X_e	0.67
X_h	0.33
X_s	0
τ_y [Pa]	0.09
K	0.29
n [Pa.s^n]	0.60
C_v	0.2
$V_{ts,\,measured}$ [m/s]	1.5
$V_{ts,\,predicted}$ [m/s]	1.39
$V_{sm,\,Xs,\,predicted}$ [m/s]	-
MODEL PERFORMANCE	
RMSE	0.0223

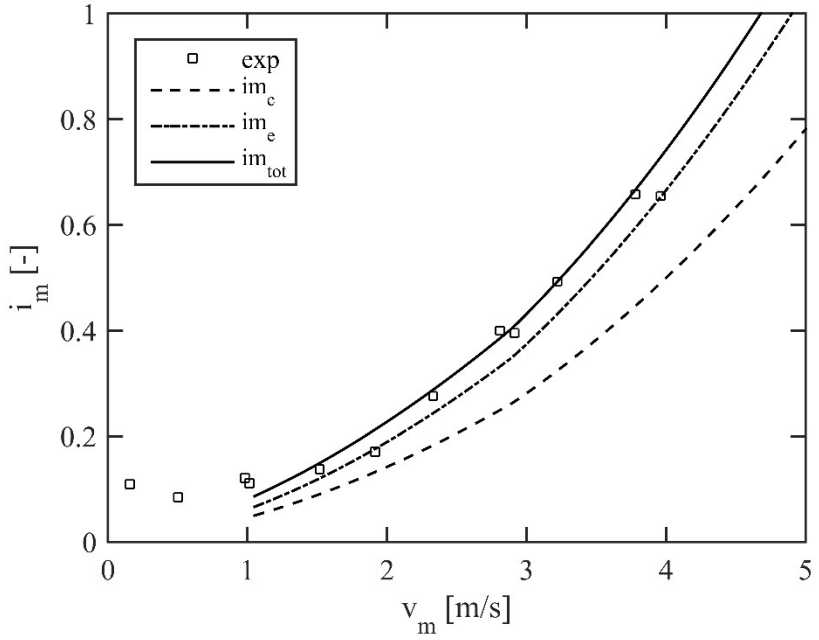

Data set CSIRO	
Test run no.	3
APPARATUS	
D [m]	0.044
material	Sand
pipe roughness	0
SLURRY PROPETIES	
X_e	0.67
X_h	0.33
X_s	0
τ_y [Pa]	0.09
K	0.29
n [Pa.s^n]	0.60
C_v	0.3
$V_{ts,\,measured}$ [m/s]	1.57
$V_{ts,\,predicted}$ [m/s]	1.39
$V_{sm,\,Xs,\,predicted}$ [m/s]	-
MODEL PERFORMANCE	
RMSE	0.0267

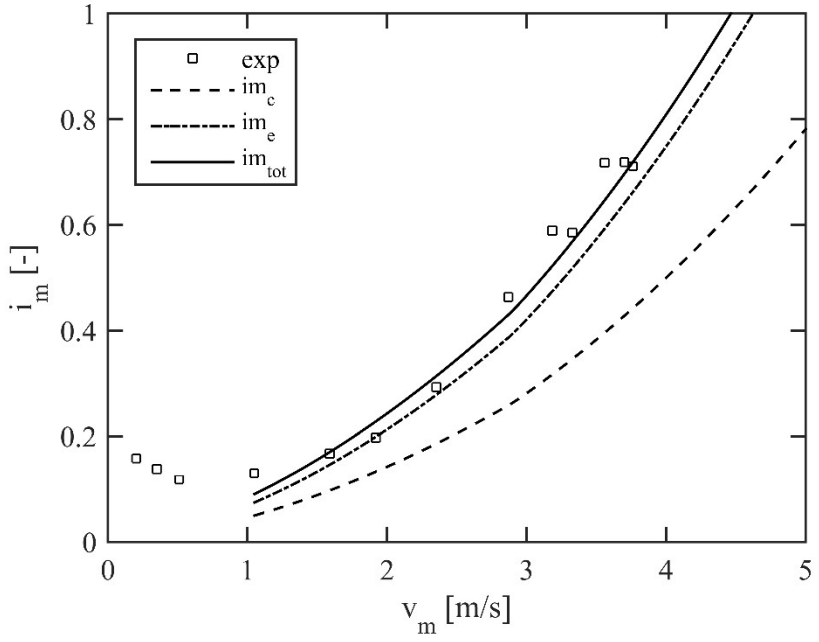

Data set 2017/2019	
Test run no.	1
APPARATUS	
D [m]	0.05
material	TK15
pipe roughness	0
SLURRY PROPETIES	
τ_y [Pa]	1.4
K	0.97
n [Pa.s^n]	0.55
μ_c	0.33
y_b/D	0.44
$V_{sm,\ measured}$ [m/s]	0.34
MODEL PERFORMANCE	
$V_{sm,\ Xs,\ predicted}$ [m/s]	0.39

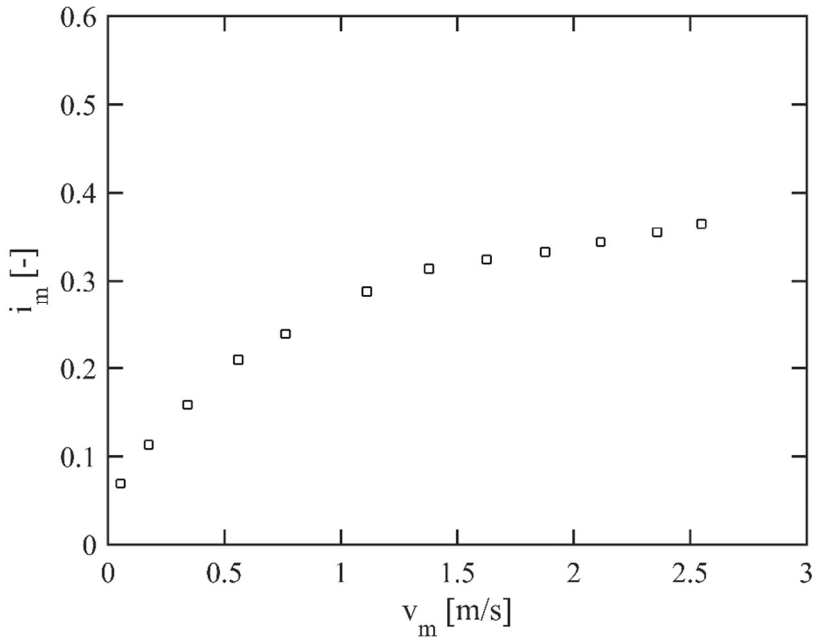

Data set 2017/2019	
Test run no.	2
APPARATUS	
D [m]	0.05
material	TK15
pipe roughness	0
SLURRY PROPETIES	
τ_y [Pa]	0.57
K	0.83
n [Pa.s^n]	0.55
μ_c	0.33
y_b/D	0.66
$V_{sm,\ measured}$ [m/s]	0.13
MODEL PERFORMANCE	
$V_{sm,\ Xs,\ predicted}$ [m/s]	0.1

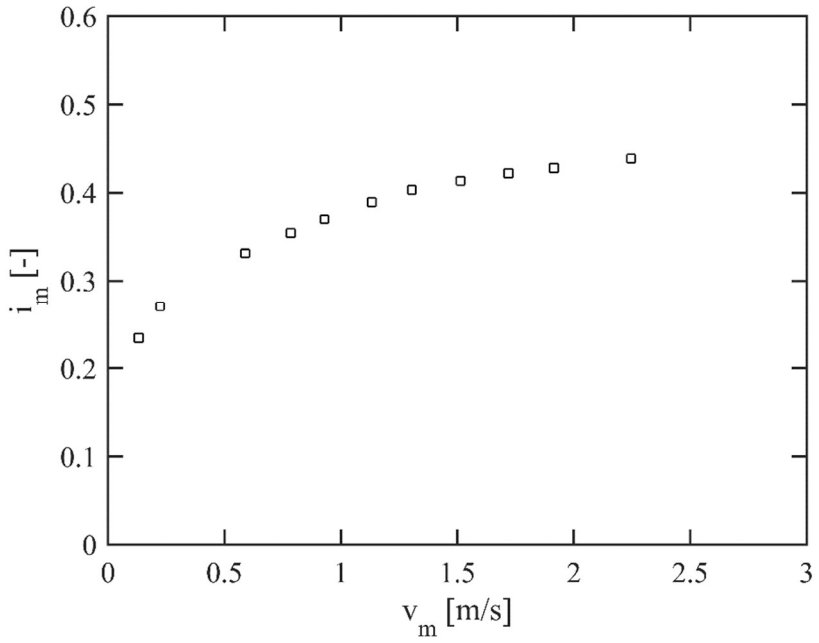

Data set 2017/2019	
Test run no.	3
APPARATUS	
D [m]	0.05
material	TK15
pipe roughness	0
SLURRY PROPETIES	
τ_y [Pa]	0.53
K	0.59
n [Pa.s^n]	0.58
μ_c	0.33
y_b/D	0.72
$V_{sm,\ measured}$ [m/s]	0.1
MODEL PERFORMANCE	
$V_{sm,\ Xs,\ predicted}$ [m/s]	0.09

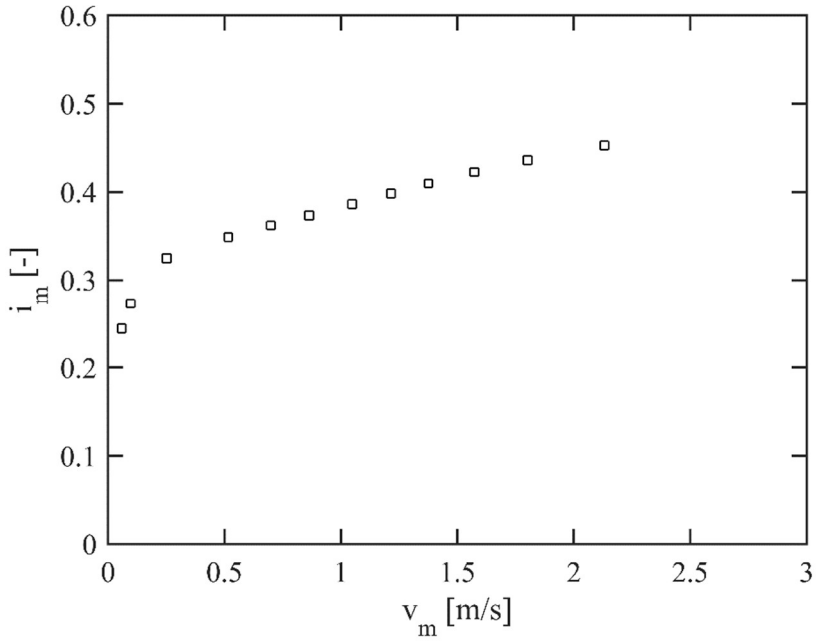

Data set 2017/2019	
Test run no.	4
APPARATUS	
D [m]	0.05
material	TK15
pipe roughness	0
SLURRY PROPETIES	
τ_y [Pa]	1.35
K	1.06
n [Pa.s^n]	0.54
μ_c	0.3
y_b/D	0.4
$V_{sm,\ measured}$ [m/s]	0.28
MODEL PERFORMANCE	
$V_{sm,\ Xs,\ predicted}$ [m/s]	0.38

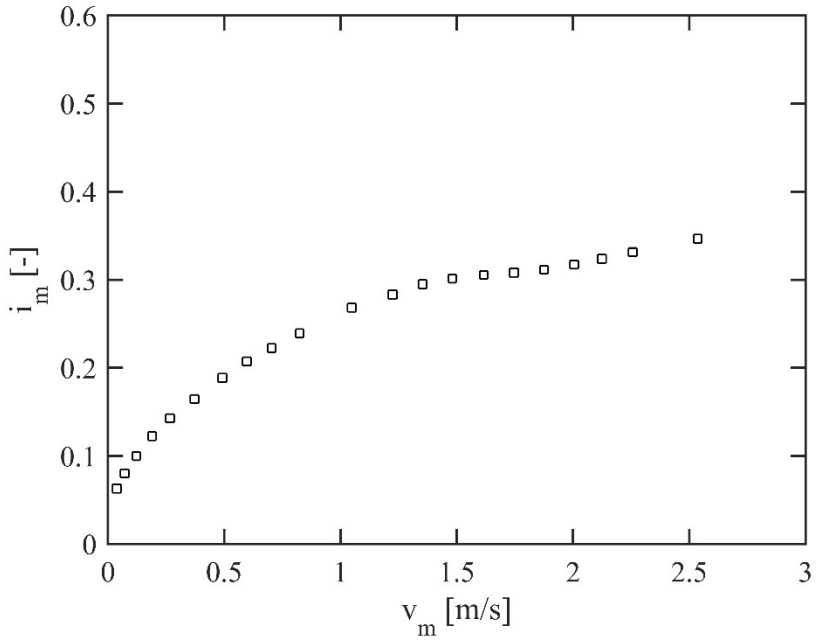

Data set 2017/2019	
Test run no.	5
APPARATUS	
D [m]	0.05
material	TK15
pipe roughness	0
SLURRY PROPETIES	
τ_y [Pa]	5.06
K	3.74
n [Pa.s^n]	0.46
μ_c	0.33
y_b/D	0.3
$V_{sm,\ measured}$ [m/s]	0.14
MODEL PERFORMANCE	
$V_{sm,\ Xs,\ predicted}$ [m/s]	0.08

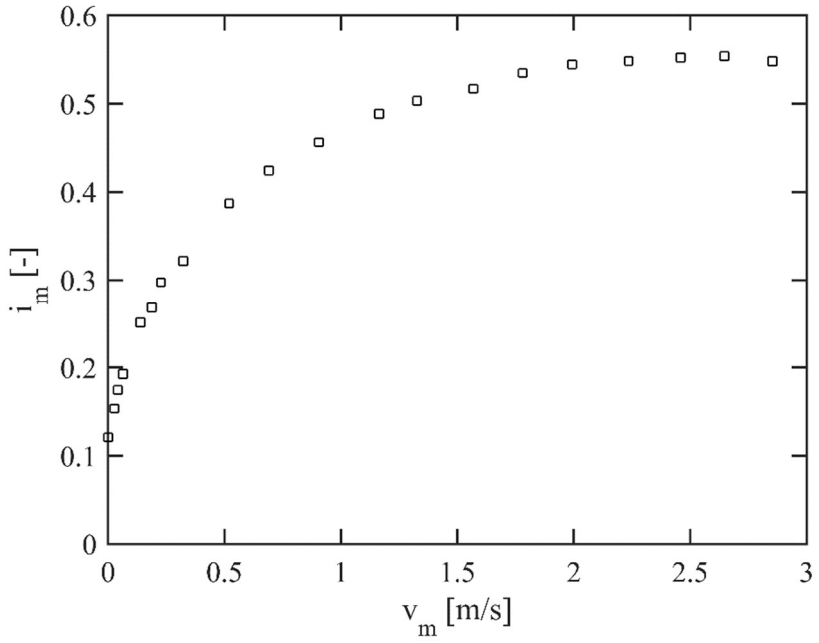

Data set 2017/2019	
Test run no.	6
APPARATUS	
D [m]	0.05
material	TK15
pipe roughness	0
SLURRY PROPETIES	
τ_y [Pa]	2.15
K	2.36
n [Pa.s^n]	0.45
μ_c	0.33
y_b/D	0.52
$V_{sm,\ measured}$ [m/s]	0.17
MODEL PERFORMANCE	
$V_{sm,\ Xs,\ predicted}$ [m/s]	0.11

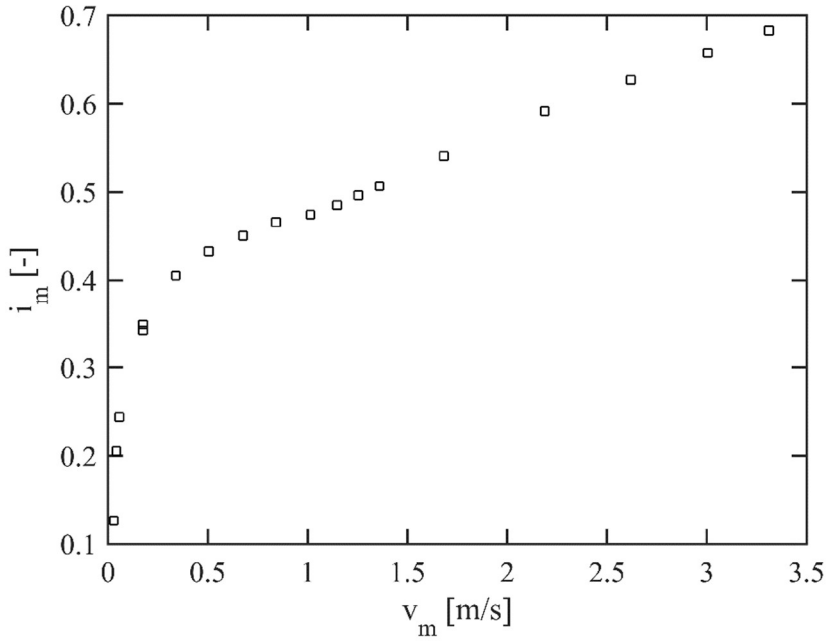

Data set 2017/2019	
Test run no.	7
APPARATUS	
D [m]	0.05
material	TK15
pipe roughness	0
SLURRY PROPETIES	
τ_y [Pa]	2.72
K	2.7
n [Pa.s^n]	0.47
μ_c	0.33
y_b/D	0.39
$V_{sm,\ measured}$ [m/s]	0.2
MODEL PERFORMANCE	
$V_{sm,\ Xs,\ predicted}$ [m/s]	0.13

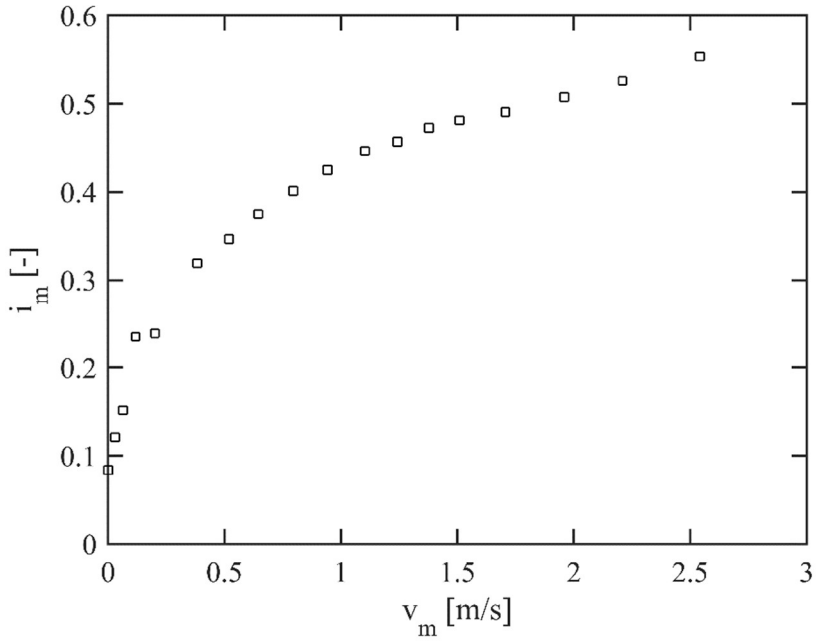

Data set 2017/2019	
Test run no.	8
APPARATUS	
D [m]	0.05
material	TK15
pipe roughness	0
SLURRY PROPETIES	
τ_y [Pa]	3.76
K	2.03
n [Pa.s^n]	0.48
μ_c	0.33
y_b/D	0.36
$V_{sm,\ measured}$ [m/s]	0.15
MODEL PERFORMANCE	
$V_{sm,\ Xs,\ predicted}$ [m/s]	0.21

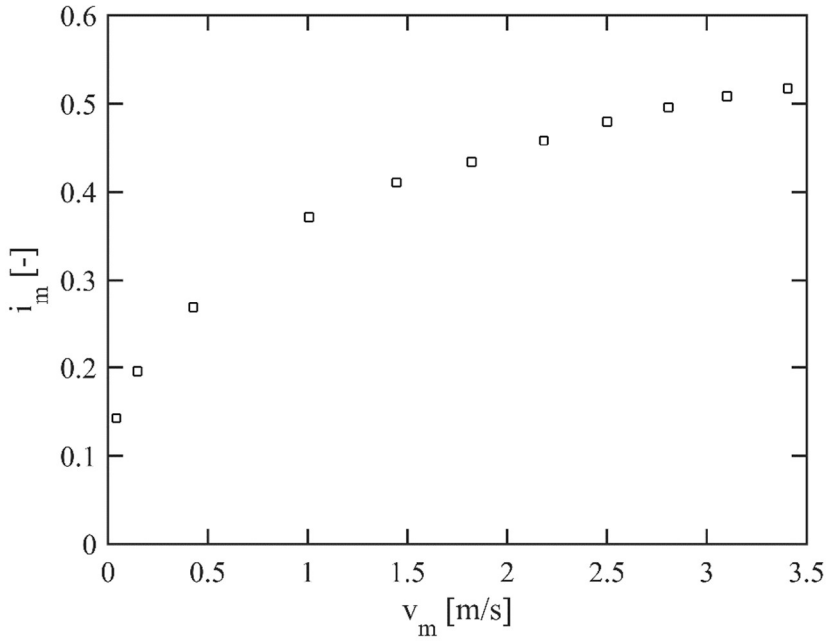

Appendix B – Photographs of the experimental test loop and instrumentation

Photograph 1. – Overview of the experimental test loop

Photograph 2. – Overview of the filling tank

Photograph 3. – Overview of the horizontal section

Photograph 4. – Overview of pressure manometers and flow meter

Photograph 5. – Overview of pressure tapings

Photograph 6. – Overview of vertical section

Appendix C– Recommended procedure for frictional head loss predictions in turbulent flows of complex slurries – straight circular pipes

C.1 INTRODUCTION

The recommended procedure for use of 3-component model, formulated in this thesis, is presented here.

C.2 DETERMINATION OF SLURRY PROPERTIES

The density of the carrier fluid should be obtained as the ratio of its mass to its volume, particle size distribution should be obtained through sieve analysis.

Slurry rheological characterisation should be performed using a viscometer. It is recommended to use a rotational viscometer, as it is more accurate than a tube viscometer. The rheological parameters are then extracted by fitting the rheological model through the experimental data.

C.3 MODEL INPUT VALUES

(i) From particle size distribution, values of mass fractions X_e, X_h and X_s should be determined, as in Fig. C.1

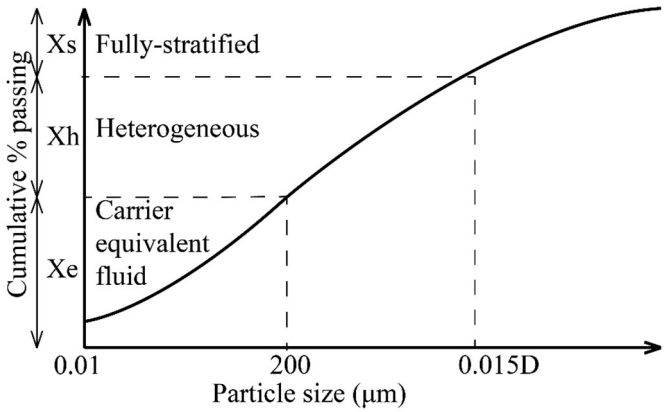

Figure C.1 – Subdivision of the particle size distribution into mass fractions

(ii) Relative densities (ratio of the actual density to that of the original carrier fluid) of model components should be calculated using:

$$S_e = S_c + X_e C_v \left(S_s - S_c \right) \tag{C.1}$$

$$S_h = S_c + \left(X_e + X_h\right) C_v \left(S_s - S_c\right) \quad \text{(C.2)}$$

(iii) Mean velocity of the flow V_m, pipeline inner diameter D, required volumetric concentration of solids C_v are chosen. Rheological parameters τ_y, K, n, are taken from rheological characterization procedure.

C.4 REGIME DETERMINATION

To determine the lower boundary of mean velocity, at which the model calculations are still valid, laminar/turbulent transition needs to be calculated. For Herschel-Bulkley type fluids, Slatter (1994) Re_3, or approach of Swamee and Aggarwal (2011) described in section 2.4.2. are recommended.

Advantage of Swamee and Aggarwal method is its simplicity and explicit calculation process. In this study however, critical value of Reynolds number for this method proved somewhat lower than 2100, which is usually regarded as the critical value, at which the laminar/turbulent transition occurs.

Slatter Re_3 is proven to be the most accurate way to predict laminar/turbulent transition (proven by this study and literature review), its disadvantage is however its implicit process of calculation, as appropriate turbulent-flow model needs to be used as an intermediary to calculate wall shear stress for given mean velocity of the flow.

If coarse particles of X_s fraction are present in the slurry, nomogram in Fig. C.2 or correlations below should be used to account for the effect of coarse particles on the laminar/turbulent transition.

$$\mathrm{Re}' = 305.5 C_{v;Xs}^{\ 2.587} + 0.6034 \qquad \text{when } Re' \leq 1 \text{ and } C_{v;Xs} > 0.05 \quad \text{(C.3)}$$

otherwise

$$\mathrm{Re}' = -0.405 C_{v;Xs}^{\ -0.367} + 2.0398 \quad \text{(C.4)}$$

where Re' is the effect of particle interference on laminar/turbulent transition as described in section 5.2. Actual critical value of Reynolds number at the point of laminar/turbulent transition is then critical value of Reynolds number of carrier fluid (typically 2100) times Re'.

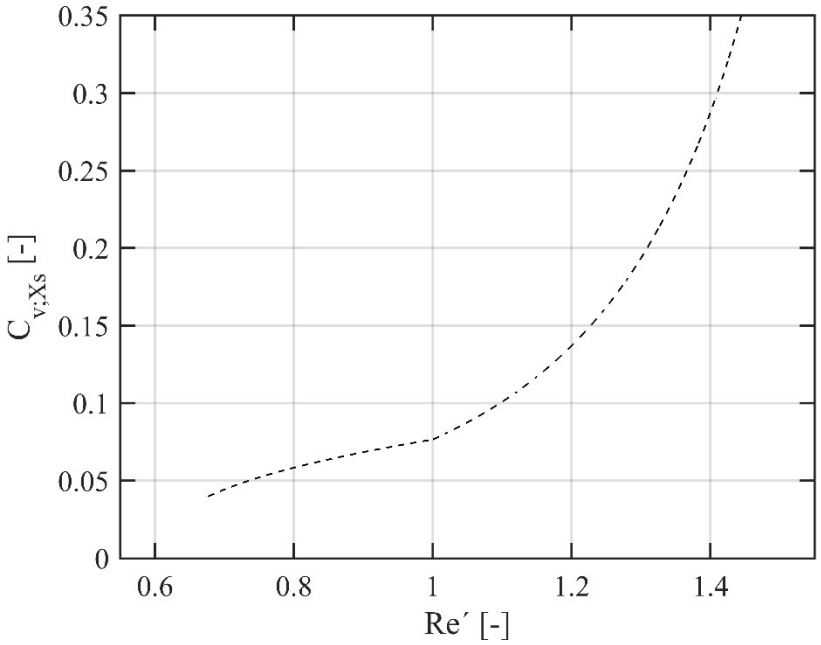

Figure C.2 – Effect of particle volumetric concentration on critical value of Reynolds number

C.5 DETERMINATION OF DEPOSITION LIMIT VELOCITY

If coarse particles of X_s fraction are present in the slurry, deposition limit velocity needs to be calculated. It is recommended to use a layered model by Matoušek et al. (2015) described in section 2.4.4.1.

Height of the X_s bed layer can be calculated directly for given volumetric concentration of solids. Assuming, that particles stop moving in fully stratified flow regime, i.e. with all particles occupying the bed at maximum concentration (for round particles $C_b = 0.55$), the height of the bed layer is then derived from its volume and geometry of the pipe.

C.6 TURBULENT FLOW HEAD LOSS

C.6. 1. Equivalent component

Pressure drop from the equivalent fluid component should be calculated:

$$\frac{dp}{dx_e} = \frac{dp}{dx_c} + k_1 \frac{dp}{dx_c}\left[\left(1-0.25X_e\right)X_e C_v \left(S_s - S_c\right)\right] \qquad (C.5)$$

where dp/dx_c should be calculated using appropriate turbulent-flow model and $k_1 = 1.8$, it is recommended to use one of the predictive models described in section 2.4.1.3.

C.6. 2. Heterogeneous fraction component

If particles of X_h fraction are present in the slurry, their contribution to the pressure drop should be calculated:

$$\frac{dp}{dx_h} = \rho_w g B X_h C_v \left(S_s - S_e\right)\left(\frac{V_{ts}}{V_m}\right)^M \tag{C.6}$$

For the exponent M, value of -1 should be used. V_{ts} should be calculated as in section C.4. and B should be derived from characteristic particle diameter d_h as follows:

$$d_h = \frac{200\mu m + \min\left(0.015D, d_{\max}\right)}{2} \tag{C.7}$$

where D is pipeline inner diameter and $B = 0.22$ when $d_h > 500$ µm, otherwise:

$$B = 0.22 \cdot \frac{d_h - 200\mu m}{300\mu m} \tag{C.8}$$

C.6. 3. Stratified fraction component

If particles of X_s fraction are present in the slurry, their contribution to the pressure drop should be calculated:

$$\frac{dp}{dx_s} = \rho_w g X_s C_v \left(S_s - S_h\right) 0.3 \left(\frac{V_m}{0.55 V_{sm}}\right)^{-0.25} \tag{C.9}$$

where deposition limit velocity V_{sm} should be calculated as in section C.5.

C.6. 4. Total pressure drop

Total pressure drop should be then calculated as:

$$\left(\frac{dp}{dx}\right)_{tot} = \frac{dp}{dx_e} + k_2 \frac{dp}{dx_h} + k_3 \frac{dp}{dx_s} \tag{C.10}$$

where scaling coefficients k_2 and k_3 are:

$$k_2 = a \cdot \exp^{b \cdot Cv} \tag{C.11}$$

$$k_3 = x \cdot \exp^{y \cdot V_{ts}} \tag{C.12}$$

where $a = 9.124$, $b = -5.405$, $x = 2.940$, $y = 0.118$ and V_{ts} should be determined as in section C.4.